LONG TERM PROPERTY PREDICTION OF POLYETHYLENE NANOCOMPOSITES

Ali Al-Abed Shaito, B.E.

Dissertation Prepared for the Degree of

DOCTOR OF PHILOSOPHY

UNIVERSITY OF NORTH TEXAS

December 2008

APPROVED:

Nandika A. D'Souza, Major Professor
Witold Brostow, Committee Member
Thomas Scharf, Committee Member
Cheng Yu, Committee Member
Reza Mirshams, Committee Member
Rick Reidy, Interim Chair of the Department of
      Materials Science and Engineering
Costas Tsatsoulis, Dean of the College of
      Engineering
Sandra L. Terrell, Dean of the Robert B. Toulouse
      School of Graduate Studies

Shaito, Ali Al-Abed, <u>Long Term Property Prediction of Polyethylene Nanocomposites</u>. Doctor of Philosophy (Materials Science and Engineering), December 2008, 184 pp. , 21 tables, 62 illustrations, references.

The amorphous fraction of semicrystalline polymers has long been thought to be a significant contributor to creep deformation. In polyethylene (PE) nanocomposites, the semicrystalline nature of the maleated PE compatibilizer leads to a limited ability to separate the role of the PE in the nanocomposite properties. This dissertation investigates blown films of linear low-density polyethylene (LLDPE) and its nanocomposites with montmorillonite-layered silicate (MLS). Addition of an amorphous ethylene propylene copolymer grafted maleic anhydride (amEP) was utilized to enhance the interaction between the PE and the MLS. The amorphous nature of the compatibilizer was used to differentiate the effect of the different components of the nanocomposites; namely the matrix, the filler, and the compatibilizer on the overall properties.

Tensile test results of the nanocomposites indicate that the addition of amEP and MLS separately and together produces a synergistic effect on the mechanical properties of the neat PE. Thermal transitions were analyzed using differential scanning calorimetry (DSC) to determine if the observed improvement in mechanical properties is related to changes in crystallinity. The effect of dispersion of the MLS in the matrix was investigated by using a combination of X-ray diffraction (XRD) and scanning electron microscopy (SEM). Mechanical measurements were correlated to the dispersion of the layered silicate particles in the matrix. The nonlinear time dependent creep of the material

was analyzed by examining creep and recovery of the films with a Burger model and the Kohlrausch-Williams-Watts (KWW) relation.

The effect of stress on the nonlinear behavior of the nanocomposites was investigated by analyzing creep-recovery at different stress levels. Stress-related creep constants and shift factors were determined for the material by using the Schapery nonlinear viscoelastic equation at room temperature.

The effect of temperature on the tensile and creep properties of the nanocomposites was analyzed by examining tensile and creep-recovery behavior of the films at temperatures in the range of 25 to -100 ^{o}C. Within the measured temperature range, the materials showed a nonlinear temperature dependent response. The time-temperature superposition principle was successfully used to predict the long term behavior of LLDPE nanocomposites.

ACKNOWLEDGEMENTS

The printed pages of this dissertation hold far more than the culmination of years of study. These pages also reflect the relationships with many generous and inspiring people I have met since beginning my graduate work. I owe my gratitude to all those people who have made this dissertation possible and because of whom my graduate experience has been one that I will cherish forever.

To my advisor Nandika D'Souza, a gracious mentor who helped me during my doctoral work. I would like to thank her for her generous time and commitment. Throughout my doctoral work she encouraged me to develop independent thinking and research skills. She continually stimulated my analytical thinking and greatly assisted me with scientific writing.

To my committee members, Dr. Witold Brostow, Dr. Thomas Scharf, Dr. Cheng Yu, and Dr. Reza Mirshams for their comments and suggestions.

I am also grateful to the following former or current staff at University of North Texas for their various forms of support during my graduate study—Alberta Caswell, Wendy Agnes, Joan Jolly , Olga Reyes, Lindsay Quinn for departmental assistance , John Sawyer for insuring a safe work environment in the labs, and David Garrett for microscopy training.

To my invaluable network of supportive and loving friends without whom I could not have survived the process: Laxmi Sahu, Siddhi Pendse, Koffi Dagnon, Sunny

Ogbomo, Shailesh Vidhate just to name few not to miss anyone. I wish all of you good luck in your work.

Most importantly, none of this would have been possible without the love and patience of my family. My immediate family, to whom this dissertation is dedicated to, has been a constant source of love, concern, support and strength all these years. I would like to express my heart-felt gratitude to my family.

TABLE OF CONTENTS

Chapters

LIST OF TABLES

LIST OF FIGURES

CHAPTER 1

INTRODUCTION

When a polymer is used as a structural material, it is important that it be capable of withstanding applied stresses and resultant strains over its service life. Polymers are generally viscoelastic materials, having the properties of solids and viscous liquids. These properties are time and temperature dependent. Poor creep resistance and dimensional stability of polymers are generally a deficiency, limiting their service durability and safety. This presents a barrier for their further expansion of their applications particularly in automotive and aviation industries. Improving the creep resistance is a key factor in ensuring their long term durability.

Creep is the time dependent strain (elongation) for materials under a constant stress. For polymers, creep deformation is an important and powerful experimental method to study many of their physical properties including viscoelastic behavior. For viscoelastic materials such as polyethylene (PE), the load response is time dependent. At very low stresses, the stress-strain relationship is time independent, and the material can be approximated as a linear viscoelastic material. However, PE is in general a nonlinear viscoelastic material and the constitutive relationship is dependent on stress/strain and temperature. When the time-dependent material properties are independent of stress/strain, a single compliance-time curve can define the creep behavior under different stress levels. Such a material is categorized as linear viscoelastic. Otherwise, the material

1

properties are dependent on stress and a group of compliance time curves are needed to describe the viscoelastic response of the material.

The creep properties of polymers can be enhanced by the addition of nanofillers. Montmorillonite layered silicate (MLS) is used as a nanofiller because of its nanometer scale dimension, which increases the interfacial interaction between MLS and the polymer. The resulting structure in the polymer and MLS is called a polymer nanocomposite. The advent of nanocomposites has led to increased interest in the creep response of these materials. In particular, polyethylene is non polar and the limited interaction with the surfactants on the clay is overcome by using a maleated compatibilizer. The contributions and synergisms of a three component system on creep are further complicated when *two* of the three components are crystallizable. Thus in this work we focus on using a maleated polyethylene as a compatibilizer.

1.1   Objectives of Dissertation

The objective of this dissertation is to investigate the individual and synergistic effects of adding montmorillonite layered silicate (MLS) and an amorphous ethylene propylene copolymer grafted with maleic anhydride (amEP) into linear-low density polyethylene (LLDPE) hence forth referred to as PE. The amorphous nature of the compatibilizer helps in separating the role of the PE structure in the nanocomposite.

The effect of adding amEP and MLS on the overall properties of PE is obtained by considering the following

2

1. Effect of amEP and MLS individually and separately on the room temperature tensile and creep properties of PE nanocomposites.

2. Correlation of crystallinity and dispersion to the improvement in the mechanical properties.

3. Effect of amEP and MLS on the stress and temperature response of PE nanocomposites.

The structure-property relationship during creep is studied by considering constitutive equations that describes the nonlinear viscoelastic behavior of the different materials

1. Burgers model and KWW function are used to correlate the morphological changes in the nanocomposites to the retardation time and breadth of relaxation.

2. Schapery's nonlinear equation is used to incorporate the structural changes in the nanocomposites.

1.2   Dissertation Outline

Chapter 2 provides an overview of materials used in this study; their synthesis and characterization and a comprehensive review of the physical models used to characterize their viscoelastic behavior.

In Chapter 3, tensile and creep properties at room temperature, crystallinity, and dispersion of the nanocomposites are studied and compared with the pure matrix. Structure-property relationship in the materials was investigated by considering nonlinear constitutive models and empirical equations that predicts the creep behavior in the nanocomposites and relates it to the presence of MLS. Retardation time and breadth of relaxation effects were examined by the Burgers and KWW models.

In Chapter 4, the effect of temperature on molecular relaxation was analyzed by examining creep and recovery of the films at temperatures in the range of 25 and -100 $^{\circ}$C. The Burgers model was used to show the relationship between creep behavior and retardation time. The individual creep compliance curves for each temperature were fitted considering a polymeric system with a distribution of relaxation times; relevant parameters such as the Kohlrausch-Williams-Watts (KWW) β relation were evaluated.

In Chapter 5, the effect of stress on the creep resistance of these materials was investigated. Creep tests were conducted at different stress levels (10, 25, and 50% yield stress). The nonlinear viscoelastic behavior of the material was modeled using Burgers viscoelastic model and was seen to fit the creep data very well. It was also possible to correlate the creep behavior to a polymeric system with a distribution of relaxation times by considering KWW stretched exponential function.

In Chapter 6, effect of stress on the nanocomposites was investigated using Schapery non-linear equation. The effects of adding MLS separately to the amEP was investigated.

In Chapter 7, the relationship between deformation, time, and temperature of PE nanocomposites was studied. For both chapters, the films were subjected to creep and recovery in the tension mode and the time/stress/temperature related creep behavior was studied. Smooth mastercurves are constructed using time-temperature-stress superposition principles (TTSSP). The temperature-related creep constants and shift factors were determined for the material using Schapery nonlinear viscoelastic equation.

The predicting results confirm the enhanced creep resistance of nanofillers even at extended time scales and low temperatures.

Chapter 8 provides summary of results.

CHAPTER 2

POLYMER –CLAY NANOCOMPOSITES : STRUCTURE-PROPERTY RELATIONSHIP

The addition of inorganic nanoparticles to polymeric systems resulted in the introduction of a new set of materials known as polymer nanocomposites (PNs). These materials exhibit multifunctional, high performance polymer characteristics beyond these found in traditional filled polymeric systems. Multifunctional features include improved thermal resistance and/or flame retardance, moisture resistance, improved mechanical properties, decreased permeability, charge dissipation, and chemical resistance.

Polymer nanocomposites have emerged as a new area of research in the past few years. The term "composite" is generally used to define a material that is made of more than one component. Depending on the matrix, three types of composites exist: polymeric, metallic, and ceramic composites. Composites consisting of components where at least 1 dimension is < 10 nm are termed nanocomposites. Organically modified layered silicates have been widely used in modern plastics as property enhancers. These properties include improvement in mechanical, thermal, and flame retardance properties .The enhancement in properties at low concentrations (2-6 wt %) has been reported by many researchers. Hambir et al. [1] studied the effect of adding 4% octadecylamine (ODA)-modified montmorillonite (MMT) clay to polypropylene (PP). They found that the incorporation of the clay in a platelet form results in a significant improvement in the thermal stability of PP. The temperature at the onset of degradation increases from about

270 to about 330 °C. The enhancement in the thermal stability of the PP/clay composites can be attributed to the decreased permeability of oxygen due to the clay platelets in the PP/clay composites. They also found that the PP/clay composite exhibits higher storage modulus over the entire temperature range. The increase in the storage modulus is about 56%. Gilman et al. [2] found that polymer layered-silicate clay nanocomposites have the unique combination of reduced flammability and improved physical properties. The mechanical properties of a nylon-6 layered-silicate nanocomposite, with a silicate mass fraction of only 5%, show excellent improvement over those for the pure nylon-6. The nanocomposite exhibits a 40% higher tensile strength, 68% greater tensile modulus, 60% higher flexural strength, and a 126% increased flexural modulus. The nylon-6 nanocomposite has a 63% lower HRR than the pure nylon-6. This suggests the improved flammability properties of the nanocomposite as compared to the pure polymer matrix. Dumont et al. [3] studied the barrier properties of PP/organoclay nanocomposites. They found that improvements in the helium barrier properties are obtained with low concentrations of the compatibilizer and filler (3 wt % each). They explained this effect by changes in the arrangement of the clay platelets and by the state of the amorphous domains.

This chapter presents an overview of polymer nanocomposites with a discussion of a) the PE matrix used for preparation of the PE nanocomposites films, b) the type of clay used in this study, c) common processing approaches to polymer nanocomposites, d) characterization techniques relevant to this dissertation, and e) physical models used to describe their viscoelastic behavior.

2.1   Matrix: Polyethylene (PE)

Polyethylene (PE) is a thermoplastic commodity heavily used in consumer products. Over 60 million tons of the material is produced worldwide every year. Polyethylene consists of long chains of the monomer ethylene. The recommended scientific name 'polyethene' is systematically derived from the scientific name of the monomer.

Polyethylene is classified into several different categories based mostly on its density and branching. The mechanical properties of PE depend significantly on variables such as the extent and type of branching, the crystal structure, and the molecular weight [4-5].

- Ultra high molecular weight polyethylene (UHMWPE)

- Ultra low molecular weight polyethylene (ULMWPE - PE-WAX)

- High molecular weight polyethylene (HMWPE)

- High density polyethylene (HDPE)

- High density cross-linked polyethylene (HDXLPE)

- Cross-linked polyethylene (PEX)

- Medium density polyethylene (MDPE)

- Low density polyethylene (LDPE)

- Linear low density polyethylene (LLDPE)

- Very low density polyethylene (VLDPE)

LLDPE differs from LDPE by having a narrower molecular weight distribution and by not containing long-chain branching. Although practically any α-olefin from C_3 to

C_{20} can be used a comonomer for LLDPE, the four commonly used are 1-butene, 1-hexene, 4-methyl-1-pentene, and 1-octene. In this dissertation, a LLDPE which is commonly used for blown films was chosen.
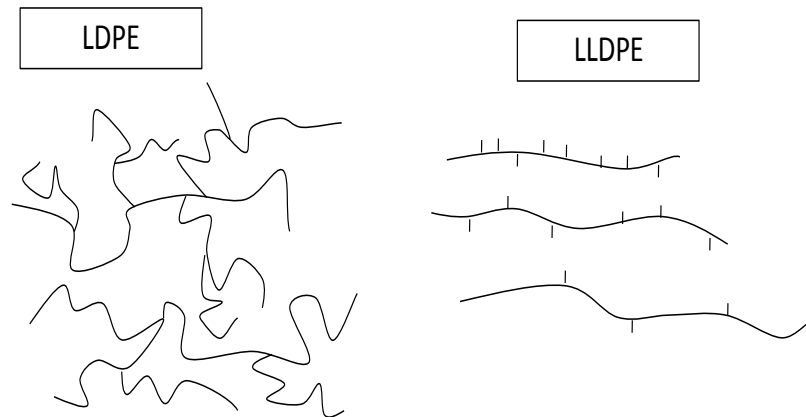
Figure 2.1. Schematic showing structural difference between LDPE and LLDPE.

2.2   Filler: Clay

PNs systems are usually made of two components: the base resin, and a modified layers silicate. A potential third component is a compatibilizer. Montmorillonite is a soft phyllosilicate mineral that typically forms in microscopic crystals, forming clay[4]. It is named after Montmorillonite in France. Montmorillonite, a member of the smectite family, is 2:1 clay, meaning that it has 2 tetrahedral sheets sandwiching a central octahedral sheet. The particles are plate-shaped with an average diameter of approximately 1 micrometer.

Figure 2.2. Montmorillonite clay.

Silica is the dominant constituent of the montmorillonite clay, with alumina being essential. The chemical structure of montmorillonite is shown in the figure. It is a sheet structure consisting of layers containing the tetrahedral silicate layer the octahedral alumina layer. The tetrahedral silicate layer consists of SiO_4 groups linked together to form a hexagonal network of the repeating units. The alumina layer consists of two sheets of closely packed oxygens or hydroxyls, between which octahedrally coordinated aluminum atoms are embedded in such a way that they are equidistant from six oxygens or hydroxyls. The two tetrahedral layers sandwich the octahedral layer. The three layers form one clay sheet that has a thickness of 0.96 nm. The chemical formula of montmorillonite clay is $Na_{1/3}(Al_{5/3}Mg_{1/3})\ Si_4O_{10}(OH)_2$. In its natural state Na^+ resides on the MMT clay surfaces.
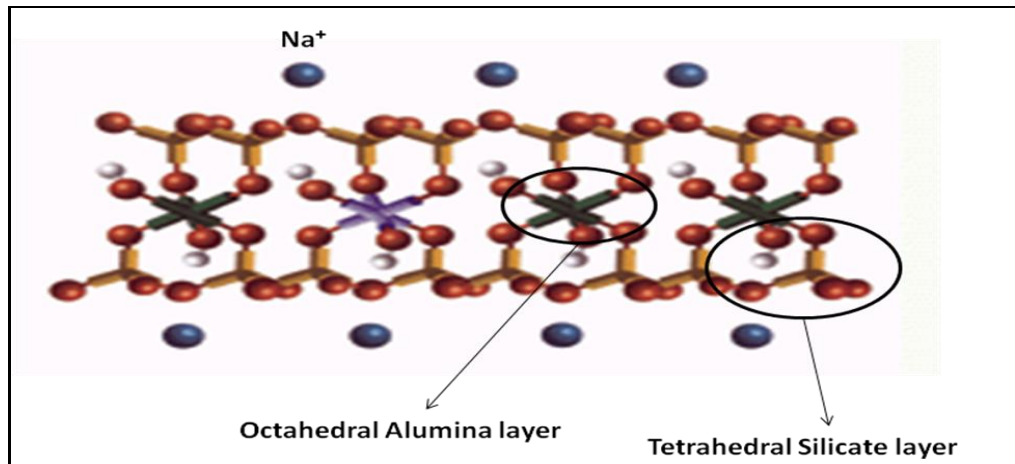
Figure 2.3. Edge view of montmorillonite structure of aluminum octahedron, which may also substitute elements of magnesium or iron, sandwiched between layers of silicon tetrahedron.

Southern clay products (SCP) manufactures and markets cloisite additives. Their montmorillonite organoclays are surface modified to allow dispersibility and miscibility with many different resin systems for which they are designed to improve properties. Cloisite MMT clays are Cloisite Na^+, 15A, 20A, 30B, 93A, 25A, and 10A.

Cloisite Na^+ is a natural montmorillonite. This additive improves various physical properties such as reinforcement, heat deflection temperature (HDT), coefficient of linear thermal expansion (CLTE), and barrier properties.

Cloisite 15A, 20A, 25A, and 30B are natural montmorillonite modified with a quaternary ammonium salt.

Cloisite 93A is a natural montmorillonite modified with a ternary ammonium salt.

Organoclays Commercial Designation	Surfactant used to make the organoclay
Cloisite 20A Cloisite 15A Cloisite 6A	$M_2(HT)_2$ $M \!-\! N^+ \!-\! HT$ with substituents HT (top) and HT (bottom), Cl^-
Cloisite 30	$(HE)_2M_1T_1$ CH_2CH_2OH $M \!-\! N^+ \!-\! T$ with CH_2CH_2OH (bottom), Cl^-
Cloisite 10A	$M_2(HT)_1B_1$ M $M \!-\! N^+ \!-\! CH_2\text{-}C_6H_5$ with HT (bottom), Cl^-

Table 1. Cloisite organoclays and their surfactants.

2.3 Compatibilizer: Thermoplastic Elastomer (TPE)

Since nanocomposites require chemical interaction between the clay and the matrix, non polar polymers like PE utilize a polar compatibilizer, typically thermoplastic elastomers. Thermoplastic elastomers (TPE) or commonly known as thermoplastic rubbers, are a class of copolymers which are usually a mixture of a plastic and a rubber. They consist of materials having both thermoplastic as well as elastomeric properties. Thermoplastic elastomers show both properties of a rubbery material and plastic material.

The principal difference between thermoset elastomers and thermoplastic elastomers is the type of crosslinking bond in their structures. Crosslinking is one of the critical structural factors which contribute to the high elastic properties. The crosslink in a thermoset polymer is a covalent bond created during the vulcanization process, while the crosslink in a thermoplastic elastomer polymer is a weaker dipole or hydrogen bond or takes place in only in one of the phases of the material.

Some generic classes of TPEs are styrenic block copolymers, polyolefin blends, elastomeric alloys, thermoplastic polyurethanes, thermoplastic copolyester and thermoplastic polyamides. Ethylene/propylene (EP) copolymers grafted with maleic anhydride are obtained from ExxonMobil Chemical, Exxelor 1803 and Exxelor 1801; the former is nearly free of crystallinity while the later has a high level of ethylene crystallinity. Exxelor 1803 was used in this study as a coupling agent between the nonpolar LLDPE matrix and MLS. Okada et al. [6] prepared blends of nylon 6 with Exxelor 1801 and 1803 by melt blending. The effect of nylon 6 content and the crystallinity of the EP copolymer on morphological, thermal and mechanical properties of

these blends were studied. The EP copolymer with some ethylene crystallinity was shown to have better mechanical properties than the amorphous EP copolymer which also had an improvement in the mechanical properties as compared to the neat nylon matrix.

Polymer	Characterization	Source
Exxelor 1803	43 wt% ethylene, 53 wt% propylene, 1.14 wt% MA, amorphous, $T_m = 127\ ^oC$	ExxonMobil Chemical
Exxelor 1801	43 wt% ethylene, 53 wt% propylene, 1.21 wt% MA, crystalline, $T_m = 127\ ^oC$	ExxonMobil Chemical

Table 2.2. Common ethylene-propylene copolymers used as elastomeric modifier [6].

2.4   Processing of Polymer Nanocomposites

Solution intercalation, in-situ polymerization, and melt processing are considered the most convenient methods to disperse layered silicates into polymer nanocomposites in an intercalated or exfoliated state.

Two types of structures are obtained from the processing techniques, intercalated nanocomposites, where the polymer chains are sandwiched between silicate layers, and exfoliated nanocomposites where the separated, individual silicate layers are more or less uniformly dispersed in the polymer matrix. This type of new materials exhibits enhanced

properties such as increased Young's and storage modulus, increased thermal stability and barrier properties, and good flame retardency at filler levels less than 2%.

Figure 2.4. Polymer-clay nanocomposite morphologies.

Layered silicates are exfoliated into single layers using a solvent in which the polymer is soluble. The layered silicates, due to the weak forces that hold the layers together can be easily dispersed in an adequate solvent. The polymer then absorbs onto the delaminated sheets, and when the solvent evaporates, the sheets reassemble sandwiching the polymer to form an ordered, multilayered structure.

Solution intercalation is a technique that has been widely used with water-soluble polymers to produce intercalated nanocomposites based on polyvinyl alcohol (PVOH) and polyethylene oxide (PEO). When polymeric aqueous solutions are added into dispersions of fully delaminated sodium layered silicate, the strong interaction between the water soluble macromolecules and the silicate layers often triggers the rearrangement of the layers as it occurs for PEO. In the presence of PVOH, the silicate layers are colloidly dispersed resulting in a colloidal distribution of the nanoparticles in PVOH.

Polymer intercalation using this technique can be also performed in organic solvents. Polyethylene oxide has been successfully intercalated in sodium MMT by dispersion in acetonitrile allowing stoichiometric incorporation of one or two polymer chains between the silicate layers and increasing the intersheet spacing from 0.98 to 1.36 and 1.71 nm, respectively.

In melt intercalation, the layered silicate is mixed with the solid polymer matrix in the molten state. Under these conditions, and if the layer surfaces are sufficiently compatible with the selected polymer, the polymer can be inserted into the interlayer space and form either an intercalated or an exfoliated nanocomposite. No solvent is required.

In the in-situ polymerization approach, the layered silicate is swollen within the liquid monomer or monomer solution so that the polymer formation can occur between the intercalated sheets. Polymerization can be initiated by different polymerization methods such as heat or radiation, diffusion of a suitable imitator, or an organic initiator or an organic initiator fixed through cationic exchange inside the interlayer before the swelling step of the monomer.

2.5 Characterization of Polymer Nanocomposites

There are three steps involved in the development of nanocomposites: (1) material preparation, (2) property characterization, (3) material performance. The material preparation involves the processing of the nanoparticles with the polymer matrix into polymer nanocomposite. The next challenge is the determination of the degree and level of dispersion of the nanoparticles in the polymer matrix. Characterization involves:

structure analysis and property measurement. Structure analysis is carried out using a variety of microscopic and spectroscopic techniques, while property characterization is diverse and depends on the individual application.

Due to the high selectivity of the size and structure of nanostructured materials, the physical properties of these materials can be diverse. An essential task to develop capability in the preparation of nanomaterials is property characterization of an individual nanostructure with a well defined atomic structure.

Characterizing the properties of an individual nanoparticle presents a challenge to many existing testing and measurement techniques because of many constraints such as the size (length and diameter) which makes their manipulation rather difficult and specialized techniques are needed for identifying and analyzing individual nanostructures. The commonly used characterization techniques for nanocomposites are

- Wide angle X-ray diffraction (WAXD) and small angle X-ray scattering (SAXS): used to study dispersion and crystallinity.

- Transmission electron microscopy (TEM), scanning electron microscopy (SEM), and spectroscopy: used to study dispersion.

- Thermal gravimetric analysis (TGA): used to study thermal stability.

- Differential scanning calorimetry (DSC): used to study thermal properties.

- Dynamic mechanical thermal analysis (DMTA): used to study thermo-mechanical properties.

- Optical microscopy: used to study dispersion.

2.5.1   X-Ray Diffraction (XRD)

Wide angle X-ray diffraction is the most commonly used technique to study the degree of nanodispersions of MMT organoclay in polymer nanocomposites. Wide angle x-ray diffraction measures the distance between the ordered crystalline layers of the organoclay.

By using Bragg's law

$$\sin \lambda = 2d \sin \theta$$

(Equation 1)

Where d is the spacing between the atomic planes in the crystalline phase and λ is the x-ray wavelength.
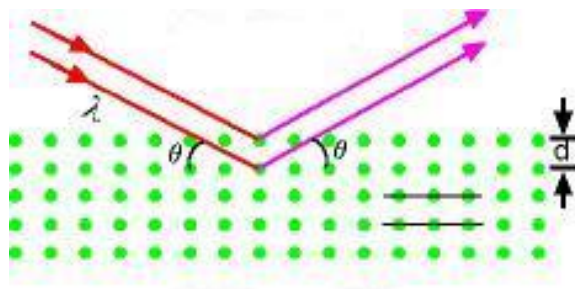
Figure 2.5. Schematic of X-ray diffraction.

The intensity of the diffracted X-ray is measured as a function of the diffraction angle 2θ and the specimen's orientation. This diffraction pattern is used to identify specimen's crystalline phases and to measure its structural properties. WAXD is a non-destructive technique and does not require excessive sample preparation which explains the wide usage of this technique in materials characterization. Spacing changes (increase

or decrease) can be used to determine the type of polymer nanocomposite formed such as:

- Immiscible: no d-spacing change.

- Decomposed/deintercalted: d-spacing decrease.

- Intercalated: d-spacing increase.

- Exfoliated: d-spacing outside the wide angle x-ray diffraction or so expanded or disordered to give a signal.

2.5.2 Transmission Electron Microscopy (TEM) and Spectroscopy

One of the characteristics of polymer nanostructured materials is their small particle size of the added particles. Direct imaging of these nanometer range particles is only possible through transmission electron microscopy and scanning probe microscopy. The uniqueness of TEM lies in the fact that it can provide a real space image of the atoms in the nanocrystals. Today's TEM provides not only atomic resolution images, but also chemical information at a spatial resolution of 1 nm or better allowing the identification of the chemistry of a single nanocrystal.

TEM sample preparation is of importance for obtaining a TEM image with good resolution. The basic requirement is that the specimen should be thin enough to be transparent to the electron beam. There are several methods for TEM specimen preparation:

- Ion-milling: for almost all kind of materials.

- Electropolishing: for conductive bulk materials.

- Microtoming: for polymeric and biological samples.

- Crushing powders: the simplest way to prepare TEM specimens, but microstructural details can be lost.

Transmission electron microscopy allows the observation of the overall organoclay dispersion in the polymer nanocomposite sample. Clay dispersion and structure observed using TEM can determine the nature of clay nanocomposites as:

- Immiscible

- Intercalated

- Exfoliated

2.5.2.1 Focused Ion Beam (FIB)

Focused ion beam, also known as FIB, is a technique used particularly in the semiconductor and materials science fields for site-specific analysis, deposition, and ablation of materials.

The FIB is a scientific instrument that resembles a scanning electron microscope. However, while the SEM uses a focused beam of electrons to image the sample in the chamber, a FIB instead uses a focused beam of gallium ions. Gallium is chosen because it is easy to build a gallium liquid metal ion source (LMIS).

Figure 2.6. Photograph of a FIB workstation.

Unlike an electron microscope, the FIB is inherently destructive to the specimen. When the high-energy gallium ions strike the sample, they will sputter atoms from the surface. Gallium atoms will also be implanted into the top few nanometers of the surface, and the surface will be made amorphous.
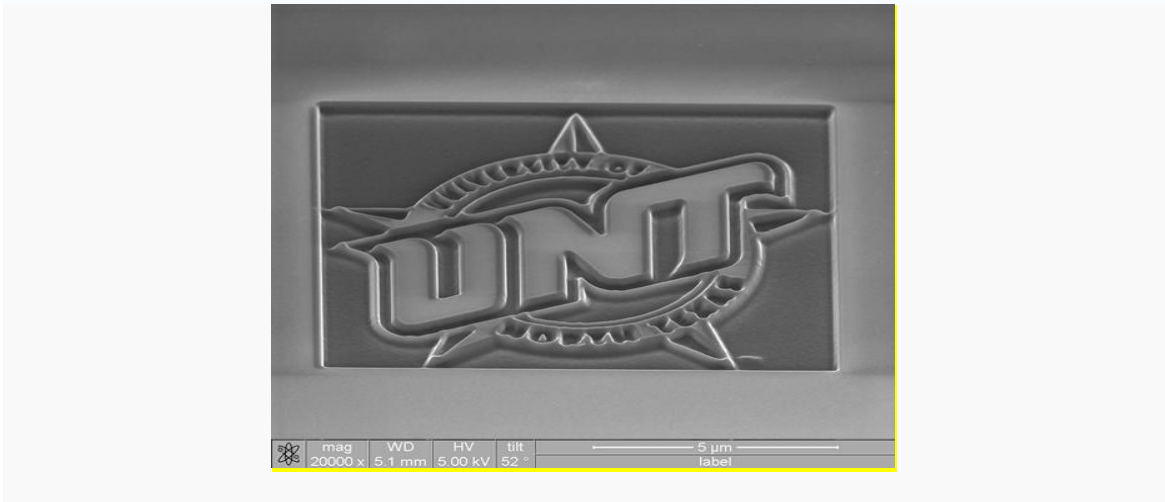
Figure 2.7. University of North Texas name and logo "tattooed" into a silicon wafer.

2.5.3   Differential Scanning Calorimetry (DSC)

Differential scanning calorimetry or DSC is a thermo-analytical technique in which the difference in the amount of heat required to increase the temperature of a sample and reference are measured as a function of temperature.
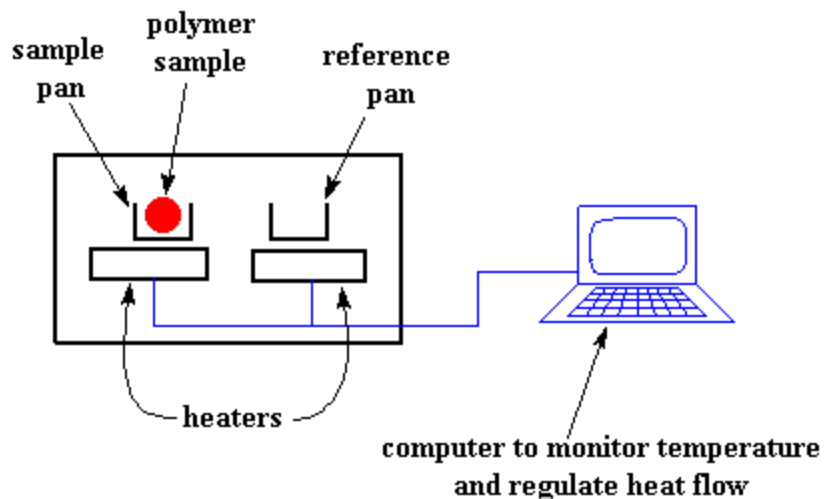
Figure 2.8. Schematic of DSC instrument [7].

In a DSC experiment, both the sample and reference are maintained at nearly the same temperature. The basic principle that this technique involves is that when the sample undergoes a physical transformation such as phase transitions, more (or less) heat will need to flow to it than the reference to maintain both at the same temperature. By observing the difference in heat flow between the sample and reference, differential scanning calorimeters are able to measure the amount of heat absorbed or released during such transitions.

2.5.4   Dynamic Mechanical Thermal Analysis (DMTA)

Dynamic mechanical properties refer to the response of the material as it is subjected to a periodic force. These properties may be presented in terms of a dynamic storage modulus, a dynamic loss modulus, and a mechanical damping factor.

For an applied stress varying sinusoidally with time, a viscoelastic material will also respond with a sinusoidal strain. The sinusoidal variation in time is usually described as a rate specified by the frequency $f = 2\ \Pi\omega$ (f = Hz; ω = rad/sec). The strain of a viscoelastic material is out of phase with the applied stress, by a phase angle, δ. This phase lag is due to the time necessary for molecular motions and relaxations to occur. For an elastic material, the phase angle is equal to zero, whereas for a viscous material the phase angle is equal to 90°.

Dynamic stress σ and strain ε can be represented by:

$$\sigma = \sigma_0 \sin(\omega t + \delta) \qquad\qquad \text{(Equation 2)}$$

$$\varepsilon = \varepsilon_0 \sin(\varpi t) \qquad\qquad \text{(Equation 3)}$$

where ω is the angular frequency.

Dividing the stress by the strain to yield a modulus and using E' and E'' for the in phase and the out-of-phase moduli respectively

$$E^* = \frac{\sigma}{\varepsilon} = \frac{\sigma_o}{\varepsilon_o}(\cos\delta + i\sin\delta) = E' + iE'' \qquad\qquad \text{(Equation 4)}$$

Equation 4 shows that the complex modulus obtained by a dynamic mechanical test consists of a "real" part and an "imaginary" part. The real (storage) part E' describes the ability of the material to store potential energy and release it upon deformation. The

imaginary (loss) part is associated with energy dissipation in the form of heat upon deformation.

2.5.4.1 Time-Temperature Superposition (TTS)

The time-temperature correspondence states that there are two methods to determine the polymer's behavior at longer times. First, one may directly measure the response at longer times. This technique is time consuming as the change is slow. Secondly, one may carry out the relaxation experiment at a temperature T_1 at experimentally accessible time scales. The temperature is then increased to a temperature T_2. The curves at temperature T_2 can be shifted horizontally to the right to give an exact superposition of the curves measured at temperatures T_1 and T_2 in the areas where the modulus values overlap. Thus, one can measure the complete modulus-time behavior by applying the time-temperature correspondence principle to experimental measurements of polymer relaxations carried out on experimental accessible time scales.
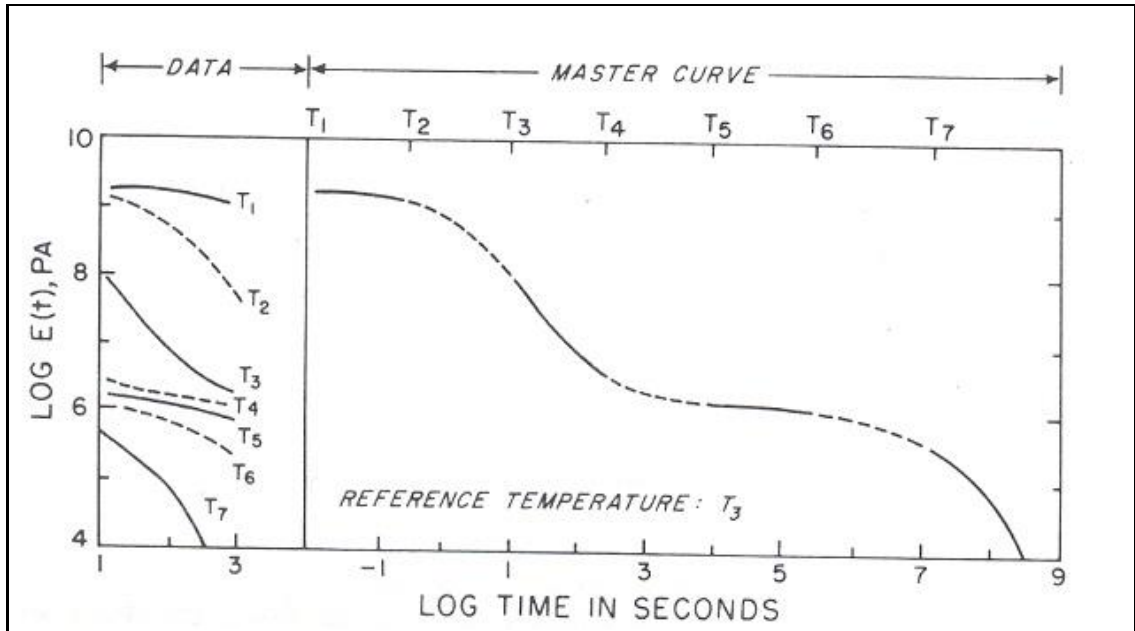
Figure 2.9. Mastercurve construction from experimental time (frequency)-temperature data.

Mathematically this is expressed as:

$$E(t_1,T) = E(T_2, t/a_T) \qquad \text{(Equation 5)}$$

where the effect of changing temperature is the same as applying a multiplicative factor to the time scale know as the temperature shift factor a_T.

When shifting horizontally, an additional correction is necessary. Since the volume of a polymer is a function of temperature, and the modulus is measured per unit cross-sectional area, the amount of matter contained in a unit volume will vary. A corresponding correction that accounts for the change of mass per unit volume should be considered. The density is thus the parameter that should be used. This will show as a vertical shifting in the modulus-time curves and is expressed as:

$$\frac{E(t_1, T)}{\rho(T_1)T_1} = \frac{E(T_2, t/a_T)}{\rho(T_2)T_2} \qquad \text{(Equation 6)}$$

Division by temperature accounts for changes in modulus due to the dependence of modulus on temperature and division by density accounts for the change per unit volume with temperature.

2.6 Modeling Long Term Properties in Polymers

Viscoelastic materials have a specific set of characteristics that differentiate them from elastic materials. Elastic materials store 100% of energy due to deformation when compared to viscoelastic materials that do not store 100% of the energy under deformation and lose or *dissipate* some of this energy. The ability to dissipate energy is one of the main reasons for using viscoelastic materials for any application to cushion shock, such as the materials used in running shoes or packing materials. The two other main characteristics associated with viscoelastic materials are stress relaxation and creep.

Stress relaxation refers to the behavior of stress reaching a peak and then decreasing or *relaxing* over time under a fixed level of strain. Creep is in some sense the inverse of stress relaxation, and refers to the ability of viscoelastic materials to undergo increased deformation under a constant stress, until an asymptotic level of strain is reached.

2.6.1 Mechanical Analogs for Viscoelastic Materials

The classic way to derive viscoelastic constitutive models is through the use of mechanical analogs [8]. These are simple mechanical models for fluid and solid

representations that are put together to produce viscoelastic effects. The simplest mechanical analog for a linear elastic material is a spring. The simple constitutive relationship for a spring relates the force (stress when force is divided by area) to the elongation or displacement (strain when displacement is normalized by length of the spring).

$$\sigma = E\varepsilon$$ (Equation 7)

Where σ is the applied stress, E is the elastic modulus, and ε represents the resultant strain. The mechanical analog for a Newtonian fluid is a dashpot. The simple constitutive relationship for a dashpot indicates that the force in the fluid depends on the rate the dashpot is displaced, or equivalently the velocity of the dashpot. The constitutive parameter that relates force (stress) to displacement rate (strain rate) is *viscosity η*.

$$\sigma = \eta \frac{d\varepsilon}{dt} = \eta \, \dot{\varepsilon}$$ (Equation 8)

By making various combinations of spring and dashpot models, we can simulate the behavior of a viscoelastic material, including stress relaxation and creep.

2.6.1.1 Maxwell Model

The simplest combination of the spring and dashpot is to put the spring in series with the dashpot. This combination is known as the Maxwell model. This model represents a fluid since it relaxes completely to zero stress and undergoes creep indefinitely.

$$\varepsilon = \varepsilon_1 + \varepsilon_2$$ (Equation 9)

Where ε_1 and ε_2 are the strains of the spring and dashpot, respectively.

Since the stresses in both the spring and dashpot are the same, the strains in the spring in the dashpot can be represented as

$$\varepsilon_1 = \frac{\sigma}{E} \; ; \quad \dot{\varepsilon}_2 = \frac{\sigma}{\eta}$$

(Equation 10)
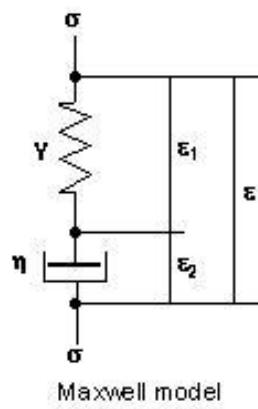
Figure 2.10.Schematic of Maxwell model.

Equations (9), (10) when combined give:

$$\dot{\varepsilon} = \dot{\sigma}/E + \sigma/\eta$$

(Equation 11)

For a constant applied stress σ

$$\dot{\varepsilon} = \frac{\sigma_0}{\eta}$$

(Equation 12)

Equation (11) allows the evaluation of the response to a step stress (creep) or step strain (stress relaxation). To solve the differential equation in Equation (11), Laplace transform is used. The Laplace transform of Equation (11) gives

$$s\varepsilon(s) - \varepsilon(0) = \frac{1}{E}[s\sigma(s) - \sigma(0)] + \frac{1}{\eta}\sigma(s)$$ (Equation 13)

The response to a stress input $\sigma(t)$ is given by

$$\varepsilon(t) = \sigma_0(\frac{1}{E} + \frac{t}{\eta})$$ (Equation 14)

Where $E = \sigma_0/\varepsilon_0$. The creep compliance function is given by

$$D(t) = \frac{\varepsilon(t)}{\sigma_0} = \frac{1}{E} + \frac{t}{\eta}$$ (Equation 15)

The response to the stress input of the Maxwell model is schematically represented in Figure 2.
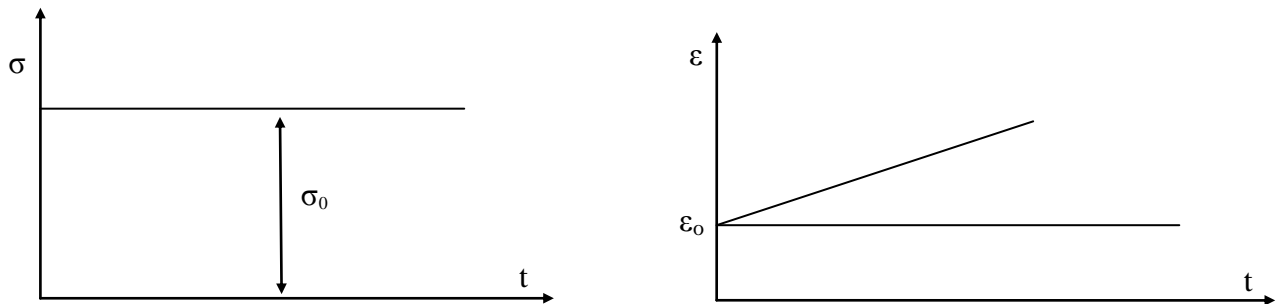
Figure 2.11. Schematic of Maxwell model response to a constant stress.

The Maxwell analog therefore reflects the instantaneous elastic deformation via the spring, but the linear time response is inadequate in reflecting the non-Newtonian viscous response of polymer systems. This is because, in creep, the dashpot undergoes continuous deformation and the strain is time dependent. The recovery response of the Maxwell analog is also inadequate. When the applied load is removed, the spring recoils

elastically while the dashpot remains deformed. The extent of this deformation depends on the viscous portion and the deformation is an irreversible process.

2.6.1.2 Kelvin-Voigt Model

In Kelvin model the spring and dashpot are connected in parallel. Based on the geometry of the model, the dashpot will constrain the spring to have the same deformation. The total stress is the sum of the stress in the spring and dashpot.

$$\sigma = \sigma_1 + \sigma_2 \qquad \text{(Equation 16)}$$

Which gives

$$\sigma = E\varepsilon + \eta\, \dot{\varepsilon} \qquad \text{(Equation 17)}$$

The above equation illustrates an important characteristic of viscoelastic materials, namely that the stress in the material depends not only on the strain, but also on the *strain rate*.
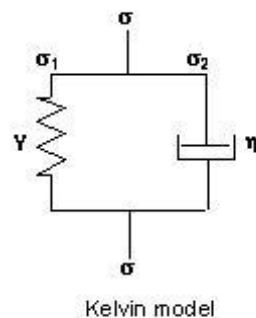
Figure 2.12. Schematic of Kelvin model.

The Laplace transform of this equation for a step stress input gives

$$\frac{\sigma_0}{s} = E\varepsilon(s) + \eta[s\varepsilon(s) - \varepsilon(0)] \qquad \text{(Equation 18)}$$

The corresponding strain can be written as

$$\varepsilon(s) = \frac{\sigma_0}{s(E + \eta s)} \qquad \text{(Equation 19)}$$

The inverse Laplace transform of Equation (14) gives the strain response of the Kelvin-Voigt element as

$$\varepsilon(t) = \frac{\sigma_0}{E}[1 - \exp(-t/\tau)] \qquad \text{(Equation 20)}$$

The response is shown schematically in Figure 4.
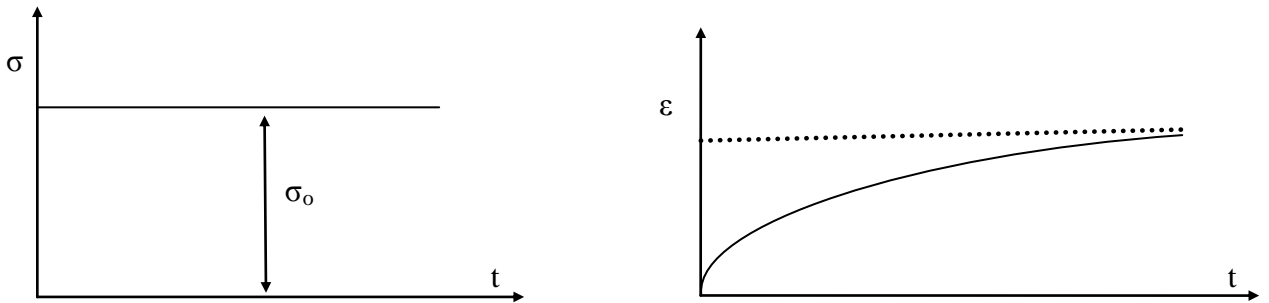
Figure 2.13. Schematic of response of Kelvin model to a constant input stress (creep).

When the load is removed in the Kelvin model, the spring tries to recoil elastically and this causes both spring and dashpot to reach their initial positions.

31

However, this process is delayed due to the presence of dashpot (viscous component). Real polymers behave viscoelastically. There is instant recoil of the elastic portion, delayed reformation of both the elastic and viscous parts, and a permanent deformation of the viscous part. Individual Maxwell and Kelvin models fail to explain the complex viscoelastic behavior of polymer systems.

2.6.1.3 Burgers Model

Burgers model is a four-element model that is a combination of Maxwell and Kelvin-Voigt models in series. The total strain is the sum of the elastic and viscous strains represented by Maxwell element and the viscoelastic strain represented by Kelvin-Voigt element.

$$\varepsilon = \varepsilon_1 + \varepsilon_2 + \varepsilon_3$$
(Equation 21)
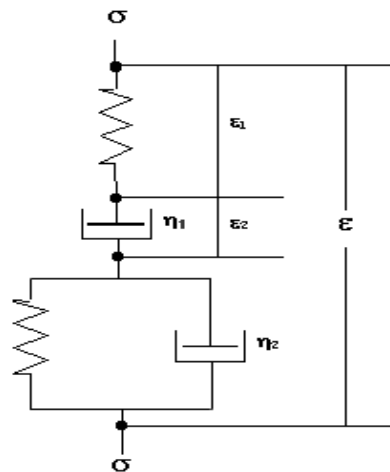
Figure 2.14. Schematic of Burgers model.

$$\varepsilon_1 = \frac{\sigma_0}{E_1} \; ; \dot{\varepsilon}_2 = \frac{\sigma_0}{\eta_1} \; ; \dot{\varepsilon}_3 + \frac{E_2}{\eta_2}\varepsilon_3 = \frac{\sigma_0}{\eta_2} \qquad \text{(Equation 22)}$$

Substituting the values of ε_1, ε_2, and ε_3 into Equation(15) , one obtains

$$\sigma + \left[\frac{\eta_2}{E_2} + \eta_1\left(\frac{1}{E_1} + \frac{1}{E_2}\right)\right]\dot{\sigma} + \frac{\eta_1\eta_2}{E_1 E_2}\ddot{\sigma} = \eta_1\dot{\varepsilon} + \frac{\eta_1\eta_2}{E_2}\ddot{\varepsilon} \qquad \text{(Equation 23)}$$

The response to a step stress input is given by

$$\varepsilon(t) = \sigma_0\left\{\frac{1}{E_1} + \frac{t}{\eta_1} + \frac{1}{E_2}\left[1 - \exp(-\frac{t}{\tau_2})\right]\right\} \qquad \text{(Equation 24)}$$

Where $\tau_2 = \eta_2/E_2$ is the relaxation time.

When a stress σ is applied, the Maxwell spring initially deforms. The Kelvin spring and dashpot show a delayed deformation at longer times. When the applied force is removed (recovery step), the Maxwell spring recovers completely. The Kelvin spring and dashpot show delayed reformation. The Burgers model resembles the behavior of a viscoelastic material and is thus used in our analysis.

2.6.1.4 Generalized Viscoelastic Constitutive Model

The strain behavior over time of a viscoelastic material is a function of the creep function and the stress. Boltzmann (1844-1906) first generalized these observations by saying that for a simple bar subject to a stress $\sigma(t)$,the increment in stress over a small time interval $d\tau$ would be:

$$d\sigma = \frac{d\sigma}{d\tau} d\tau \qquad \text{(Equation 25)}$$

This assumes that the stress is continuous and differentiable in time. Given that the stress is related to the strain via the creep function, Boltzmann postulated that an increment of strain dε, which depends on the complete stress history up to time t, would be related to the increment of stress dσ at the specific time increment from τ to t through the creep function D at the time t - τ as:

$$d\varepsilon(t) = D(t-\tau)\frac{d\sigma}{d\tau} d\tau \qquad \text{(Equation 26)}$$

The complete strain at a time t would then be obtained by integrating the strain increments from time 0 to time t, over all the increments dτ:

$$\varepsilon(t) = \int_0^t D(t-\tau)\frac{d\sigma(\tau)}{d\tau}d\tau \qquad \text{(Equation 27)}$$

2.6.2   Findley Power Law

Considering the creep curves of many polymers are similar to those of some metals, many authors proposed several empirical mathematical models to represent the creep data of polymers. Among then Findley, used the following empirical power equation which could describe the creep behavior of many polymers with good accuracy over a wide time scale

$$\varepsilon_F = \varepsilon_{F0} + \varepsilon_{F1}t^n \qquad \text{(Equation 28)}$$

where the subscript F indicates the parameters associated with the Findley power law; n is a constant independent of stress and generally less than one.; ε_{F0} is the time independent strain; and ε_{F1} is the time dependent strain. ε_{F0} and ε_{F1} are functions of stress and temperature.

The power law has been widely used to express stress-strain relationship for viscoelastic materials.

2.6.3   Kohlrausch -Williams-Watts (KWW) Relation

The initial (for small strains) stress-strain behavior of polymers can be described by the classical viscoelasticity theory. In the linear viscoelastic region, the strain, ε, evolution with time can be obtained from Boltzmann superposition principle. For the case of creep, the total strain may be expressed by

$$\varepsilon(t) = \int_{-\infty}^{t} D(t-\tau)d\sigma \qquad \text{(Equation 29)}$$

For systems with single retardation time τ, the creep compliance, D, is given by

$$D(t) = D_0[1 - \exp(-t/\tau)] \qquad \text{(Equation 30)}$$

where D_0 is the initial creep compliance.

Real systems are characterized by a distribution of characteristic times. A simple empirical equation based on the KWW stretched function can be used to express the exponential growth of the creep compliance, and the creep compliance is given by

$$D(t) = D_0[1 - \exp(-t/\tau_c)^{\beta_c}] \qquad \text{(Equation 31)}$$

where β_c takes values between 0 and 1. It quantifies the degree of retardation time distribution; the KWW function implies a spectrum of retardation times whose breadth is related to β_c. τ_c is the mean retardation time of the retardation spectrum.

2.6.4   Schapery Integral Representation

In general, creep compliance is defined as the time dependent strain per unit stress during a creep experiment. It is expressed as

$$D(t) = \frac{\varepsilon(t)}{\sigma} \qquad \text{(Equation 32)}$$

The nonlinear viscoelastic constitutive equation derived by Schapery [9-11] has the advantage of having a single time-integral form, even in the nonlinear region. The stress-strain relation of this model is expressed as

$$\varepsilon(t) = g_0 D_0 \sigma + g_1 \int_0^t \Delta D(\psi - \psi') \frac{dg_2 \sigma}{d\tau} d\tau \qquad \text{(Equation 33)}$$

Where D_o and $\Delta D(\psi)$ are defined as initial and transient components of the creep compliance, g_0, g_1, and g_2 are the stress and temperature dependent material parameters.

The total linear viscoelastic compliance is given by

$$D(\psi) = D_0 + \Delta D(\psi) \qquad \text{(Equation 34)}$$

Where D_o represents the elastic value and $\Delta D(\psi)$ represents the time dependent portion of the compliance.

The function $\Delta D(\psi)$ is called the "master curve" and is commonly presented as the log of the transient compliance as a function of the log of "reduced time" ψ. The reduced time ψ is a critical parameter in any viscoelastic characterization and is defined symbolically as:

$$\psi \equiv \int_0^t \frac{dt'}{a_\sigma} \qquad \text{and} \qquad \psi' \equiv \psi(\tau) \equiv \int_0^\tau \frac{dt'}{a_\sigma} \qquad \text{(Equation 35)}$$

Where a_σ is a temperature dependent shift factor.

Substituting a constant stress σ into Eq. 33; $dg_2\sigma/dt=0$ and Eq. 34 gives

$$\varepsilon(t) = g_0 D_0 \sigma + g_1 g_2 \Delta D\left(\frac{t}{a_\sigma}\right) \sigma \qquad \text{(Equation 36)}$$

The time dependent creep function can be written as a power law

$$\Delta D(\psi) = C_1 \psi^n \qquad \text{(Equation 37)}$$

This gives

$$\varepsilon_c(t) = g_0 D_0 \sigma + \frac{C_1 g_1 g_2}{a_\sigma^n} t^n \sigma \qquad \text{(Equation 38)}$$

Equation 38 has a number of unknown parameters, so that additional information is needed to obtain all parameters. The initial condition is at small strain levels where Schapery equation becomes identical to the known linear viscoelastic creep equation ($g_0 = g_1 = g_2 = a_\sigma = 1$).

Schapery derived another expression for the recovery strain [10]

$$\varepsilon_r(t) = \frac{\Delta \varepsilon_a}{g_1} [(1 + a_\sigma \lambda)^n - (a_\sigma \lambda)^n] \qquad \text{(Equation 39)}$$

Where $\Delta\varepsilon_a$ is the strain before unloading at t_a and λ is the reduced time $(t-t_a)/t_a$.

Creep and recovery strains in Eqs 38 and 39 can be rewritten as

$$\varepsilon_c(t) = \varepsilon_0 + \Delta\varepsilon_1 t^n \qquad \text{(Equation 40)}$$

$$\varepsilon_r(t) = A[(1 + a_\sigma \lambda)^n - (a_\sigma \lambda)^n] \qquad \text{(Equation 41)}$$

Where $\varepsilon_{0=}g_0 D_0 \sigma$ (the instantaneous strain after unloading), $\Delta\varepsilon_1 = \dfrac{C_1 g_1 g_2}{a_\sigma^n} \sigma$ (the transient strain), and $A = \Delta\varepsilon_a / g_1$ ($\Delta\varepsilon_a$ is the net strain at time just before unloading).

2.7. References

1. S Hambir, N Bulakh, P Kodgire, R Kalgaonkar, J Jog, *Journal. of Polym. Sci.: Part B: Polym. Phy.* ,**39**, 446–450 (2001)

2. J. Gilman , *Appl. Clay Sci.*, **15,** 31–49 (1999)

3. MJ Dumont, A Reyna-Valencia, JP Emond, M Bousmina, *Journal of Appl. Polym. Sci.* ,**103,** 618–625 (2006)

4. A Guide to IUPAC Nomenclature of Organic Compounds, Blackwell Scientific Publications, Oxford (1993)

5. J Kahovec, RB Fox, K Hatada, *Pure and Applied Chemistry,* **74,** 1921–1956 (2002)

6. O. Okada, H. Keskkula, D.R. Paul ", *Polymer*, **42,** 8715-8725 (2001)

7 . http:// pslc.ws/mactest/dsc.htm

8. J.J. Aklonis and W.J. MacKnight. *Introduction to Polymer Viscoelasticity*, John Wiley & Sons: New York (1983).

9. R Schapery, *Journal of Solids and Structures*,**2**, 407-425 (1966)

10. R Schapery, *Polymer Engineering and Science,* **9**,295-310 (1969)

11. R Schapery, *International Journal of Solids and Structure,***37**,359-366 (2000)

CHAPTER 3

NONLINEAR CREEP DEFORMATION IN POLYETHYLENE NANOCOMPOSITES:
EFFECT OF COMPOSITION OF ETHYLENE-PROPYLENE COPOLYMER ON
ROOM TEMPERATURE CREEP DEFORMATION

3.1. Introduction

Polymer nanocomposites are a class of materials composed of a polymeric matrix
in which fillers with nanoscale dimensions are embedded. The fillers improve the
physical and mechanical macroscopic properties of the nanocomposites dramatically.
Polymer nanocomposites show increased modulus, higher heat distortion temperature,
better barrier properties, and decreased thermal expansion coefficient [1, 2]. These
properties make them the material of choice in different applications such as the
construction of stratospheric balloons. However, because the application of polymer
nanocomposites can be limited by their poor dimensional stability, knowledge of the
creep resistance of polymer nanocomposites over a long period of time is of great
interest. The importance of creep resistance in polymers is underscored both in thick
sample geometries in automotive applications and in thin films (0.01 mm) for use in
scientific balloon applications. Balloons experience harsh stratospheric conditions that
require a material with good ductility. Balloons are made of thin polymeric films (10- to
20-μm thickness) [3,4] with a number of properties, including low permeability, high
toughness, and structural stability.

The mechanical properties of polyethylene (PE) nanocomposites have been
studied by many researchers [5-7]. Liang et al. [6] studied the mechanical properties of

PE- montmorillonite layered silicate (MLS) nanocomposites compatibilized with maleated polyethylene and found that increasing the content of maleated PE with a silicate modified by a cationic surfactant could enhance the extent of intercalation. A maximum increase in mechanical properties was achieved when a combination of 6 wt% maleated PE and 3 wt % MLS was used. Wang et al. [8] investigated exfoliation and intercalation in maleated PE/clay nanocomposites prepared by melt compounding. In their investigation, the nanocomposites were completely exfoliated, and the mechanical properties were dramatically improved when the PE had a higher grafting level of MA than the critical level of 0.1%. A clay weight fraction of 5 wt % was used. Quintanilla et al. [9] studied the effect of maleated polypropylene (PP) content on the mechanical properties of PP nanocomposites. They found that clay dispersion and interfacial adhesion are strongly affected by maleated PP content. The increase in content of polar groups gave better interfacial adhesion and improved mechanical properties.

Creep resistance in nanocomposites can be ascribed to clay dispersion as well as matrix properties. Thus, variations in clay content, compatibilization by maleated PE, and the degree of dispersion are all parameters that affect creep [10-17]. Pegoretti et al. [11] studied the creep deformation of polyethylene terephthlate (PET) filled with 1, 3, and 5 wt % layered silicate. An increase of 30% in modulus was obtained at a clay loading of 5 wt%. The creep compliance decreased slightly with the addition of clay. This decrease suggests the beneficial effect of clay on the dimensional stability of the nanocomposite. Yang et al. [14] studied the tensile creep resistance of polyamide 66 nanocomposites with different filler shapes. The volume content of the nanoparticles was set to 1%. The creep

resistance of the nanocomposites was significantly enhanced by the nanoparticles without sacrificing the tensile properties. The improvement was attributed to the good dispersion of the surface-modified particles.

Previous work by our laboratory [18] studied the creep and tensile properties of semicrystalline LLDPE/maleated PE/MLS nanocomposite to determine the effect of semicrystalline maleated PE/MLS on room temperature creep. We showed synergistic increase in tensile strength and modulus. The highest increase in strength (35%) was obtained for the addition of 1% of both MLS and maleated PE. The results were attributed to the addition of maleated PE, which acted as a coupling agent between PE and MLS. The miscibility between PE and MLS was increased because of MA's polar nature. Non-linearity in creep behavior was analyzed by using the Burgers model. Diffraction analysis and optical microscopy showed more uniform dispersion in the maleated nanocomposite. Maleated nanocomposites showed lower retardation time. Since the maleated PE contributed to crystallinity, determining the influence of MLS separately from crystallinity changes was hindered. To demarcate the effect of the compatibilizer and its crystallinity, we use an amorphous maleated PE. We investigate the tensile and creep properties of this PE nanocomposite and correlate the synergistic improvement in properties to the addition of MLS and compatibilizer to the PE matrix.

3.2. Experimental

3.2.1. Materials

LLDPE DOWLEX™ 2056G (Dow chemical company) was used to prepare the PE nanocomposite films (density = 0.92 g/cc; Melt Index= 1.0 gm/10min). MLS (Cloisite 15A™), supplied by southern clay products, was used as the nanofiller. An amorphous maleic anhydride functionalized elastomeric copolymer (amEP); ExxonMobil Exxelor™ VA 1803 was used as a compatibilizer between the layered silicate and the PE matrix. Exxelor VA 1803 has a nominal density of 0.86 g/cm3 and a melt index of 3 g/10 min (ASTM D1238, 230 $^{\circ}$C, 2.16 kg). The MA level is in the range of 0.5% to 1%.

3.2.2. Sample Preparation

Seven different batches with different concentrations of MLS and amEP were prepared. The compositions of the different batches are displayed in Table 3.1. The effects of amEP and MLS were individually investigated through addition of these individual components to the PE matrix. One batch of the PE nanocomposites was made without addition of amEP (1% MLS). Another had amEP alone (1% amEP). Four separate batches were made with different amEP: MLS ratio to investigate the combined effects of amEP and MLS. The effects of the combined amEP + MLS systems were investigated by preparing blends having 1:1 1:2, 2:1, and 2:2 of amEP:MLS. Also to study the effects of MLS on amEP, blends of amEP with 1% and 3% MLS were included in this study.

In order to achieve dispersion of MLS in the PE matrix, MLS and the amEP were simultaneously compounded with the base PE matrix. Since MLS exhibits affinity to

43

moisture, it was dried for 48 hours in a forced air convection oven at 60ºC prior to compounding. All samples were compounded with a Haake TW100 twin-screw extruder with a temperature profile of 200, 200, 205, and 210 ºC for zones 1 to 4. PE films 1.5 mil (0.04 mm) thick were processed with a Killion single-screw extruder (L/D = 24:1), fitted with a dual-lip air ring and a die diameter of 50 mm (2 inches)

Sample	LLDPE (wt %)	Exxelor VA 1803 (wt %)	MLS (wt %)
LLDPE	100	0	0
PE/MLS 1	99	0	1
PE/amEP 1	99	1	0
PE/amEP 1/MLS 1	98	1	1
PE/amEP 1/MLS 2	97	1	2
PE/amEP 2/MLS 1	97	2	1
PE/amEP 2/MLS 2	96	2	2
amEP	0	100	0
amEP/MLS 1	0	99	1
amEP/MLS 3	0	97	3

Table 3.1. Summary of concentrations used.

3.2.3. X-Ray Diffraction (XRD)

XRD was conducted on a Rigaku X-ray generator (Cu Kα radiation with λ = 0.15406 nm) at room temperature. The diffractograms were scanned between 2θ ranges of 1 to 10 ^{o} at 2 ^{o}/min with a 0.03 step size.

3.2.4. Focused Ion Beam/Scanning Electron Microscopy (FIB/SEM)

A high-resolution focused ion beam/scanning electron microscope (FIB/SEM) (FEI Nova 200 dual-beam FIB/field emission gun SEM) was used to observe the

dispersion of MLS. A section of 30 μm $\times$ 15 μm $\times$ 5 μm was created by the Ga+ ion source using an ion beam of 1 nA at 30 kV of accelerating voltage. The section was imaged by using an electron beam of 1.7 nA at 30 kV of accelerating voltage.

3.2.5. Differential Scanning Calorimetery (DSC)

The thermal behavior of the samples was characterized with a Perkin Elmer DSC with Pyris software. The DSC was calibrated with indium as a reference. Sample weights of 5 to 10 mg were tested. The temperature was ramped at 10 $^{\circ}$C /min in a range of 30 to 150 $^{\circ}$C. Melting and crystallization temperatures were calculated.

3.2.6. Tensile Testing

Yield stress, ultimate tensile strength, and elastic modulus E were determined by using a rheometric solids analyzer (RSA III) by TA instruments, Inc. (New Castle, DE, USA) films fixture with an extension rate of 0.208 mm/min. The mean sample dimensions are 5 mm $\times$ 25 mm with a mean thickness of 40 μm. Five samples were tested as described by ASTM D882 (standard test method for tensile properties of thin plastic sheeting).

3.2.7. Creep Testing

Uniaxial tensile creep tests were performed by using RSA III with films attachment using the same sample geometry as that for tensile tests. The desired constant stress to be applied for each measurement was calculated to be 50% of the yield stress for the corresponding material. The constant stress was applied for 1 hour of loading

followed by 1 hour of unloading. A linear displacement transducer with a force capacity of 35 N was used to monitor the strain during the experiment.

3.3. Results and Discussion

3.3.1. Dispersion of MLS in the LLDPE Matrix

The XRD patterns of LLDPE and am/PE/MLS nanocomposites are shown in Figure 3.1. The MLS used in this study has three characteristic peaks at $2\theta = 2.9\ ^{o}$ (001), $4.5\ ^{o}$ (002), and $7.3\ ^{o}$ (003). The (001) reflection corresponds to a d-spacing of 2.99 nm using the Bragg equation. The results are tabulated in Table 3.2.

Sample	MLS, 2θ (001)	d (nm)	PE, 2θ (110)	FWHM, MLS (001)	Particle size (nm)	FWHM, PE (110)	Lamella size (nm)	Average plate thickness from SEM (nm)	No. of plates (plate thickness/d spacing)
MLS	2.95	2.99	-	0.81	9.83	-	-	-	-
LLDPE	-	-	20.76	-	-	0.46	18.48	-	-
PE/MLS 1	2.71	3.25	20.7	0.72	11.05	0.42	20.24	24±4	6-9
PE/amEP 1	-	-	20.56	-	-	0.46	18.46	-	-
PE/amEP 1/MLS 1	2.44	3.62	20.66	0.63	12.63	0.44	19.31	12±4	3-6
PE/amEP 1/MLS 2	2.94	2.99	20.43	0.64	12.44	0.42	20.20	35±5	11-14
PE/amEP 2/MLS 1	3.19	2.76	20.42	0.46	17.31	0.45	18.85	28±2	8-10
PE/amEP 2/MLS 2	3.16	2.79	20.44	0.44	18.10	0.42	20.20	35±5	9-12

Table 3.2. Values of 2θ and d for LLDPE/amEP/MLS nanocomposites.

When MLS is introduced into PE, a slight drop in 2θ occurs from 2.95 °C to 2.71, which corresponds to an increased d-spacing from 3 to 3.25 nm. In contrast, when the MLS is added to the amEP, a complete annihilation of the (001) peak occurs for the 1% and 2% samples. The intercept at $\theta = 2°$ increases substantially when 3% MLS is present,

indicating that more MLS does correspond to a lower degree of exfoliation and a possible intercalated-exfoliated dispersion. The nominal particle thickness was estimated to be 9.8 and 11 nm. These values were calculated from the full width half maximum (FWHM) determined from the instrument software for the (001) MLS peak using the Debye-Scherer equation: $D = 0.9*\lambda/B \cos\theta$, where B is the fwhm in radians, λ is the x-ray wavelength (0.15418 nm for Cu-K_α radiation), and θ is the diffraction angle. A PE/amEP with 1% amEP was compounded, and 1% and 2% MLS were added to the matrix (PE/amEP1/MLS1 and PE/amEP1/MLS2, respectively).

As can be seen, the 2θ value for (001) reflection for the 1% MLS compound shifted from 2.95 for pure MLS to 2.44 for the PE/amEP1/MLS1 and remained at 2.94 for PE/amEP1/MLS2. This shift corresponds to an increase in d-spacing from 2.99 to 3.62 in PE/amEP1/MLS1 and no change for PE/amEP1/MLS2. This indicates that increased MLS content for the same PE: amEP ratio results in decreased interaction between the MLS and the matrix.
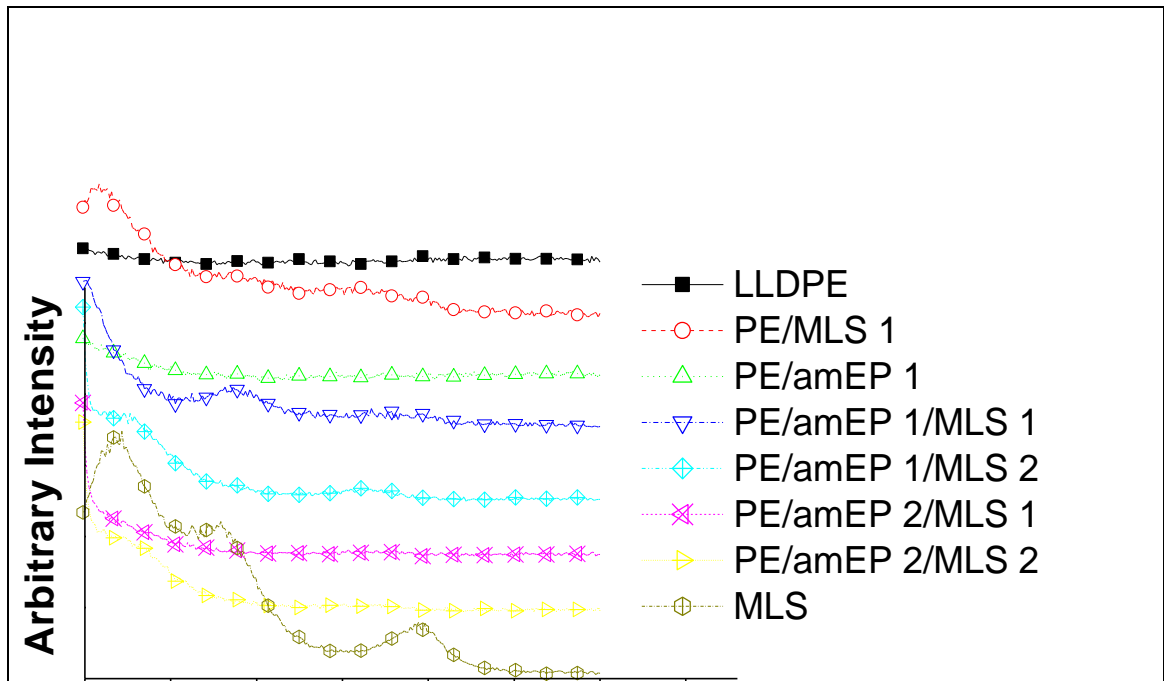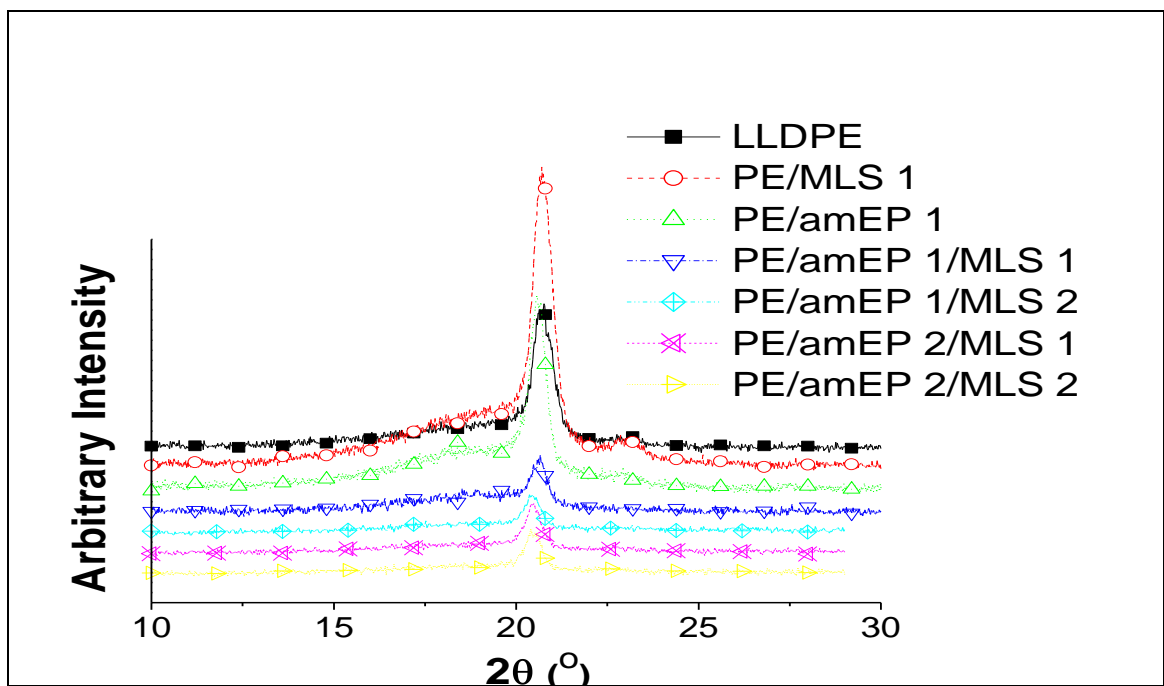
Figure 3.1. XRD patterns of LLDPE and amEP/MLS nanocomposites: (a) MLS (001) reflections, (b) PE (110) reflections.

It was then examined whether enhanced amEP presence would improve dispersion by comparing a PE/amEP with 2% amEP added. Both 1% and 2% MLS were added to this compound (PE/amEP2/MLS1 and PE/amEP2/MLS2, respectively). For both these samples, the 2θ peak shifts to the right, indicating a decreased d-spacing. The decrease in d-spacing has been observed in other polymer systems [19-20]. The decrease can been related to a collapse of the intergallery chains of the surfactant (dimethyl, dehydrogenated tallow, quaternary ammonium) between the MLS plates and a transition from pendant bilayers to a lateral monolayer.
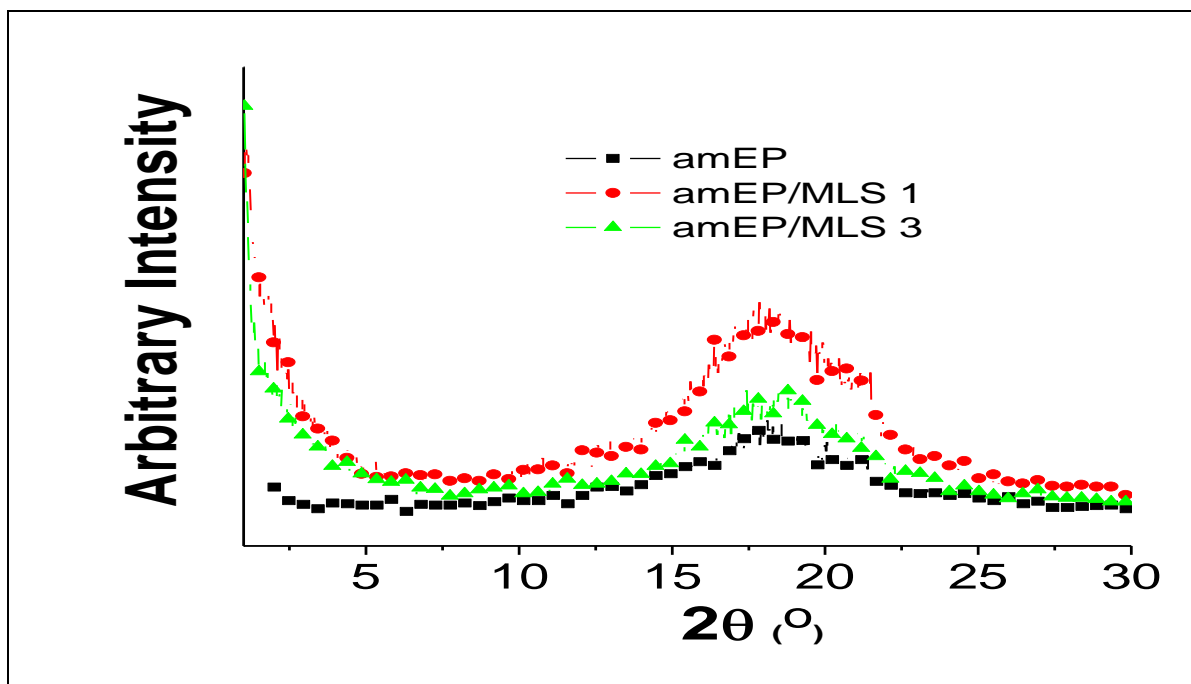
Figure 3.2. XRD patterns of amEP/MLS nanocomposites showing amEP amorphous halo.

The FIB/SEM images of LLDPE nanocomposites in Figure 3.3 show good dispersion of the stacked platelets. The d spacing of the MLS is 2.99 nm. The average thickness of the platelets for LLDPE with 1% MLS is 24 ± 4 nm (determined with FEI Nova software). This thickness indicates that six to nine plates are stacked together. The addition of 1% amEP reduces the average thickness to 12 ± 4 nm. This reduction in thickness is an indication that three to six plates are stacked together. The number of stacked platelets increases for the addition of 2% MLS while keeping the amEP at 1%.

The same increase is observed for the addition of 1% and 2% MLS with 2% amEP into LLDPE. The average distance between these stacked platelets is 200 ± 50 nm for the PE with MLS alone, 300 ± 50 nm for the LLDPE/1% amEP/1% MLS, 250 ± 50 nm for the LLDPE/1% amEP/2% MLS, 350 ± 50 nm for the LLDPE/2% amEP/1% MLS, and 300 ± 50 nm for the LLDPE/2% amEP/2% MLS nanocomposite. Thus, it can be inferred that while platelet stacking continues, the dispersion of the stacks within the matrix material is significant and enhanced by the presence of amEP. Figure 3.4 shows the good dispersion obtained for the addition of 1 and 3% MLS into amEP which further confirms the synergistic effect of adding amEP into the bulk PE matrix.

The results of dispersion indicate that PE/amEP1/MLS1 provides maximum dispersion and extent of intercalation in the system.

(a)

(b)

mag	WD	HV	tilt	
100 020 x	5.4 mm	5.00 kV	52 °	1 μm

(c)

mag	WD	HV	tilt	
80 000 x	5.8 mm	5.00 kV	52 °	1 μm

(d)

mag | WD | HV | tilt
80 000 x | 5.3 mm | 5.00 kV | 52 °
1 μm
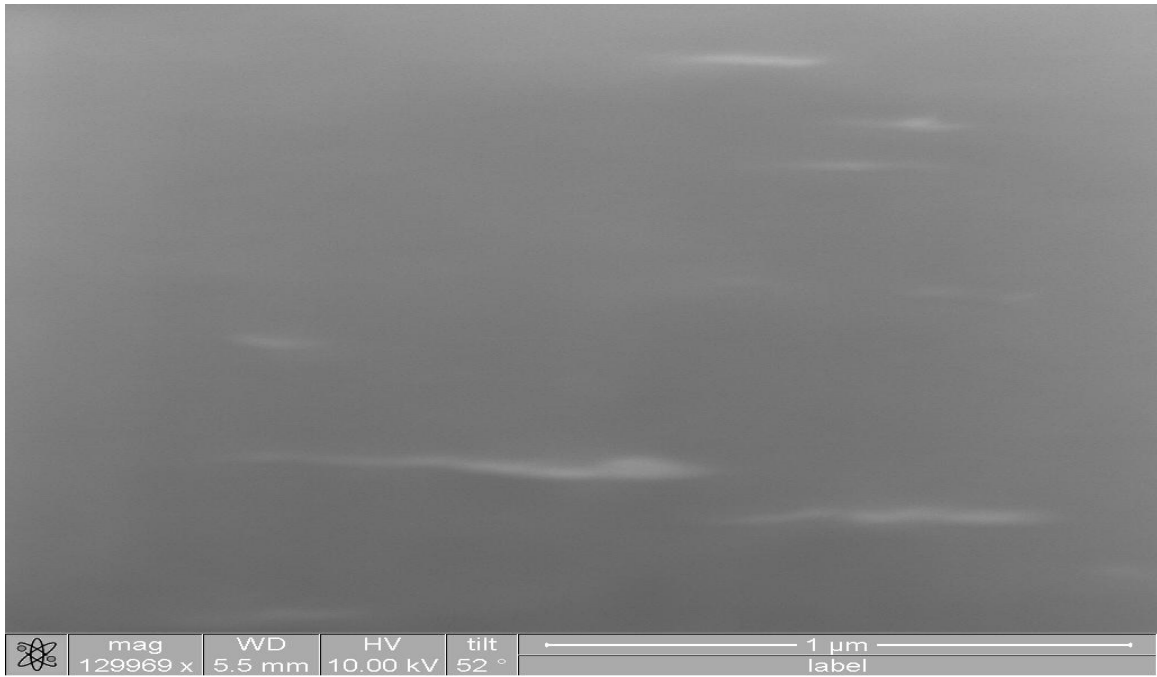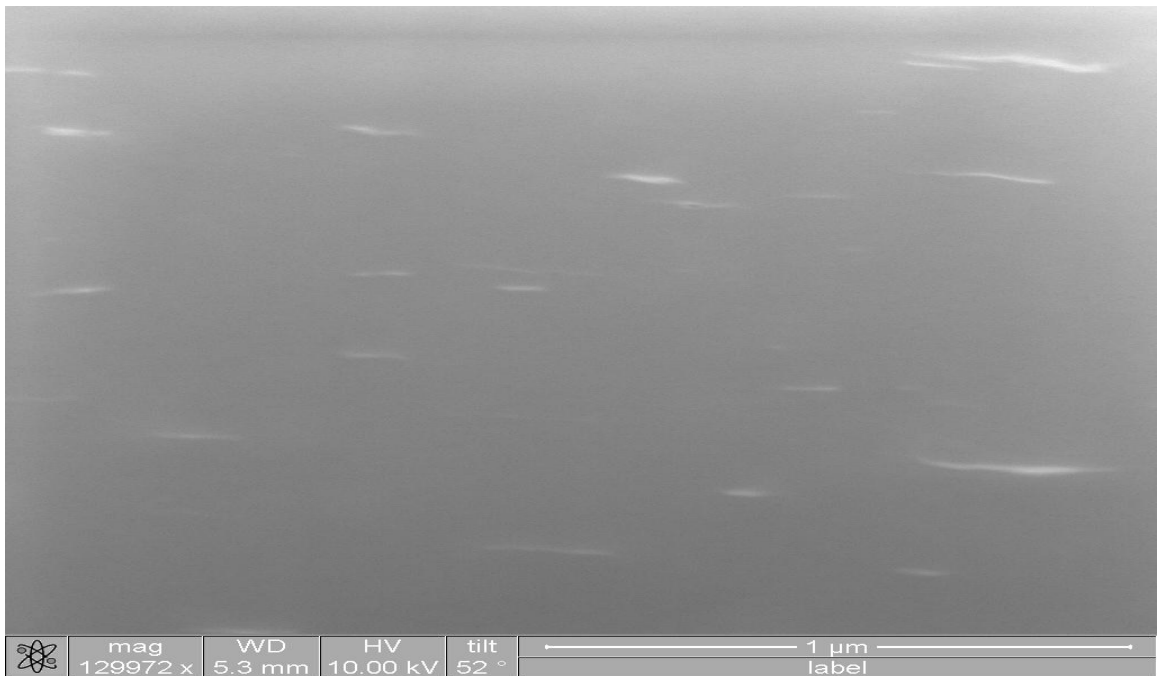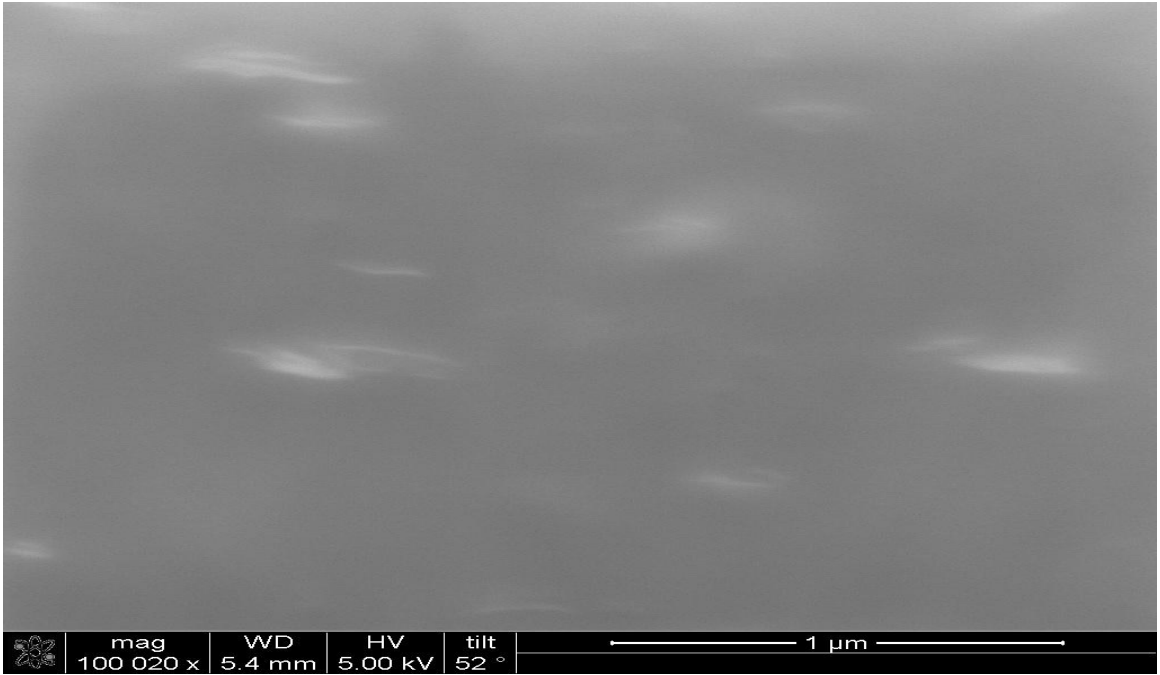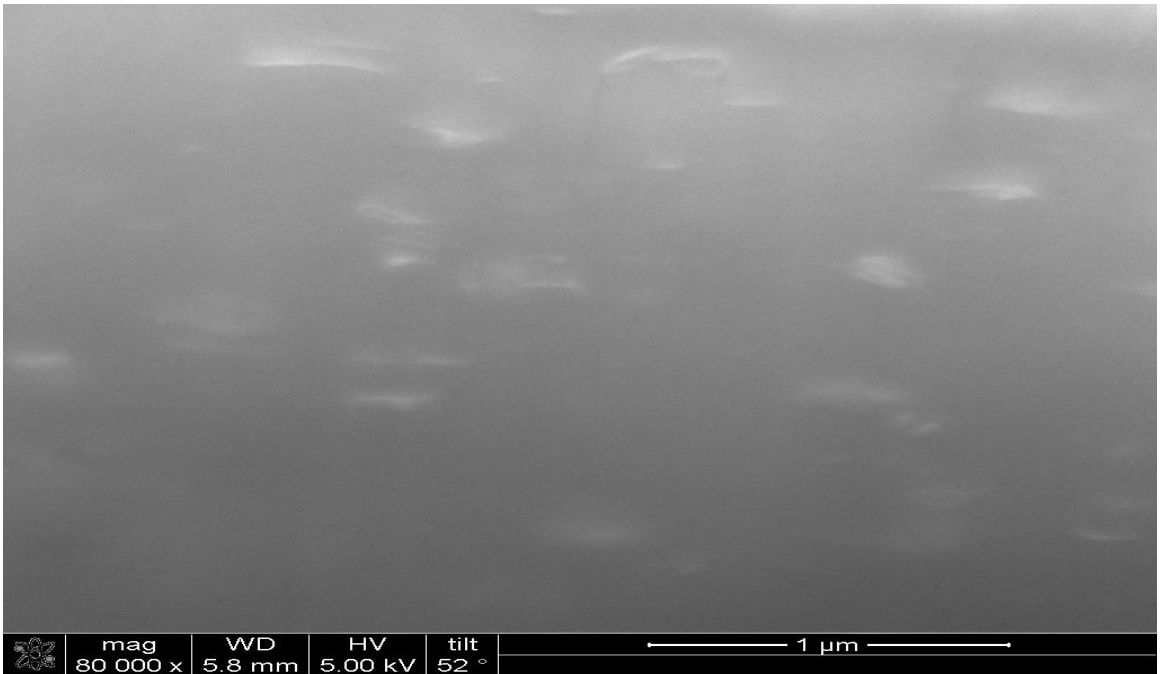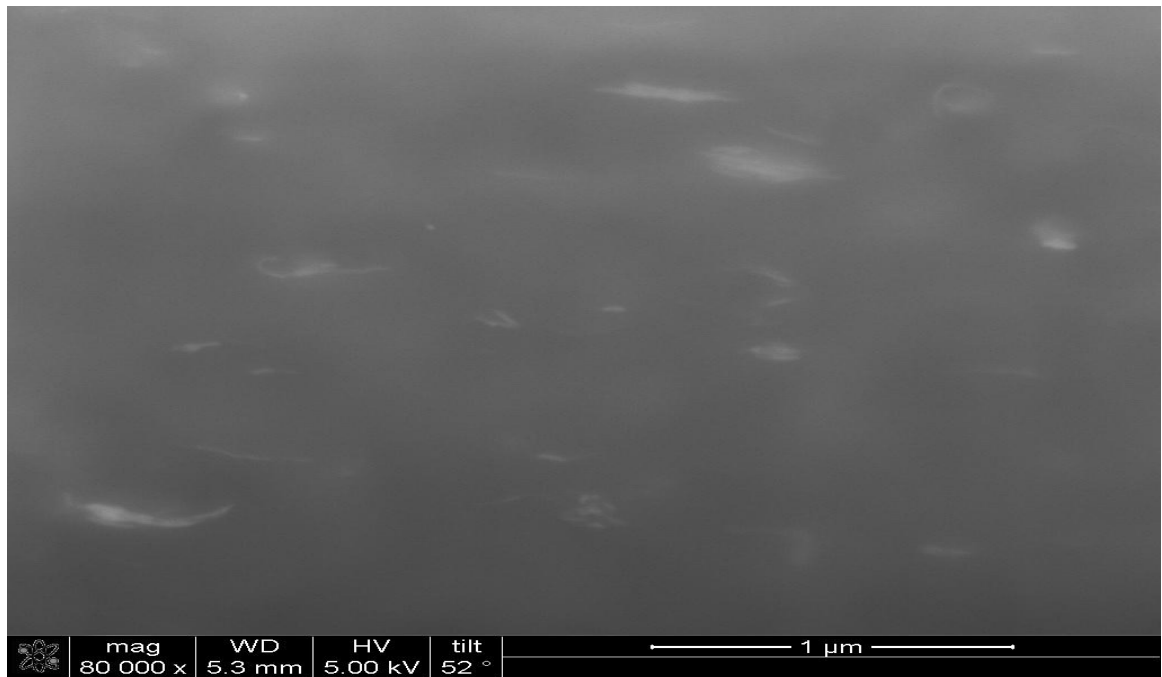
(e)

Figure 3.3. FIB/SEM images of (a) LLDPE/1% MLS nanocomposite, (b) LLDPE/1% amEP/1% MLS, (c) LLDPE/1% amEP/2% MLS, (d) LLDPE/2% amEP/1% MLS, and (e) LLDPE/2% amEP/2% MLS nanocomposites.
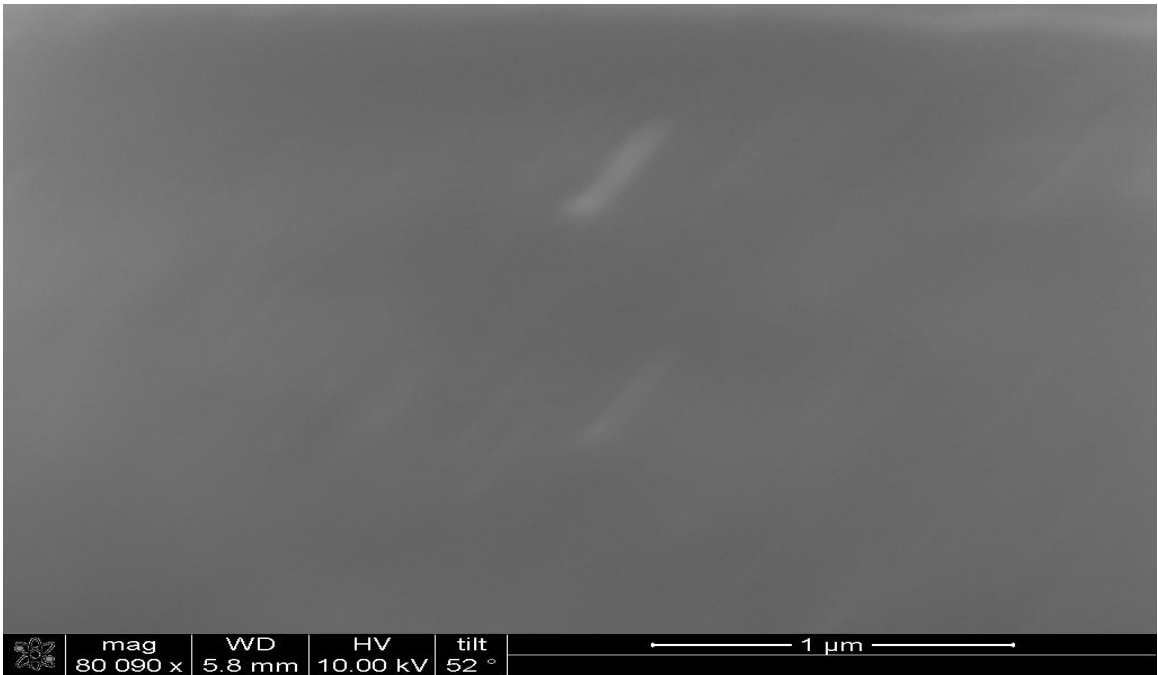
(a)
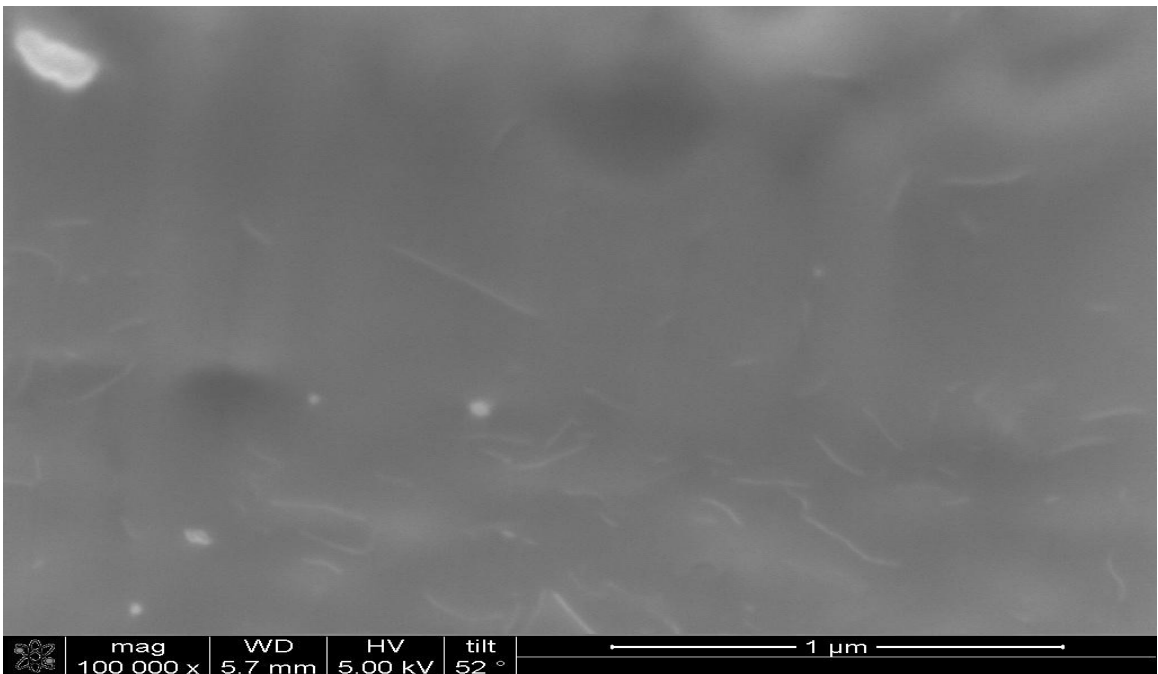
(b)

Figure 3.4. FIB/SEM images of (a) amEP /1% MLS nanocomposite, (b) amEP/ 3% MLS.

3.3.2. Crystallization Effects

Crystallization was probed by examining both the XRD peaks of the PE and the DSC heating and cooling thermograms. XRD results are shown in Figures 3.1 and 3.2. The (110) reflection of PE is analyzed in Table 3.1.

As it can be seen, the 2θ values for the (110) reflections of PE are not affected by the variations in the PE: amEP ratio or the extent of MLS present in the composites. The amEP results indicate an amorphous halo corresponding to a peak of 18° 2θ. The lamella thicknesses, however, are affected. When MLS is introduced into PE, a decrease in FWHM from 0.46 to 0.42 corresponds to an increase in lamella thickness from about 18 to 22 nm. Blending amEP into PE shows no impact on lamella thicknesses. The PE/amEP with 1% amEP was compounded, and 1% and 2% MLS were added to the matrix (PE/amEP/MLS1 and PE/amEP/MLS2, respectively). These compositions showed an increase in lamella thickness with MLS concentration with its being 19 and 20 nm as the MLS concentration increased from 1% to 2%. Increased maleation served to show similar trends in crystalline lamella. That is, PE/amEP2/MLS1 and PE/amEP2/MLS2 had the same changes in lamella thicknesses as PE/amEP1/MLS1 and PE/amEP2/MLS1 did. It can be thus concluded that MLS had a small effect on the PE crystallization but that amEP was not a participant in either the 2-part or 3-part compounds. These results were complemented by the DSC results.

Figure 3.5 shows the DSC results of the neat LLDPE films and the nanocomposites. The melting temperature (T_m), enthalpy of melting (ΔH_m), melt crystallization temperature (T_{mc}), enthalpy of melt crystallization (ΔH_{mc}), and the

percentage of crystallinity (X_C) were obtained from the second heating and cooling thermograms and are summarized in Table 3.3.
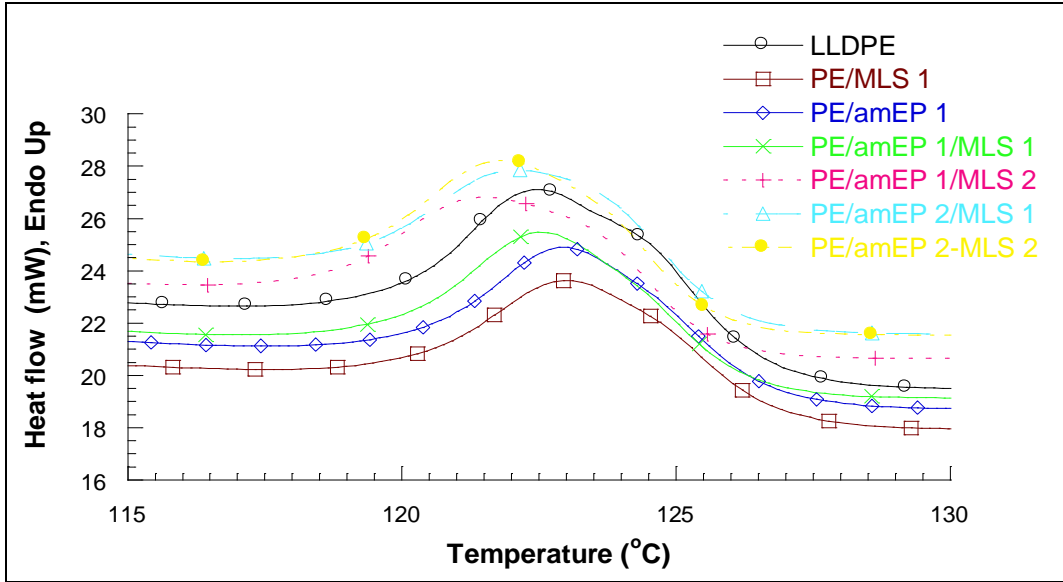
(a)
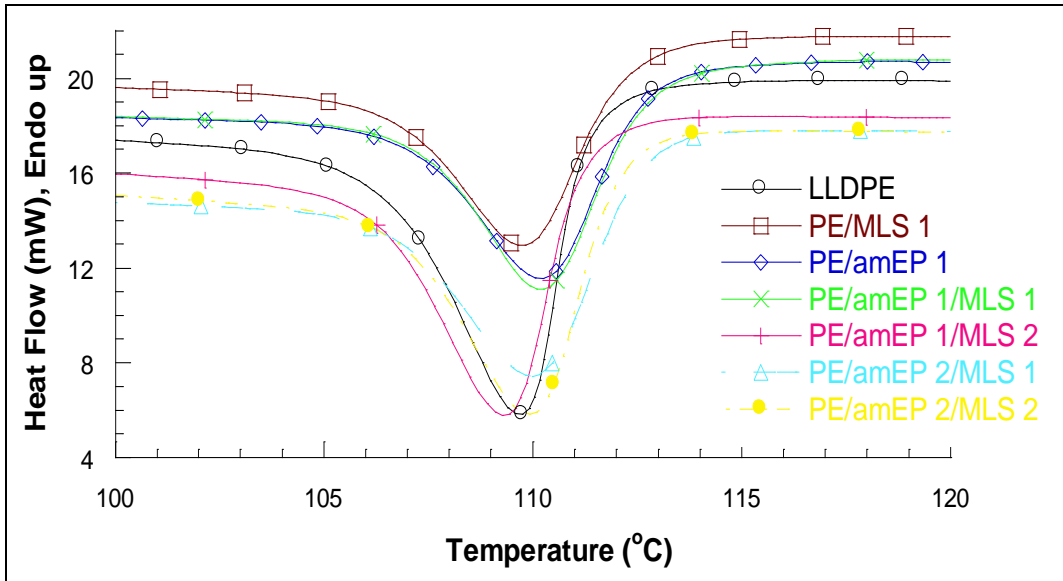
(b)
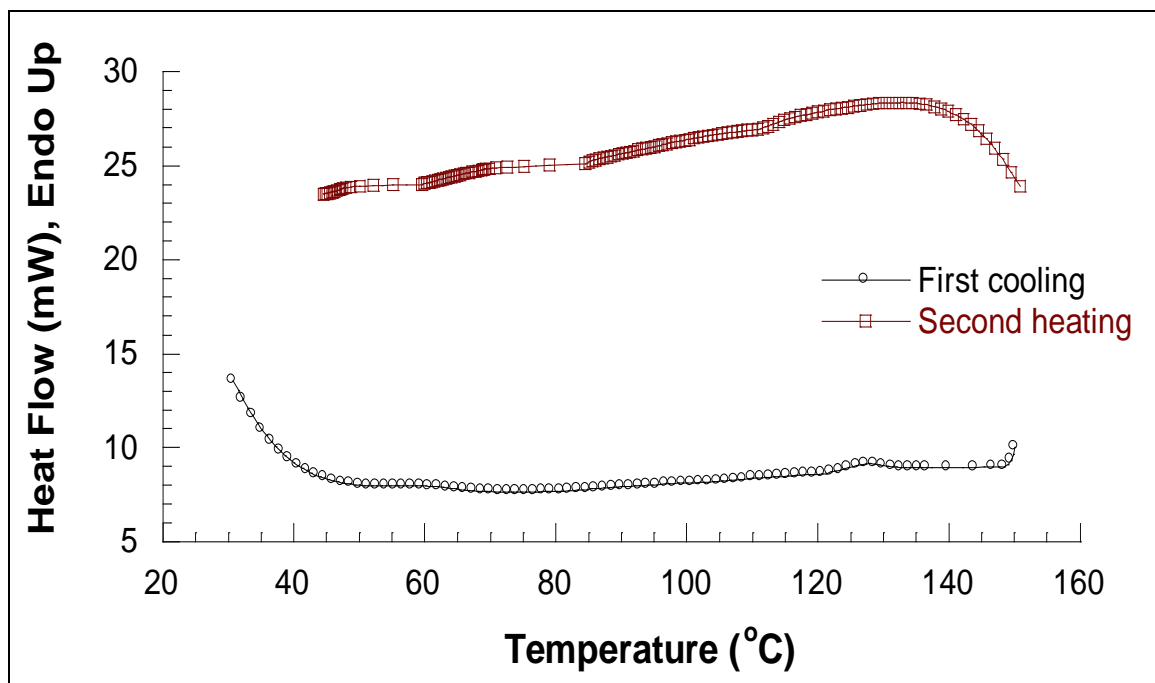
(c)

Figure 3.5. DSC thermograms: (a) second heating; (b) first cooling of
LLDPE/amEP/MLS nanocomposites; (c) second heating and first cooling of amEP.

Sample	Melting temperature (^{o}C)	Crystallization temperature (^{o}C)	ΔH_m (J/g)	ΔH_{mc} (J/g)	X_C (%)
LLDPE	122.6	109.8	128.5	85.0	44.0
PE/MLS 1	123.0	110.0	127.1	86.0	43.4
PE/amEP 1	123.1	110.2	124.9	88.3	42.6
PE/amEP 1/MLS 1	122.5	110.3	123.9	89.0	42.3
PE/amEP 1/MLS 2	121.6	109.3	130.5	88.0	44.5
PE/amEP 2/MLS 1	122.2	110.0	129.6	85.3	44.2
PE/amEP 2/MLS 2	122.0	109.9	131.4	84.3	44.8

Table 3.3. DSC results for LLDPE nanocomposites.

LLDPE shows an endothermic T_m at around 122.6 ^{o}C, corresponding to its
crystalline phase, and an enthalpy of melting of 128.5 J/g. No change in T_m was
observed, whereas ΔH_m changed. In fact, the enthalpies of melting indicate that when

amEP and MLS are individually added to PE, the enthalpies of melting are lower than that of the nanocomposite containing both additives. This change indicates a smaller distribution of crystallite sizes for these nanocomposites.

The cooling thermogram of the neat LLDPE shows an exothermic peak at around 109.8 $^{\circ}$C, which corresponds to T_{mc} and a melt crystallization enthalpy of 85 J/g. T_{mc} stayed the same, whereas ΔH_{mc} changed. Indeed, the enthalpy of crystallization shows a small increase when MLS and amEP were added separately and in combination at ratios of 1:1 and 1:2 (amEP: MLS). A decrease in ΔH_{mc} was observed in the nanocomposites having amEP and MLS ratios of 2:1 and 2:2.

The degree of crystallinity of the neat LLDPE and the nanocomposites was calculated according to the relation $X_c = \Delta H_m/\Delta H_{mo}$, where ΔH_{mo} is the equilibrium heat of fusion of PE which was taken as 293 J/g [16]. The overall crystallinity does not change, which suggests that MLS does not act as a nucleating site in the LLDPE matrix and negates the possibility that increased crystallinity could be responsible for the improved mechanical properties.

3.3.3. Tensile Stress-Strain Results

A stress-strain curve of LLDPE nanocomposites at room temperature is shown in Figure 3.6. The tensile properties, which include yield stress and Young's modulus, are tabulated in Table 3.4. The decreased crystallinity of the PE resin used in this study is reflected in the modulus value of 0.12 GPa compared to the value of 0.58 GPa previously reported [16].
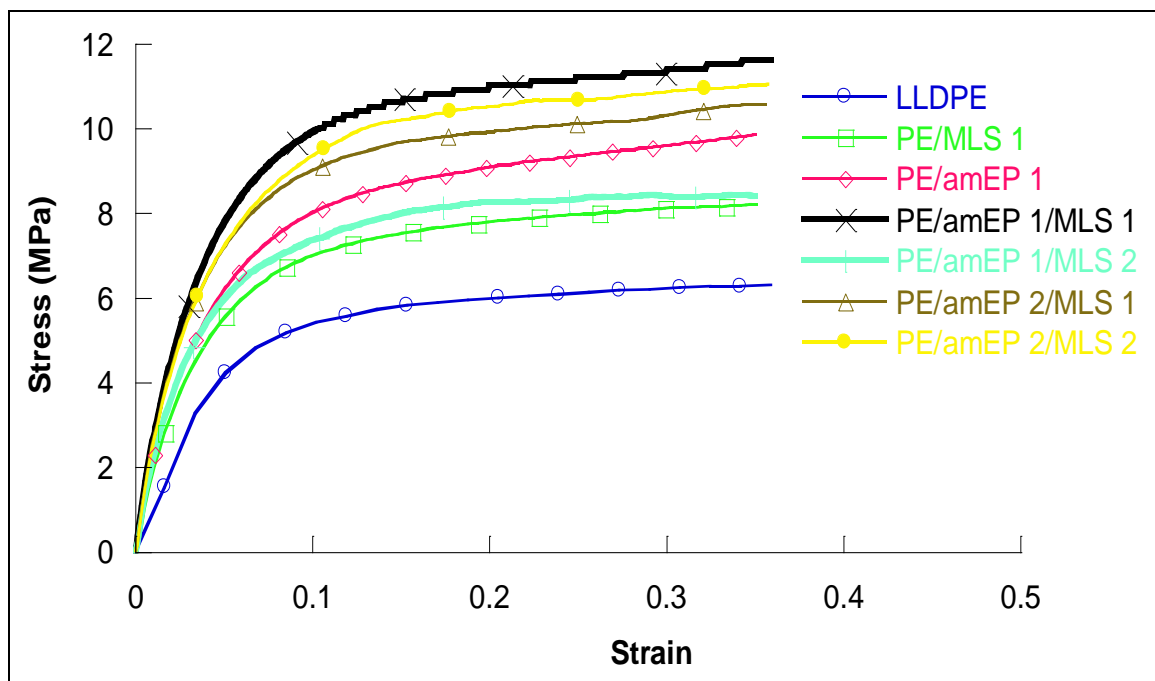
Figure 3.6. Stress-strain curve of LLDPE nanocomposites at room temperature.

Sample	Yield stress (MPa)	Elastic modulus E (GPa)
LLDPE	4.86 ± 0.09	0.12 ± 0.02
PE/MLS 1	5.12 ± 0.10	0.18 ± 0.03
PE/amEP 1	5.61 ± 0.11	0.22 ± 0.03
PE/amEP 1/MLS 1	6.92 ± 0.13	0.32 ± 0.04
PE/amEP 1/MLS 2	5.51 ± 0.11	0.16 ± 0.02
PE/amEP 2/MLS 1	6.41 ± 0.12	0.25 ± 0.03
PE/amEP 2/MLS 2	6.75 ± 0.13	0.24 ± 0.03
amEP	0.325 ± 0.006	0.09 ± 0.02
amEP/MLS 1	0.362 ± 0.006	0.12 ± 0.02
amEP/MLS 3	0.429 ± 0.008	0.17 ± 0.02

Table 3.4. Tensile test results of LLDPE nanocomposites.

There is a noticeable increase in yield stress and elastic modulus when MLS is added to the PE matrix (Figure 3.6). The addition of 1% amEP resulted in an 80% increase in elastic modulus, whereas the addition of 1% MLS caused an increase of 50%. Adding 1% amEP/2% MLS, 2% amEP/1% MLS, and 2% amEP/2% MLS in LLDPE caused increases of 33, 108, and 100% in modulus, respectively. The highest increases in elastic modulus (166%) are for samples in which a combination of 1% amEP and 1% MLS is used. The yield stress values follow the same trends as observed in the elastic modulus. The yield stress increased from 4.86 MPa for neat PE to 6.92 MPa for the LLDPE/1% and amEP/1% MLS. The yield stress and modulus of 1% amEP/2% MLS, 2% amEP/1% MLS, and 2% amEP/2% MLS into LLDPE also shows a significant increase compared to the neat PE. This increase indicates the combined effect of amEP and MLS, which is distinct from a previous report [18] in the positive impact that amEP has on the PE matrix.

Figure 3.7 shows the effect of adding MLS to the amEP in an approach to separate the effect of adding MLS and the amEP in combination and separately to the LLDPE matrix. The addition of 1% MLS to amEP increases the yield stress and elastic modulus by 10% and 12 %, respectively. An increase of 35% and 90 % is observed with the addition of 3% MLS. The results, which are presented in Table 3.4, show that MLS has a similar effect on amEP and LLDPE, suggesting the significant role of MLS as an effective nanofiller in the LLDPE nanocomposites.

It is clear, therefore, that all maleated LLDPE nanocomposites show an increase in the tensile properties compared to the neat PE. The results also highlight the synergistic effect of adding amEP and MLS together.
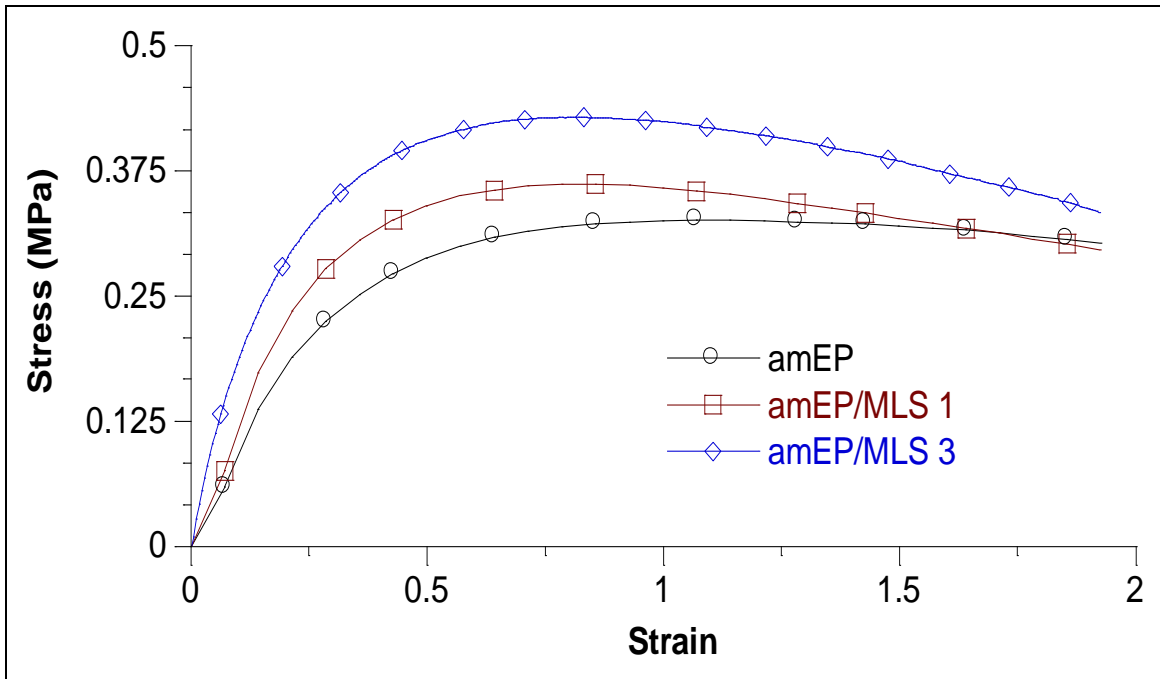
Figure 3.7. Stress-strain curve of amEP/MLS nanocomposites at room temperature.

3.3.4. Creep Response

Figure 3.8 shows the creep-recovery curves of LLDPE/amEP/MLS nanocomposites at room temperature. The stress level applied is 50% of yield stress. All samples showed an irrecoverable permanent deformation although the applied load was well within the linear region. When MLS is added, the creep compliance decreases and the material recovers more. This decrease can be explained by the addition of an elastic

component (MLS), which gives the matrix its stiffness (less creep) and elasticity (more recovery). The addition of the elastomeric amEP improves the recovery in the LLDPE/amEP blend. The creep compliance further decreases with the addition of 1% amEP/2% MLS, 2% amEP/1% MLS, and 2% amEP/2% MLS into LLDPE.
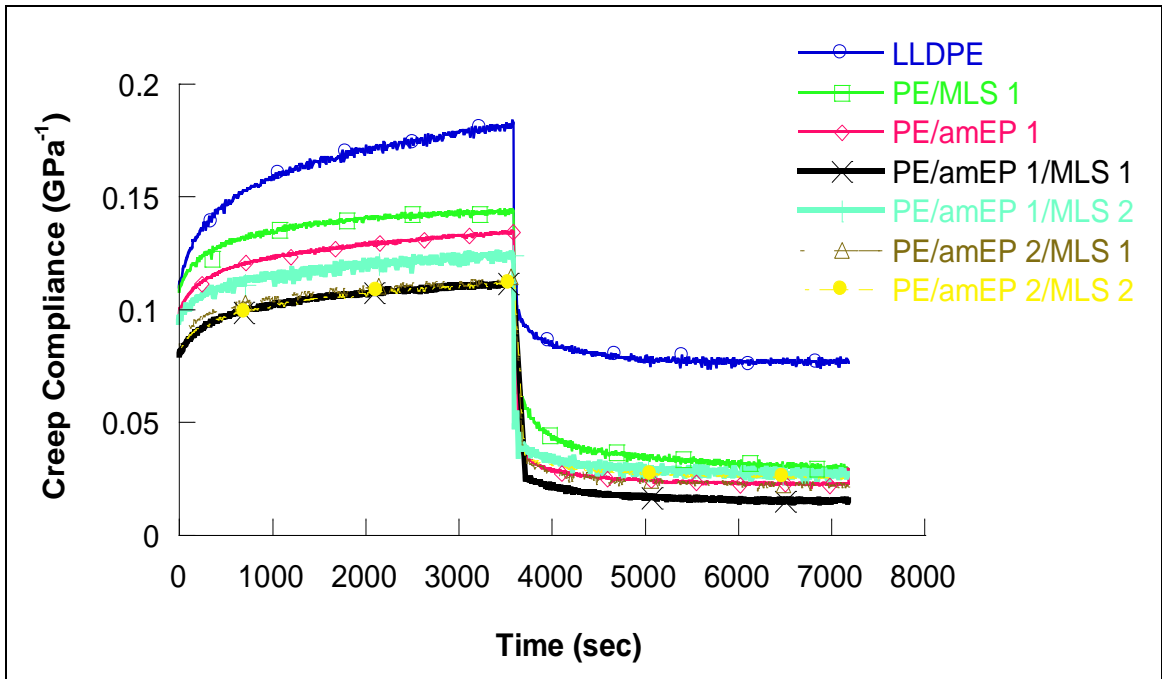
Figure 3.8. Creep-recovery curves of LLDPE/amEP/MLS nanocomposites at room temperature.

When a combination of 1% amEP and 1% MLS is added, the material shows the lowest creep compliance and the lowest unrecoverable deformation, as shown in Figure 3.8. This behavior mirrors the tensile test results in which LLDPE/1% amEP/1% MLS films show the highest yield stress and modulus (Table 3.4).

To study the effect of the different components on the viscoelastic response of LLDPE nanocomposites, 1% and 3% MLS were added to the amEP matrix. Figure 3.9 shows a creep-recovery plot of amEP/MLS nanocomposites. The addition of 1% MLS

causes amEP to have lower creep compliance, and the amount of recovery increases from 72% to 75%. Increasing the concentration of MLS to 3% further decreases the creep compliance, and the amount of recovery shows a noticeable increase to 85%. It is clear, then, that MLS improves creep resistance and acts as a damping material in both amEP and LLDPE nanocomposites.
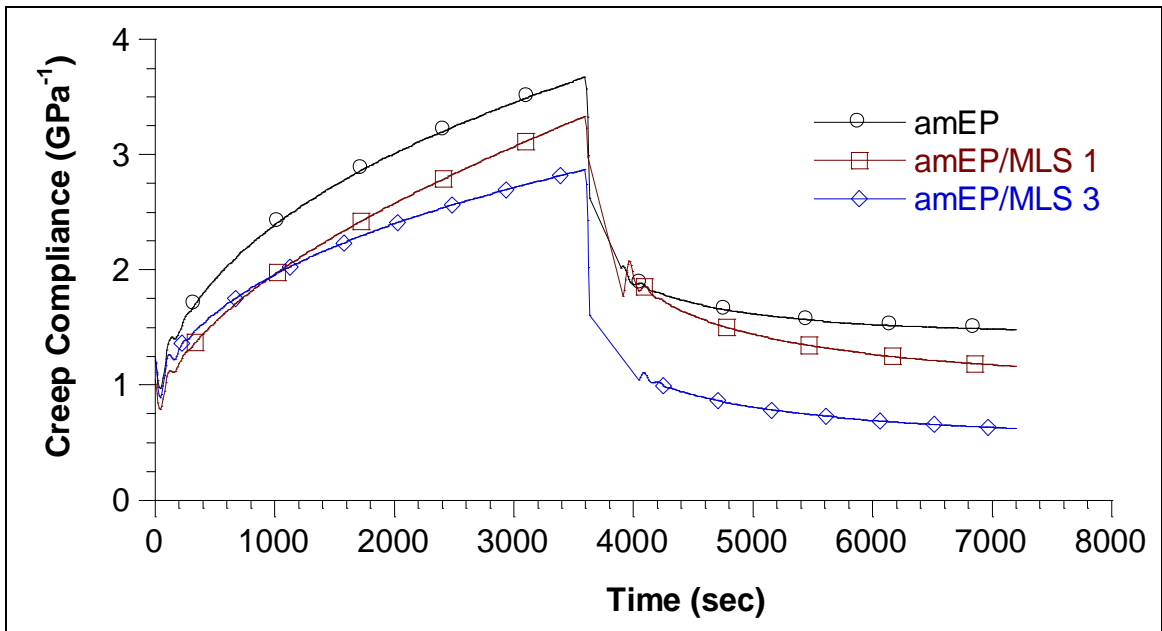
Figure 3. 9. Creep-recovery curves of amEP/MLS nanocomposites at room temperature.

These effects are shown by analyzing the recovery and creep curves and applying a Lai and Baker approach [21]. In linear viscoelasticity,

$$\varepsilon_c(t - t_a) = \varepsilon_r(t - t_a)$$

where ε_c and ε_r are the creep and recovery strains, respectively; and t_a is the time at unloading. The comparison between creep and recovery is shown schematically in Figure 3.10 with ε_p as the unrecovered plastic strain.
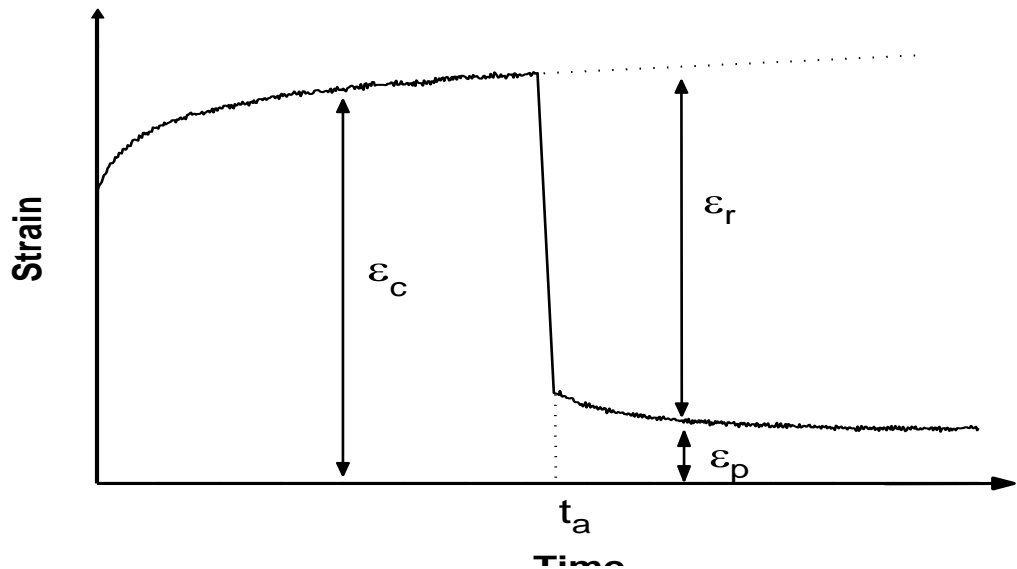
Figure 3.10. Creep-recovery schematic.

If the strain is completely recoverable after removal of the applied load, the recovered strain should coincide with the recovered strain from creep. However, if the material behaves in a non- linear viscoelastic manner, $\varepsilon_c(t-ta)$ doesn't coincide with $\varepsilon_r(t-ta)$ after the load is removed. Divergence of the creep strain from the creep strain shows that an irrecoverable plastic strain is produced by the applied load. Lai and Baker [21] applied this concept to high-density polyethylene (HDPE) at different low-stress levels.

Divergence of the creep strain from the recovered strain was observed for HDPE at low stress levels and was correlated to the strong non-linearity of the material. Drozdov and Christiansen [22] also predicted that viscoplasticity is restricted in polymer nanocomposites. They suggested that the applied load produces an irrecoverable plastic strain. Figure 3.11 shows the comparison of creep and recovery compliance of LLDPE and its nanocomposites at room temperature. It can be seen that the recovered compliance

does not coincide with creep compliance. Divergence of the recovery strain from the creep strain suggests that an irrecoverable deformation exists. Addition of 1% MLS into LLDPE decreases the degree of divergence. The degree of divergence further decreases with the addition of 1% amEP to LLDPE. Addition of a combination of amEP and MLS gives the lowest divergence, which is supported by the increased elasticity observed in the tensile results of the LLDPE/amEP/MLS combination.
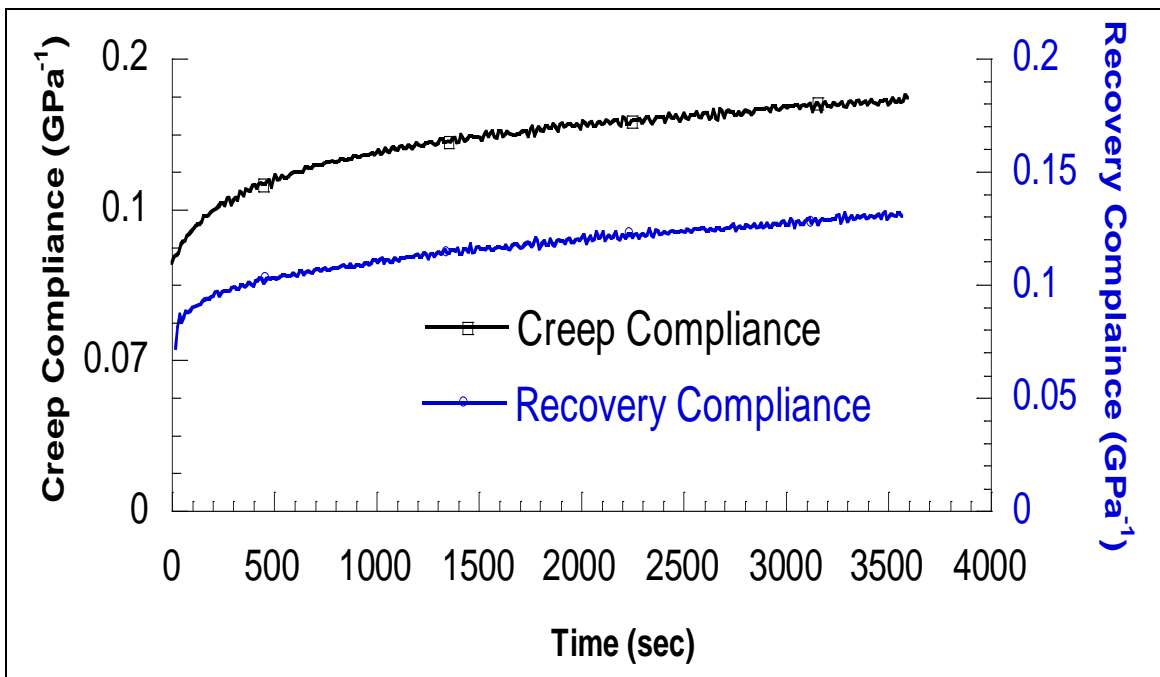
(a)
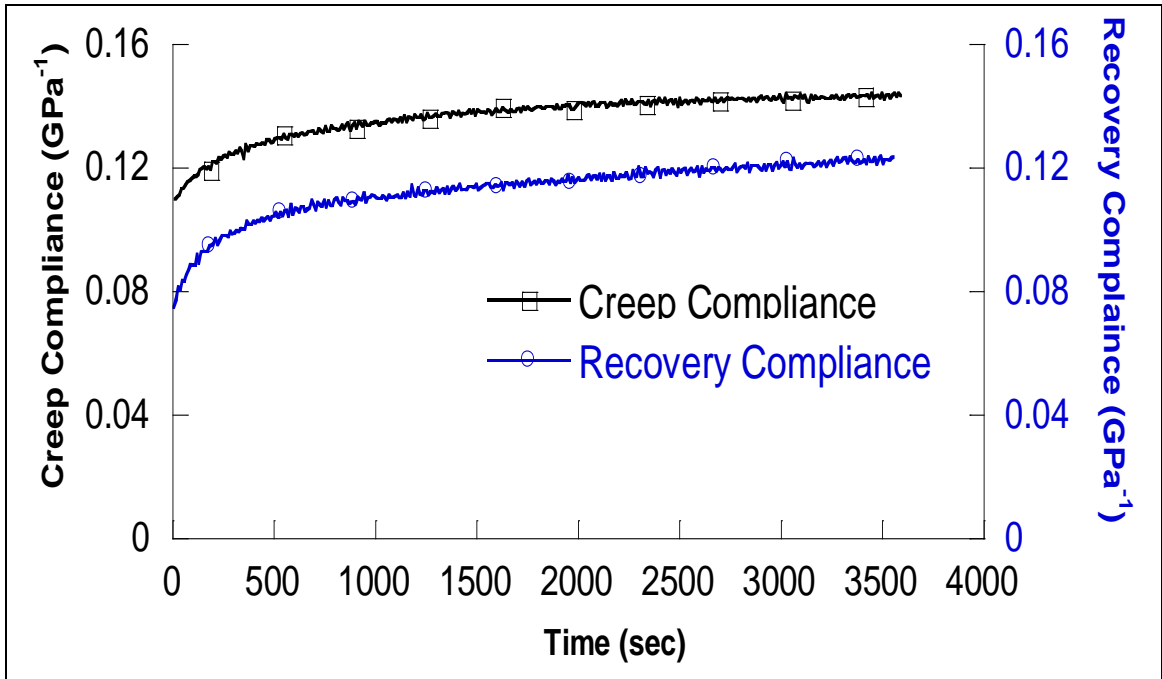
(b)
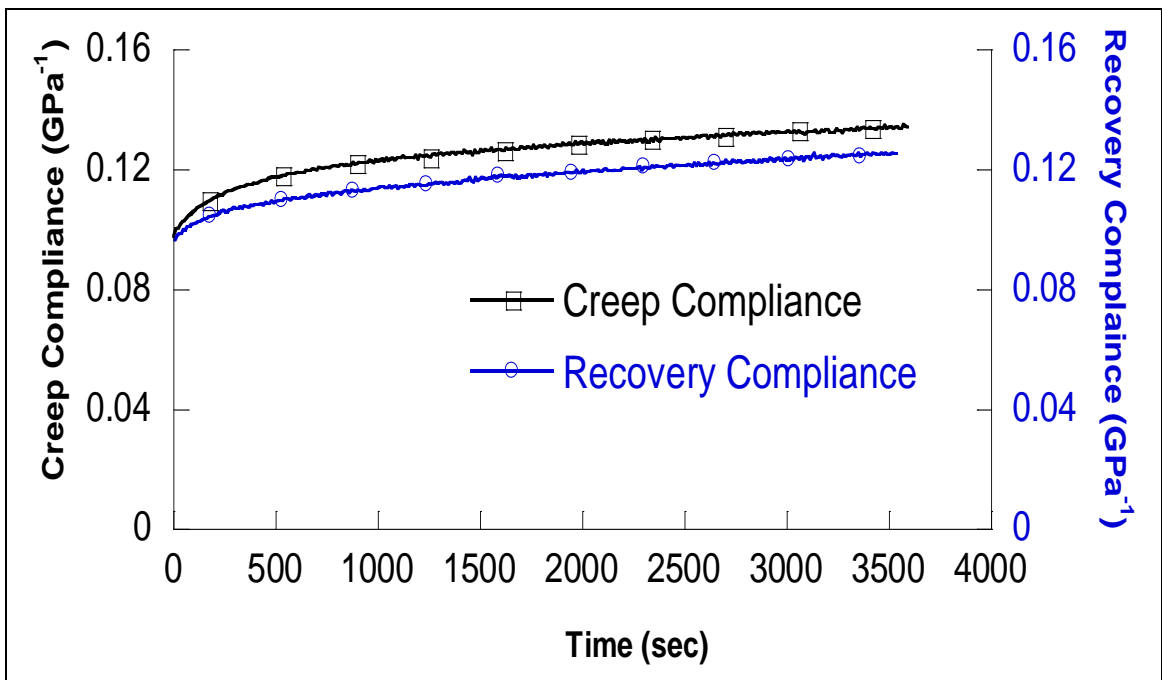
(c)
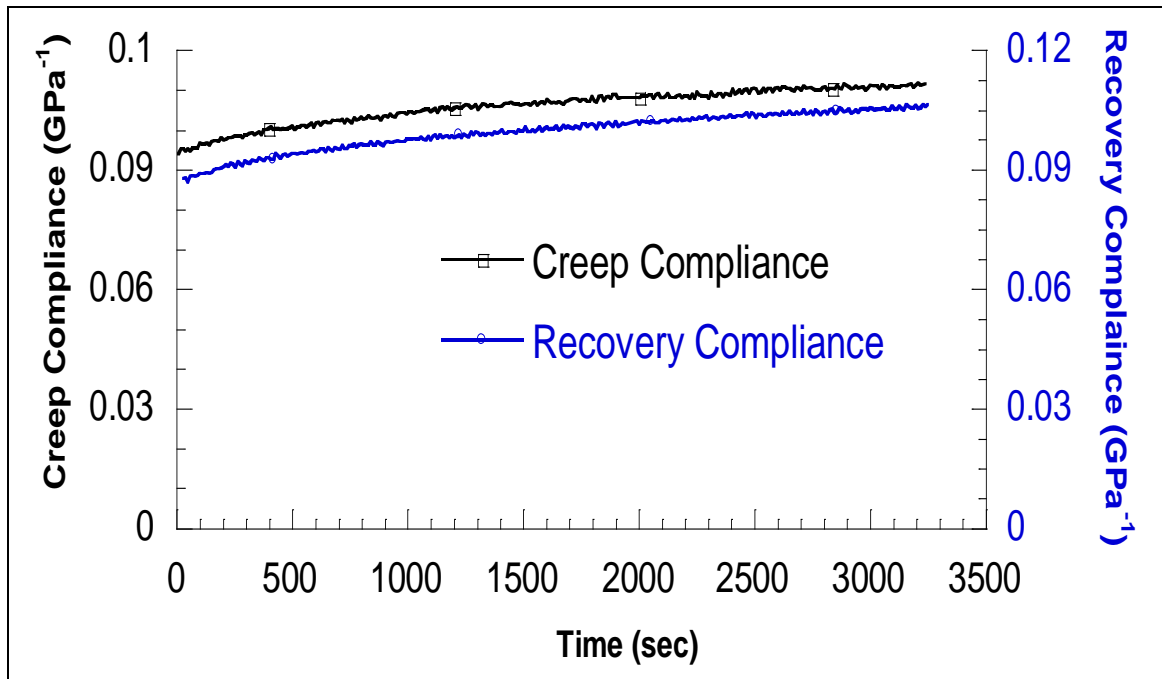
(d)

Figure 3.11. Comparison of creep-recovery compliance of LLDPE and its nanocomposites at room temperature: (a) pure LLDPE, (b) LLDPE/1% MLS, (c) LLDPE/1% amEP, and (d) LLDPE/1% amEP/1% MLS.

To evaluate the changes of the material properties with the addition of amEP and MLS, Burgers model was used to fit the creep data of the different LLDPE and amEP nanocomposites. Figure 3.12 shows the experimental and theoretical creep results of different LLDPE nanocomposites. It is clearly seen that there is agreement between theoretical and experimental results. The results of the Burgers fit parameters for all samples are tabulated in Table 3.5.
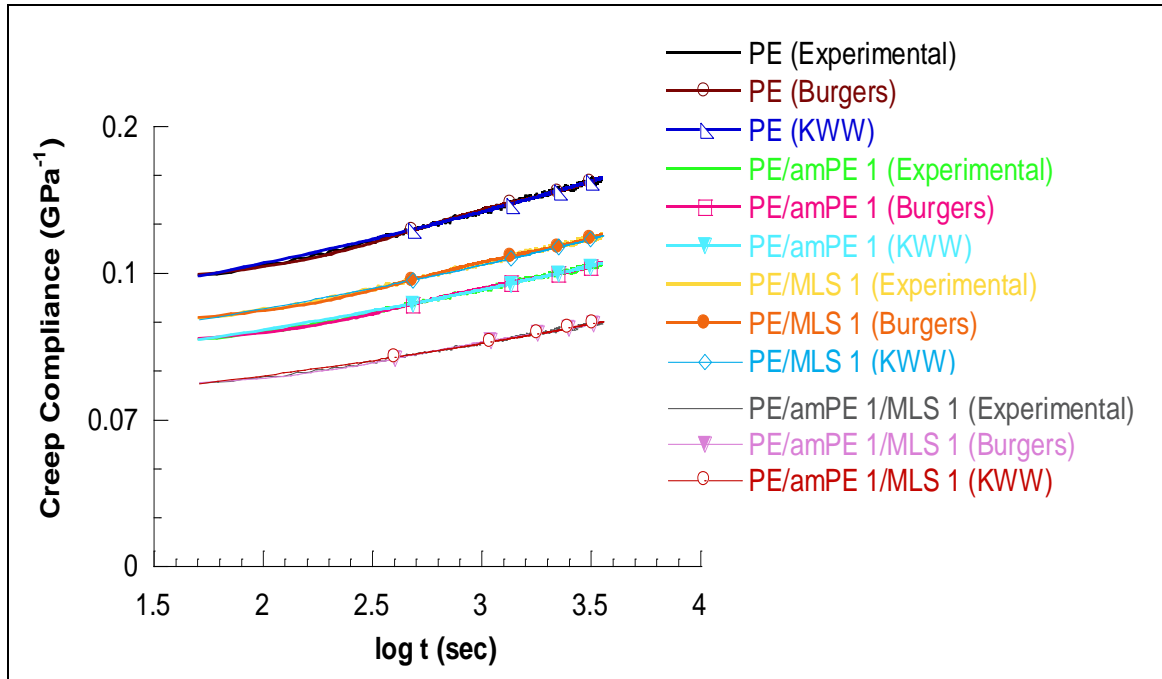
Figure 3.12. Comparison of experimental data to the Burgers model and the KWW function.

Sample	EM (109 Pa)	EK (109 Pa)	ηK (1011 Pa.s)	ηM (1012 Pa .s)	τ (sec)	% recovery
LLDPE	0.09	0.29	1.52	1.32	528	72
PE/MLS 1	0.08	0.31	1.54	2.75	493	95
PE/amEP 1	0.09	0.52	2.64	3.39	482	88
PE/amEP 1/MLS 1	0.12	0.66	3.53	4.83	472	95
PE/amEP 1/MLS 2	0.10	0.25	1.07	1.42	422	82
PE/amEP 2/MLS 1	0.13	0.40	1.65	1.89	413	80
PE/amEP 2/MLS 2	0.14	0.65	2.72	1.94	418	85
amEP	0.64	0.95	7.50	1.70	690	72
amEP/MLS 1	0.79	1.07	8.49	2.73	621	75
amEP/MLS 3	0.86	1.32	10.51	3.83	597	85

Table 3.5. Burgers fit parameters of LLDPE nanocomposites.

According to the Burgers constitutive equation, the modulus E_M of the Maxwell spring determined the instantaneous elastic creep strain, which could be immediately recovered on the removal of stress. In general, the nanocomposites showed higher values of E_M compared to neat matrix. Among the nanocomposites, LLDPE/amEP 1/MLS 1 behaved with the highest elasticity. In the case of LLDPE/MLS systems, the nanoclay layers could bear load because of the large aspect ratio of the individual platelet while discounted by the slippage of stacks and large amount of unexfoliated layers. Hence, the resulting E_M of LLDPE/amEP 1/MLS 1 was higher than the neat matrix. This increase reflects the tensile test results in which the nanocomposites with amEP and MLS had higher yield stress and modulus (Table 3.5). The instantaneous elasticity E_M reasonably corresponded to the elasticity of the crystalline part of the polymer, which took the immediate load because of high stiffness compared to the amorphous polymer. The crystallinity of each specimen was not obviously altered with the addition of the MLS particles, which implied that the load bearing parts were not greatly different between the neat LLDPE matrix and the nanocomposites.

The time-dependent E_K and η_K in the Kelvin unit might be associated with the stiffness and viscous or oriented flow of amorphous polymer chains in short term, respectively. E_K and η_K of the nanocomposites increased considerably with the addition of amEP and MLS. The addition of 1% amEP and 1% MLS showed a maximum in these values. The materials with a relatively higher bulk modulus deformed very little, and the Kelvin unit behaved with a higher modulus and very difficult viscous flow. E_K and η_K of the neat PE showed a small change with the addition of 2% MLS while keeping amEP at

1%, whereas an increase is observed with the addition of 1% and 2% MLS with 2% amEP into LLDPE. The addition of amEP and MLS showed reinforcement effectiveness on the Kelvin unit and showed to be effective to retard the deformation of the Kelvin unit.

E_K and η_K were used to determine the retardation time. Ideal elastic materials display an immediate recovery after loading and subsequent removal of the load. In the case of viscoelastic materials, there is a time delay for recovery. The retardation time is the delayed response to an applied force or stress. Figure 3.13 shows the retardation time behavior of LLDPE nanocomposites.
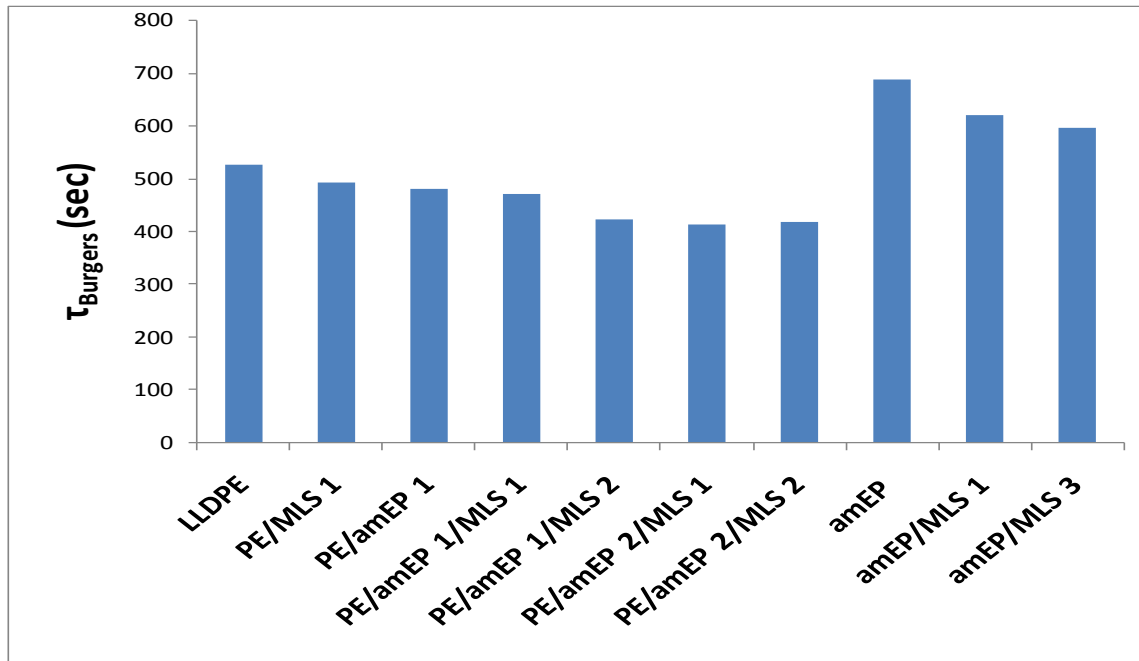
Figure 3.13. Burgers retardation time comparison of LLDPE and amEP nanocomposites.

The retardation time decreases from 528 sec for LLDPE to 493 sec with the addition of 1% amEP. The addition of 1% MLS further decreases the retardation time. Adding a combination of amEP and MLS with different ratios into LLDPE gives smaller retardation times. The results show that both E_M and retardation time reflect the final percentage recovery of LLDPE nanocomposites.

Another important parameter to consider in the Burgers constitutive equation is η_M that describes the irrecoverable creep as compared to the instantaneous and time-dependent parameters that showed enhancement with the addition of amEP and MLS. From Table 3.5, it can be seen that η_M increases with the addition of amEP and MLS. It can be considered that η_M is associated with the damage from crystallized polymer or oriented noncrystalline regions, such as the pulling out of chain folds by a crystal slip process and the breaking of an intercrystalline tie molecule or the irreversible

deformation from amorphous regions, such as breaking of bridging segments between the clay particles and the polymer chains. The enhanced resistance to deformation was obtained with the addition of amEP and MLS. Addition of 1% of amEP and 1% MLS separately or combined increases η_M reflecting the fact of a decrement of the irrecoverable deformation. The results are reflected in the higher % recovery for the composites containing 1% amEP and 1% MLS. Addition of 2% MLS while keeping amEP at 1% shows lower η_M values indicating an increase in the amount irrecoverable deformation and hence a lower % recovery value. The results can be attributed to the ease of mobility of the polymer chains.

To assess both the retardation time and the breadth of relaxation times, creep compliance curves were fitted with the KWW [23-24] stretched exponential function

$$D(t) = D_0[1 - \exp(-t/\tau)^\beta]$$

where D(t) is the creep compliance, τ is the characteristic retardation time, and β is a creep shape parameter. The numerical analysis of the creep compliance curve fits was performed using OriginLab™ nonlinear least-squares data analysis software.

Figures 3.13 and 3.14 compare the KWW fit parameters of LLDPE and amEP nanocomposites. A retardation time represents resistance offered by the microstructure to the elastic deformation of the system. As the retardation time decreases (i.e., as less resistance occurs), the system response becomes more elastic. The results of the sample investigated are tabulated in Table 3.6.
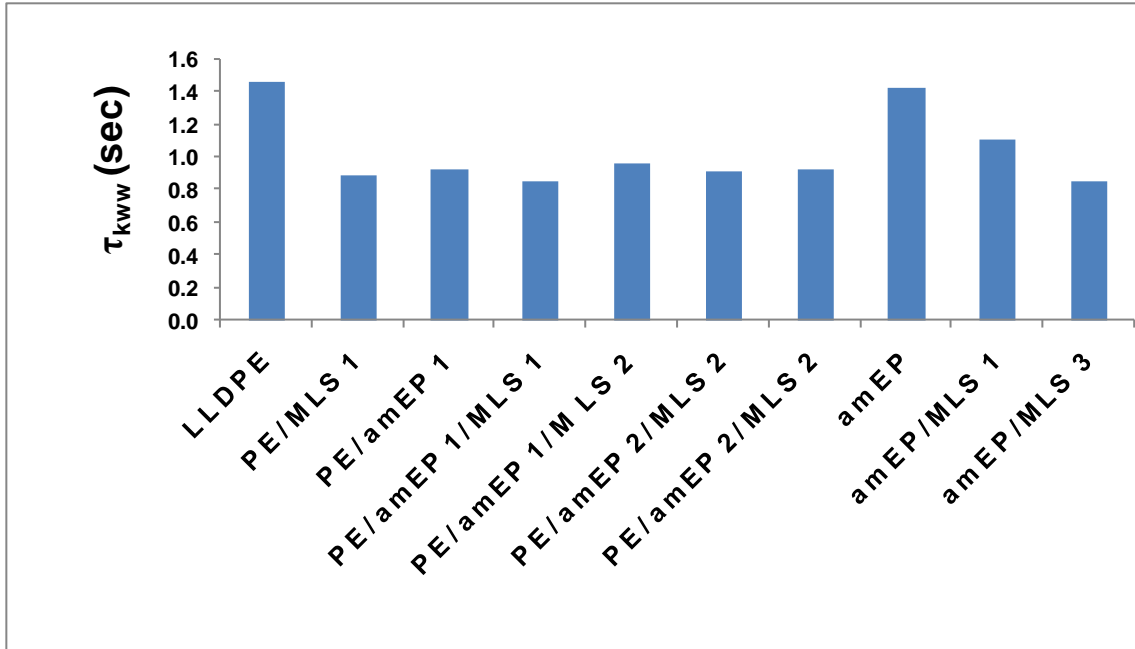
Figure 3.14. Retardation time comparison of LLDPE and amEP nanocomposites.
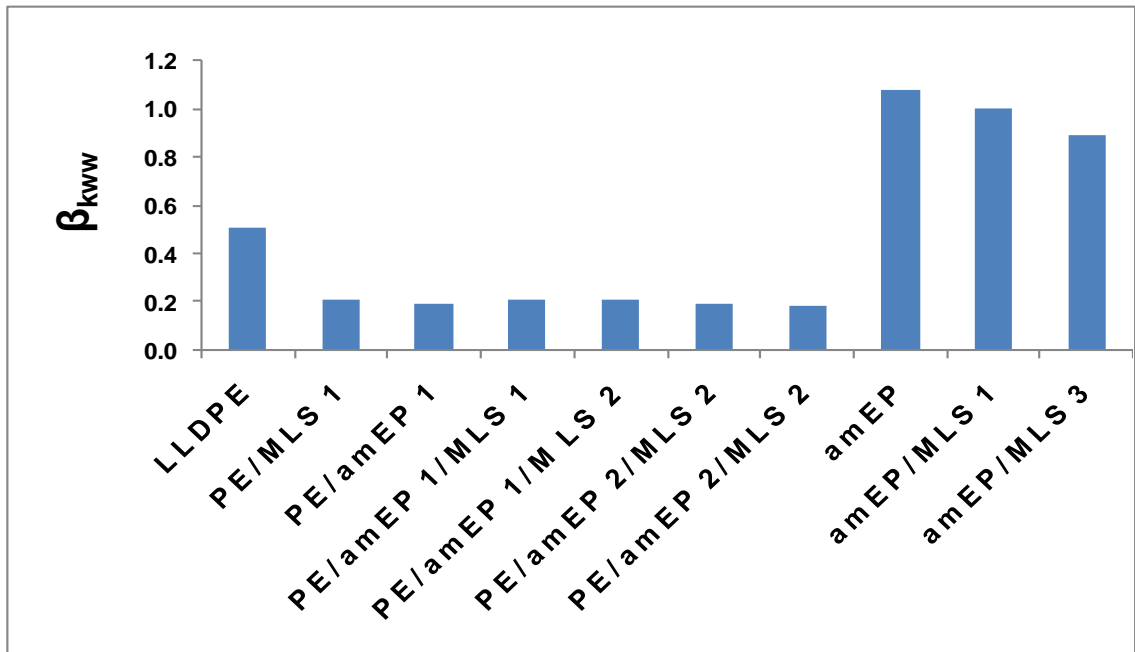
Figure 3.15. Comparison of β_{kww} for the different LLDPE and amEP nanocomposites.

Sample	τ_{kww}(sec)	β_{kww}
LLDPE	1.47	0.50
PE/MLS 1	0.89	0.21
PE/amEP 1	0.93	0.19
PE/amEP 1/MLS 1	0.86	0.21
PE/amEP 1/M LS 2	0.96	0.20
PE/amEP 2/MLS 1	0.92	0.19
PE/amEP 2/MLS 2	0.92	0.18
amEP	1.43	1.08
amEP/MLS 1	1.11	1.00
amEP/MLS 3	0.86	0.89

Table 3.6. KWW curve fitting parameters.

Pure LLDPE and amEP had a similar retardation time at room temperature. The breadth of the relaxations, which are inversely related to β, show that the LLDPE had a larger breadth than the amEP. For LLDPE nanocomposites, the addition of 1% MLS decreases the retardation time from 1.47 sec for LLDPE to 0.89 sec for PE/1% MLS. For amEP nanocomposites, the addition of 1% MLS also causes a decrease in the retardation time. The retardation time decreases from 1.43 sec for amEP to 1.11 sec for amEP/1% MLS. The addition of 3% MLS to amEP further decreases the retardation time to 0.86 sec. The results can be explained by the addition of the rigid MLS particles, which act to increase the elasticity of the matrix and hence reduce the retardation time. The retardation time increases to 0.93 when 1% amEP is used. The corresponding effect on the breadth of relaxations indicates that the effect on the LLDPE is to increase it substantially, whereas marginal impact on relaxation breadth is obtained in the amEP + MLS composites. The combined nanocomposites based on both LLDPE and amEP show values similar to those

obtained in the PE +MLS systems. The values of β remained constant ($\beta = 0.19 \pm 0.02$) despite the different amounts of MLS and amEP that have been added into the PE matrix.

For amEP nanocomposites, the β values decrease from 1.08 for neat amEP to 1 and 0.89 with the addition of 1% and 3% MLS to amEP, respectively. A decrease in the β parameter can be interpreted as a strengthening of the coupling between the relaxing species and the medium and is related to an overall decrease of the molecular mobility. A minimum in the values of retardation time is obtained when a combination of 1% MLS and 1% amEP is used. The addition of 2% amEP with 1% and 2% MLS to PE retains the value of 0.92 sec for the retardation time. The results obtained for LLDPE nanocomposites suggest that a combination of 1%MLS and 1% amEP gives the lowest retardation time. The enhanced recovery observed for the combination of amEP and MLS is reflected in lower τ values. We note that the addition of MLS to either PE or amEP influences retardation time and relaxation breadth. We also note that the blend of LLDPE + amEP indicates a larger relaxation breadth and a decrease in retardation time of the pure PE and amEP.

3.4. Error Analysis

All experiments were validated as follows:

For DSC, a set of two samples were used to ensure reproducibility of the data. Enthalpies of melting and crystallization were calculated using the Pyris software on the Perkin Elmer DSC6.

For XRD, a set of two samples were used to ensure reproducibility of the data. The 2 theta values, the d spacing, and the FWHM were calculated using the Rigaku Ultima III software.

For Tensile testing, a total of five samples were tested according to ASTM D882. Figure 3.16 shows a representative curve for tensile test of LLDPE showing the overlay of three samples. The error analysis was presented in Table 3.4. The yield stress was calculated as the deviation of the stress from the linear region on the stress-strain curve.

For creep testing, two samples were used to ensure reproducibility of the data. The creep compliance was calculated as the ratio of the strain obtained from RSA III software divided by the constant stress applied during the creep test.
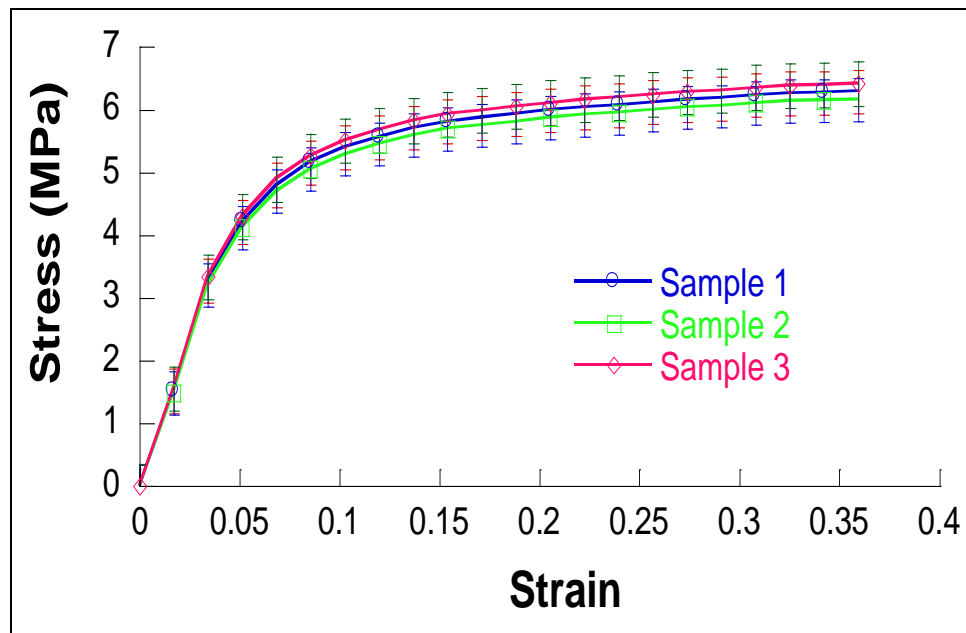
(a)
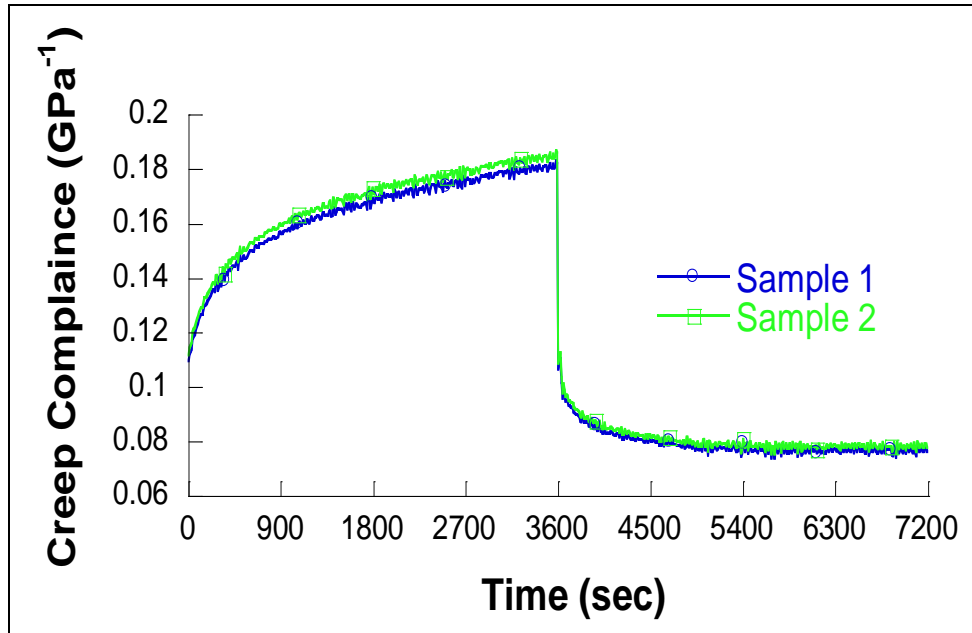
(b)
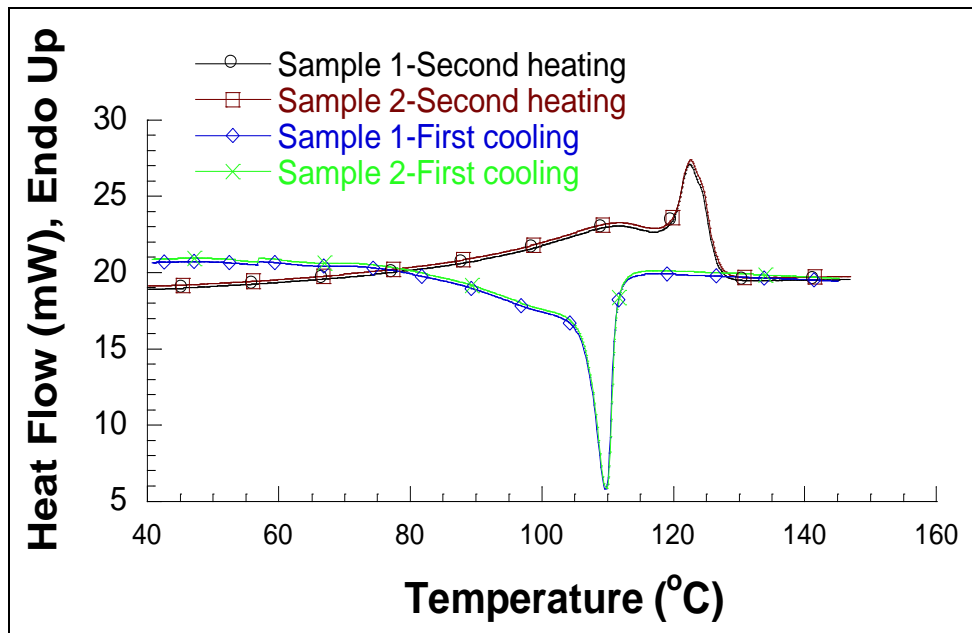
(c)

Figure 3.16. Error analysis showing overly of (a) tensile test; (b) creep test; (c) DSC test for pure LLDPE samples.

3.5. Conclusions

XRD and microscopy of LLDPE nanocomposite films showed some intercalation effects for samples in which a combination of 1% amEP and 1% MLS was used. An increase in the interlayer distance was observed for this sample. The amEP proved to be an effective factor in the dispersion behavior of the nanocomposites and resulted in improved tensile and creep properties.

Both the Burgers model and the KWW relation model creep behavior (Figure 3.12). The trends in retardation time were more clearly depicted in the KWW relation. The LLDPE nanocomposite showed a nonlinear viscoelastic behavior. A permanent deformation was observed in all systems with LLDPE nanocomposite having the lowest creep. Struik [25] proposed that since the polymer chains adhere to the filler particles, the segmental mobility near the particles' surface would be reduced. Far from the particles, the mobility of the matrix will be similar; thus, a distinction between "disturbed" and "undisturbed" regions is made. Lai and Baker [21] used this network model to understand the mechanism of plastic deformation in HDPE at low stress levels. The model assumes that the time-dependent behavior of a semicrystalline or filled polymer is due to the amorphous phase only and that crystals do not contribute to viscoelasticity of the polymer and act as inert fillers or crosslinks behaving elastically. On application of a load, the deformation from the disturbed amorphous regions and the crystals is recoverable. The undisturbed amorphous regions undergo an irrecoverable deformation. This behavior can be seen in the LLDPE/amEP/MLS nanocomposites. The percentage recovery in LLDPE/amEP/MLS nanocomposites is higher than that of pure LLDPE. This suggests the role of MLS particles in the absence of crystallites. MLS particles act as hinges in the

amorphous matrix; this action is reflected in higher modulus, higher yield strain, and more recovery. MLS lowers retardation time in all materials but the crystallinity in the host matrix acts in a similar way. For the pure amorphous material with MLS, the retardation time values are higher (recovery is lower) as compared to the PE+ amEP +MLS, in which a higher recovery and a lower retardation time are experienced. The relaxation breadth is increased when MLS was added to either PE or amEP.

3.6.   References

1. K.K. Maniar., *Polymer-Plastics Tech. and Eng.*, **43**, 427-443 (2004).

2. F. Hussain, M. Hojati, M. Okamoto, and R. Gorga, *J. Composite Materials*, **40**, 1511-1575 (2006).

3. J.L. Rand, D.A. Grant, and T. Strganac, AIAA 34th Aerospace Sciences Meeting and Exhibit (1996).

4. J.L. Rand and W.J. Sterling, 35th COSPAR Scientific Assembly; Adv. Space Research, Paris (2004).

5. D. Martin, P. Halley, R. Truss, M. Murphy, O. Jackson, and O.Y. Kwon, *Polym Int,* , pp. 1774-1779 (2003).

6. G. Liang, J. Xu, S. Bao, and W. Xu , *J. Appl. Polym. Sci.*, **91**, 3974-3980 (2004).

7. G. Malucelli, S. Ronchetti, N. Lak, A. Priola, N.T. Dintcheva, and F.P. La Manta, *Eur. Polym. J.*, **43**, 328-335 (2007).

8. H. Wang, D.G. Thompson, J.R. Schoonover, S.R. Aubuchon, and R.A. Palmer, *Macromolecules*, **34**, 7084-7090 (2001).

9. M.L. Quintinilla, S.S. Valdez, L.F. Ramos, and R.G. Miranda, Polym. Bulletin, pp. 385-393 (2006).

10. A. Lee and D. Lichtenhan, *J. Appl. Polym. Sci.*, **73**, 1993-2001 (1999).

11. A. Pegoretti, J. Kolarik, C. Peroni, and Cilgiaresi, *Polym.*, **4**, 2751-2759 (2004).

12. J. Morawiec, A. Pawlak, M. Slouf, A. Galeski, E. Piorkowska, and N. Kransikowa, *Eur. Polym. J.*, **41**, 1115-1122 (2005).

13. R.W. Truss and T.K. Yeow, *J. Appl. Polym. Sci.*, **100**, 3044-3049 (2006).

14. J.L. Yang, Z. Zhang, A. Schlarb, and K. Friedrich, *Polym.*, **47**, 2791-2801 (2006).

15. U. Gurmendi, J.I. Eqiazabal, and J. Nazabal, *Macromol. Mater. Eng.*, **292**, 169-175 (2007).

16. F.C. Chiu, Q. Wang, Q. Fu, P. Honigfort, S. Cheng, B.S. Hsiao, F. Yeh, M.Y. Keating, E.T. Hsieh, and C.C. Tso, *J. Macromolecular Sci., Part B*, **39**, 317-331 (2000).

17. M. Niaounakis and E. Kontou, *J. Polym. Sci.: Part B: Polymer Physics*, **43**, 1712-1727 (2005).

18. A. Ranade, K. Nayak, D. Fairbrother, and N.A. D'Souza, *Polym,* **46**, 7323-7333 (2005).

19. Z. Shen, G.P. Simon, and Y.B. Cheng, *Polym,* **43**, 4251-4260 (2002).

20. M. Costache, M.J. Heidecker, E. Manias, and C. Wilkie, *Polym. Adv. Technol.*, **17**, 764-771 (2006).

21. L. Lai and A. Bakker, *Scripta Metallurgica et Materialia*, **28**, 1447-1452 (1993).

22. A.D. Drozdov and J. Christiansen, *Eur. Polym.*, **43**, 10-25 (2007).

23. F. Kohlrausch, Pogg. Ann Physics, **12**, 393 (1847).

24. G. Williams, D.C. Watts, Trans Faraday Soc, **66**, 80 (1970).

25. LCE Struik , *Physical aging in amorphous polymers and other materials*; Elsevier: New York (1978)

CHAPTER 4

EFFECT OF TEMPERATURE ON MOLECULAR RELAXATIONS IN
POLYETHYLENE NANOCOMPOSITES

4.1.   Introduction

Polymer nanocomposites are hybrid materials composed of an organic polymer matrix in which organic fillers with nanoscale dimensions are embedded. The inorganic fillers dramatically improve the physical and mechanical properties of the polymer [1-4]. For these materials, the ability to model viscoelastic response determines the understanding of deformation mechanisms and facilitates solutions to their long-term performance.

Mechanical analogs are commonly used to model long-term performance, the simplest being the Maxwell model (spring and dashpot in series) and the Voigt model (spring and dashpot in parallel). The Maxwell model is commonly used for representation of stress relaxation, whereas the Voigt model is used for creep and recovery representation. More complex models involve three or four elements, such as the Burgers model, which is a combination of the Maxwell and Voigt models and can be used for creep and recovery representation [5].

Creep behavior is an important property of polymer nanocomposites that controls the dimensional stability, especially in applications where the material supports loads for long periods [6-11]. This mechanism can cause undesirable deformation that leads to structural failure. Yang et al. [7] investigated the creep behavior of polyamide 66 (PA66) nanocomposites at various temperatures for use in aviation and automotive applications.

The creep deformation and the creep rate of the matrix were reduced by the addition of the nanofillers. Ranade et al. [8] studied the potential use of linear low-density polyethylene (LLDPE) nanocomposites based on montmorillonite-layered silicates (MLS) as load bearing materials for stratospheric scientific balloons. The creep resistance and modulus of the polymer was increased by the incorporation of the layered silicate. The results were attributed to the dispersion effects due to the presence of MLS. Nunez et al. [9] analyzed the creep properties of polypropylene (PP) composites prepared from wood flour at different temperatures for use in industrial applications such as automotive components and domestic appliances. The effect of filler content, addition of compatibilizing agent, and temperature was investigated. The Burgers model was found to give a good description of the viscoelastic behavior. The parameters were found from best-fitting of experimental data. The results showed that the creep deformation decreased when wood flour concentration was increased. The addition of a small amount of maleated PP greatly improved creep behavior. The composite showed a strong dependence of the creep behavior on temperature; the Maxwell modulus E_0 showed a reduction with increasing temperature as a result of material softening.

Morphology plays an important role in the creep behavior of real polymeric systems. For amorphous polymers, creep behavior can be represented by the Kohlrausch-Williams-Watts (KWW) function, which states that creep compliance increases according to a stretched exponential function. The KWW function can be also used for creep characterization of semicrystalline polymers [12-13]. McKenna et al. [12] studied the effect of physical aging on the creep behavior of syndiotactic polystyrene (sPS) by using

the KWW function. The effect of aging time and temperature was considered. Cheriere et al. [13] studied the three stages of creep of polymethyl-methacrylate (PMMA) between 55 and 90 $^{\circ}$C. After stress application, creep starts by a logarithmic function. It is followed by a KWW creep stage with an exponent of 0.36. The third stage follows a power law with an exponent of 0.8.

In our previous experimental studies, the creep behavior of maleated and non-maleated LLDPE nanocomposites at room temperature was studied [14]. Creep compliance was significantly reduced with the addition of different ratio of an amorphous maleated polyethylene (amEP) and MLS. The results were attributed to the good dispersion of MLS particles which was facilitated by the addition of the compatibilizer. In this chapter, the modeling of creep behavior by using traditional creep models was conducted. An attempt to understand the structure-property relationship was carried out by analyzing the parameters of the Burgers model since variations in these parameters illustrate the influence of nanofillers on the creep performance of the bulk matrix. Moreover, the distribution of retardation time was considered by using the KWW function.

4.2. Experimental

4.2.1. Sample Preparation

Nanocomposites were compounded by using a Haake TW100 twin-screw extruder with a temperature profile of 200, 200, 205, and 210 ^{o}C for zones 1 to 4, respectively. PE films 1.5 mil (0.04 mm) thick were processed with a Killion single-screw extruder (L/D = 24:1), fitted with a dual-lip air ring and a die diameter of 2 inches. Blends of PE + amEP + MLS were made, and the mixtures were compounded and pelletized. The compounded pellets were then extruded into blown films. Table 4.1 summarizes the concentrations used.

Sample	LLDPE (wt %)	Exxelor VA 1803 (wt %)	MLS (wt %)
LLDPE	100	0	0
PE/MLS 1	99	0	1
PE/amEP 1	99	1	0
PE/amEP 1/MLS 1	98	1	1

Table 4.1. Summary of concentrations used.

4.2.2. Dynamic Mechanical Analysis (DMA)

DMA experiments were performed with a rheometric solids analyzer (RSA III) instrument (TA instruments Inc.). The mode of deformation applied is tension, and the mean sample dimensions are 5 mm $\times$ 25 mm with a mean thickness of 40 μm. The temperature ranged from -100 ^{o}C to 100 ^{o}C at a heating rate of 3 ^{o}C/min, and the frequency was set at 1 Hz. The storage and loss modulus as well as tan δ versus

temperature were evaluated as described in ASTM D5026 (standard test method for plastics: dynamic mechanical properties in tension).

4.2.3. Tensile Testing

Yield stress, ultimate tensile strength (UTS), and elastic modulus E were determined by using RSA III film fixture with an extension rate of 0.208 mm/min. The effect of temperature was studied by running experiments at different temperatures of 25, 10, -10, -30, -50, -70, -90, and -100 ^{o}C. A convection oven with a temperature range of -150 ^{o}C to 600 ^{o}C was used for this purpose.

4.2.4. Creep Testing

Uniaxial tensile creep tests were performed by using the RSA III with a film attachment. The desired constant stress to be applied for each measurement was calculated to be 50% of the yield stress. The constant stress was applied for 1 hour of loading followed by 1 hour of unloading. A linear displacement transducer with a force capacity of 35 N was used to monitor the strain during the experiment. Creep tests were also performed at the same set of temperatures as the tensile tests, and the liquid nitrogen controller connected to the environmental chamber was used for cooling.

4.3. Results and Discussion

4.3.1. DMA Results

LLDPE usually shows three transition temperatures in DMA designated as α, β, and γ, which are best obtained from tan δ curve. The α transition ranges from 0 to 120 ^{o}C,

the β-transition ranges from -30 to 10 ^{o}C, and the γ transition ranges from -150 to -120 ^{o}C. For the temperature range tested, all samples showed a β transition at around -30 ^{o}C and an α transition between 50 and 60 ^{o}C. The transition temperatures and relative change in magnitude of the $E^{'}$, E" and tan δ corresponding to the β and α transitions for the different compositions are shown in Figure 4.1, and the results are tabulated in Table 4.2.
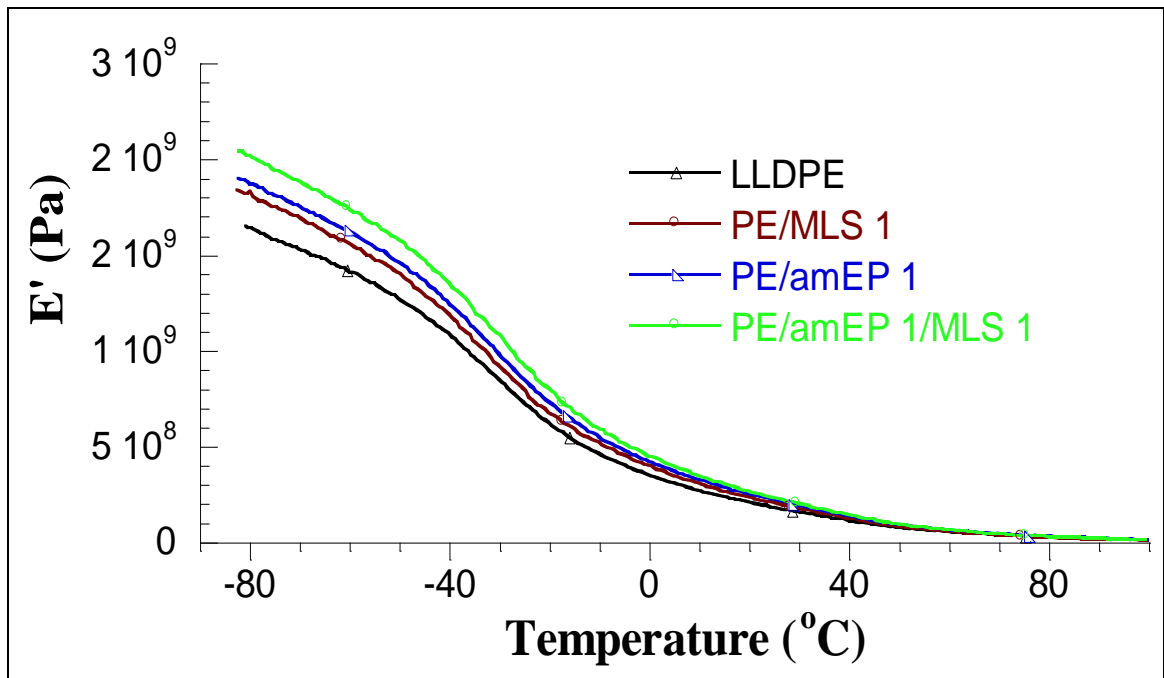
(a)
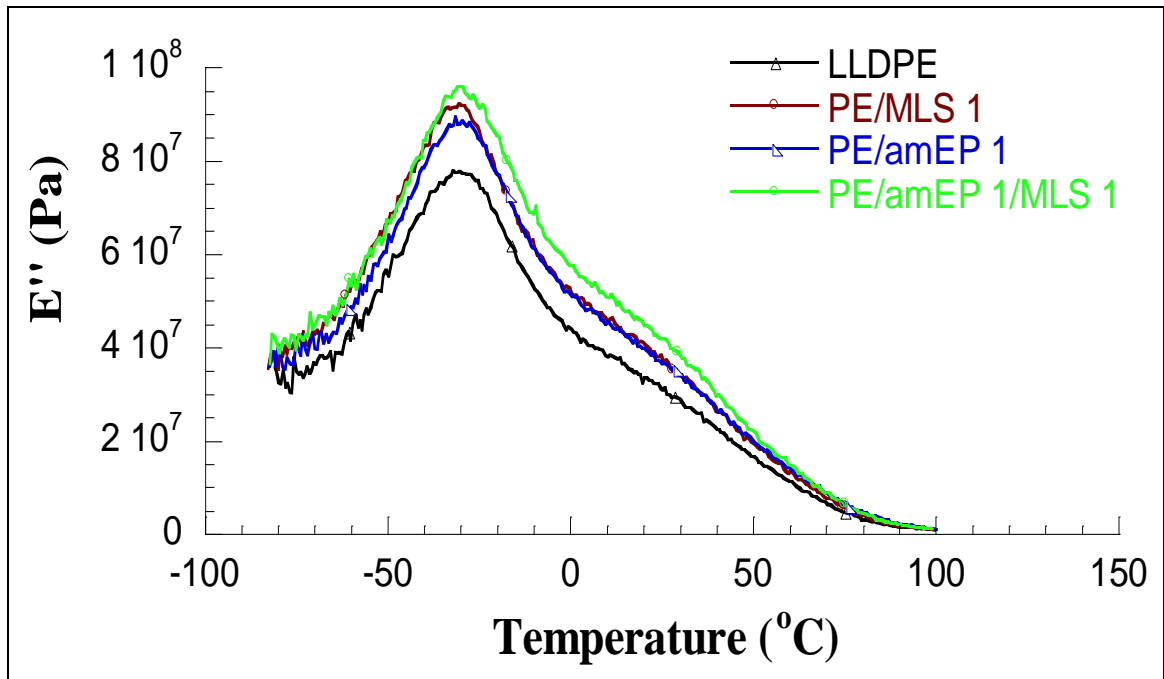
(b)
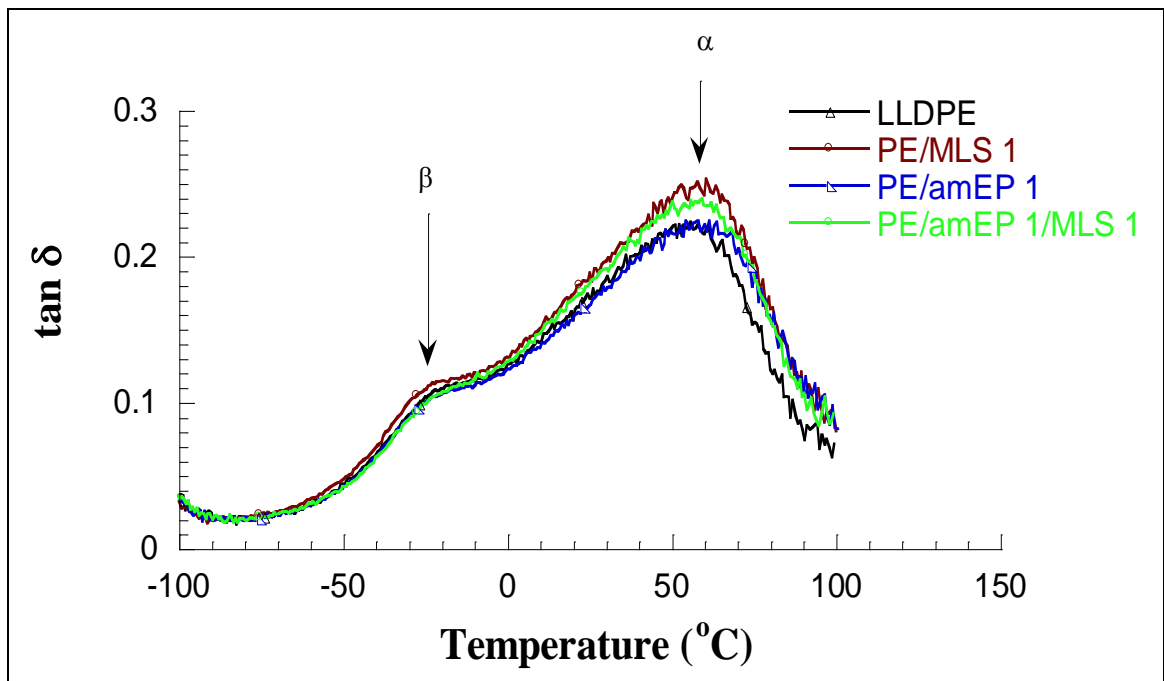
(c)

Figure 4.1. DMA results showing (a) E', (b) E″, and (c) tan δ versus temperature of LLDPE nanocomposites.

Sample	E' (GPa) -80 °C	E' (GPa) 25 °C	β-Transition		α-Transition	
			Temperature (°C)	E'' peak intensity (Pa)	Temperature (°C)	tan δ peak intensity
LLDPE	1.65	0.18	-31.91	7.78E+07	59.28	0.22
PE/MLS 1	1.84	0.21	-30.22	9.22E+07	54.15	0.25
PE/amEP 1	1.90	0.22	-31.23	8.92E+07	60.52	0.22
PE/amEP 1/MLS 1	2.04	0.23	-29.86	9.59E+07	55.77	0.24

Table 4.2. DMA results showing variations in E', E'', and tan δ.

The β-transition temperature is not affected by the addition of either amEP or MLS, which is expected since this transition corresponds to the motions of chain units in the interfacial region [15]. However, the presence of MLS is found to have a pronounced impact on the α-transition temperatures. The addition of MLS into the PE matrix caused a decrease of 5 °C in α-transition temperature for all compositions. This decrease indicates that MLS acts to increase the chain mobility of the PE matrix.

The storage moduli E' of the nanocomposites were higher than those of the pure LLDPE over the entire temperature range. At low temperatures (-80 °C), the storage modulus increased by 11% and 15 % with the addition of 1% MLS and 1% amEP, respectively. At 25 °C, the storage modulus increased by 16% and 22%, respectively. The highest increase in storage modulus (23% at -80 °C and 27% at 25 °C) was for samples in which a combination of 1% amEP and 1% MLS was used (Table 4.2). This increase can be explained by the synergic interaction between amEP and MLS at these loading conditions.

The selection of relative values for E″ and tan δ peaks was based on the clarity of a peak for the β and α transitions, respectively. Adding 1% amEP had a slight impact on the PE for the β transition. However, the addition of 1% MLS with or without the amEP increased the peak intensity by 23% and 18%, respectively (Table 4.2). This increase indicates that the polymer-clay interfacial region played a role in the time response of the PE. The increases noted in the α-transition peak maxima are even higher. The amEP did not affect the maxima of the PE for the α transition, indicating no influence on the amorphous compatibilizer on segmental relaxation. However, the presence of MLS had a pronounced effect on the maxima, supporting the conclusion that MLS provides an interface that affects the relaxation in the PE matrix. The change in transition temperatures and E" peak maxima for composites containing MLS with or without amEP indicates that the vibrational and orientational motion within the crystals is altered by the addition of MLS. The increase in E' and E" values indicates benefits in both the elastic and the viscous response in the modified PE. The MLS rigid platelets linked to the PE matrix via the reactive surfactants serve as rigid crystals and can act as anchors in the PE matrix.

4.3.2. Tensile Test Results

A stress-strain curve of LLDPE nanocomposites at room temperature is shown in Figure 4.2. The results, which include yield stress and elastic modulus E, are tabulated in Table 4.3. The decreased crystallinity of the PE resin used is reflected in the modulus value of 0.12 GPa compared to 0.58 GPa in the previous work [8].

The addition of 1% amEP resulted in an 80% increase in modulus, whereas the addition of MLS caused an increase of 50%. It can be seen that the highest increase in modulus (166%) occurred for samples in which a combination of 1% amEP and 1% MLS was used. The yield stress values follow the same trends as observed in the modulus. The yield stress increased from 4.86 MPa for neat PE to 6.92 MPa for the LLDPE/amEP 1/MLS 1 nanocomposite. This increase indicates the combined effect of amEP and MLS, which is distinct from the previous work, on the positive impact that amEP has on the PE matrix.
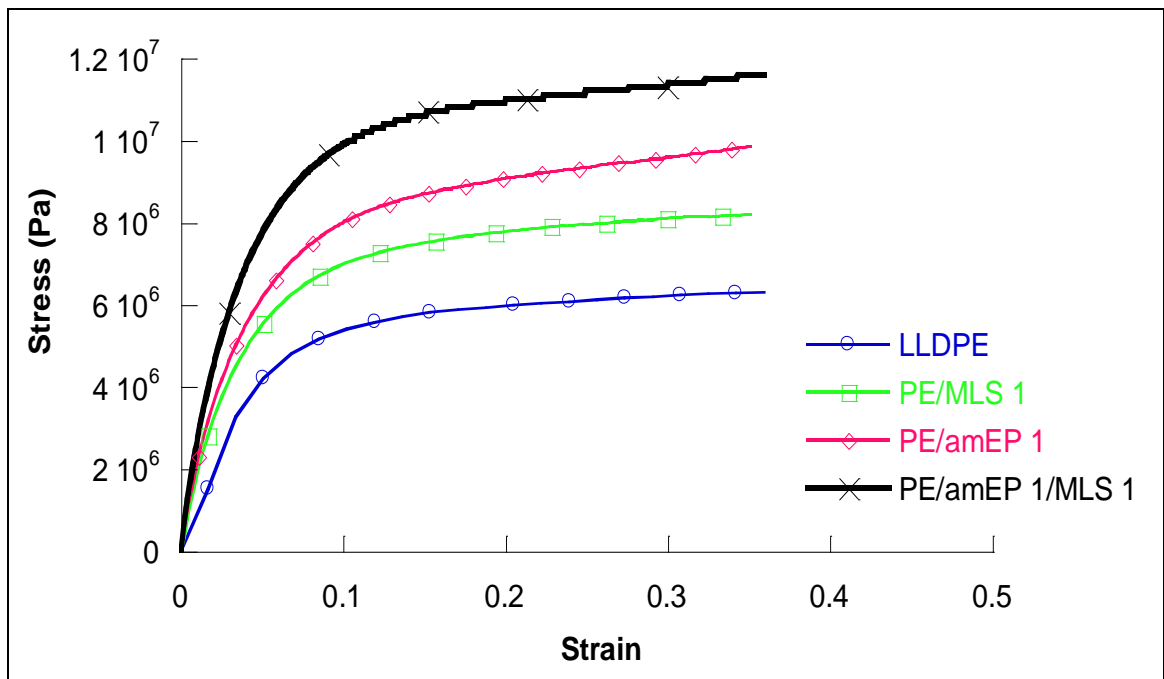
Figure 4.2. Stress-strain curve of LLDPE nanocomposites at room temperature.

The effect of temperature on the tensile properties is important in applications where temperatures can fall down to -100 $^{\circ}$C, particularly in high-altitude balloon films. Figure 4.3 shows the stress-strain curve of LLDPE and LLDPE/amEP 1/MLS 1 at

different temperatures. The results are tabulated in Table 4.3. It is worth mentioning that all the temperatures showed a similar trend in the stress-strain curves as that observed in the room temperature measurements.
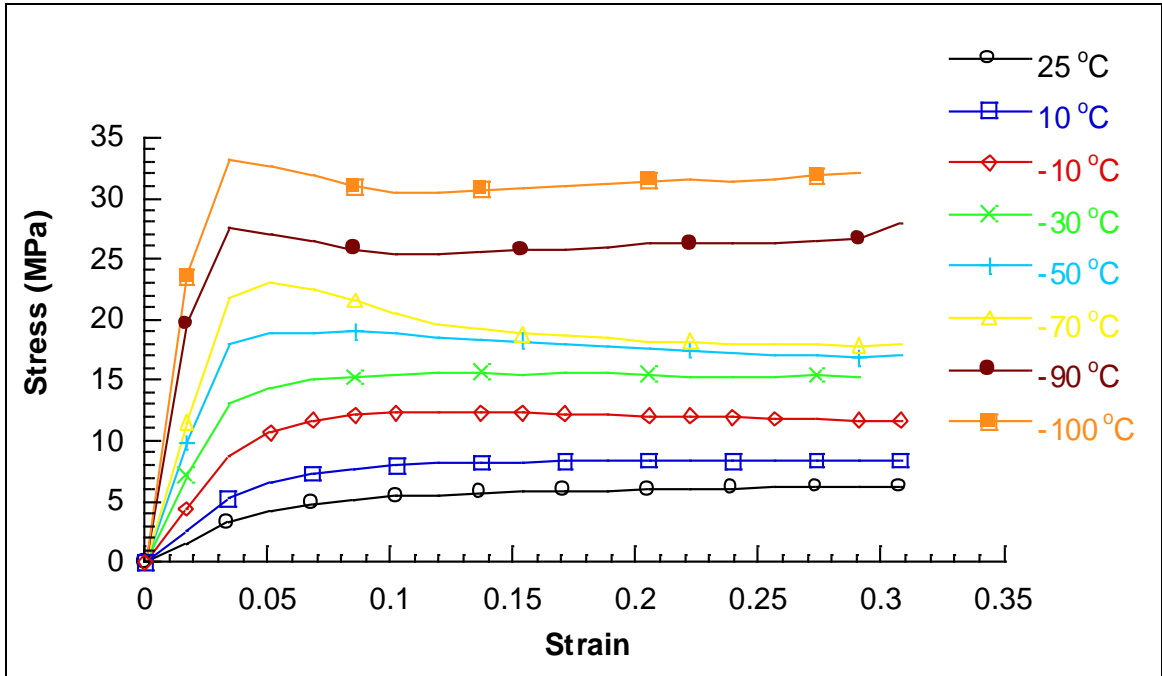
(a)
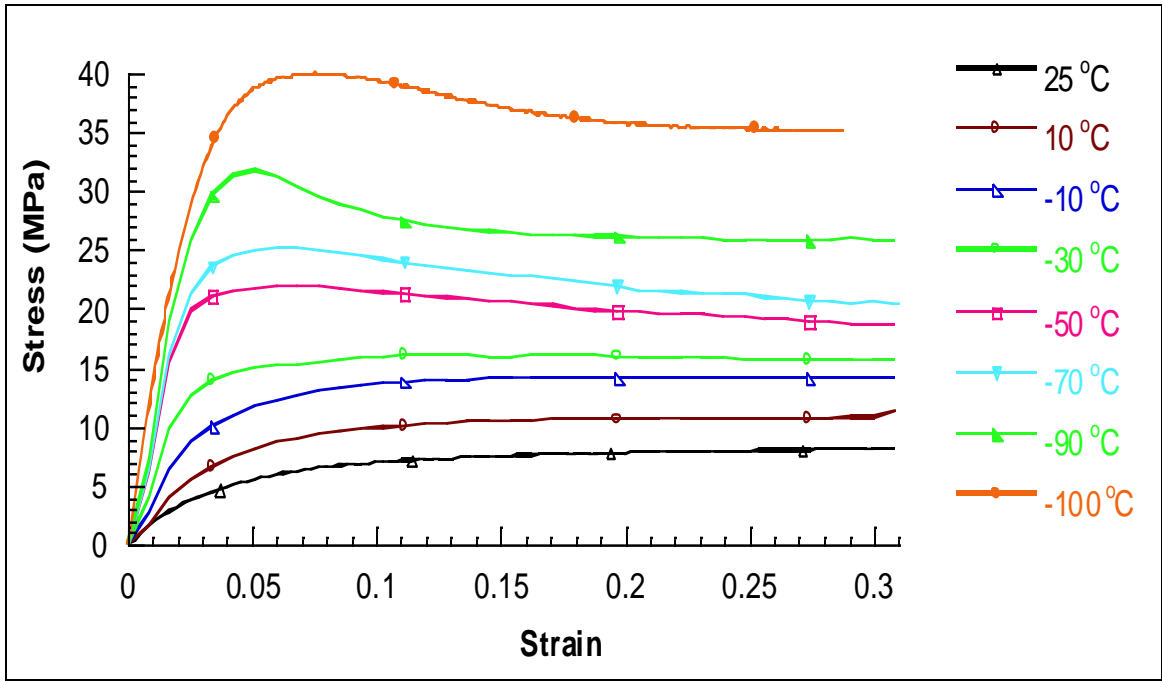
(b)
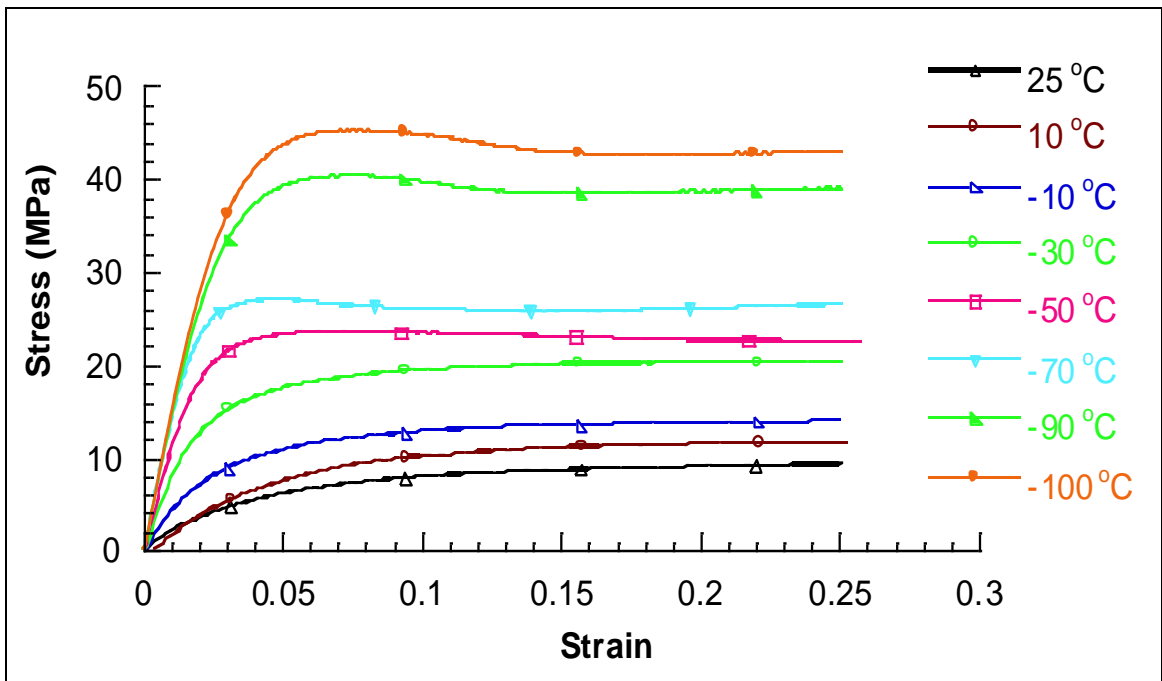
(c)
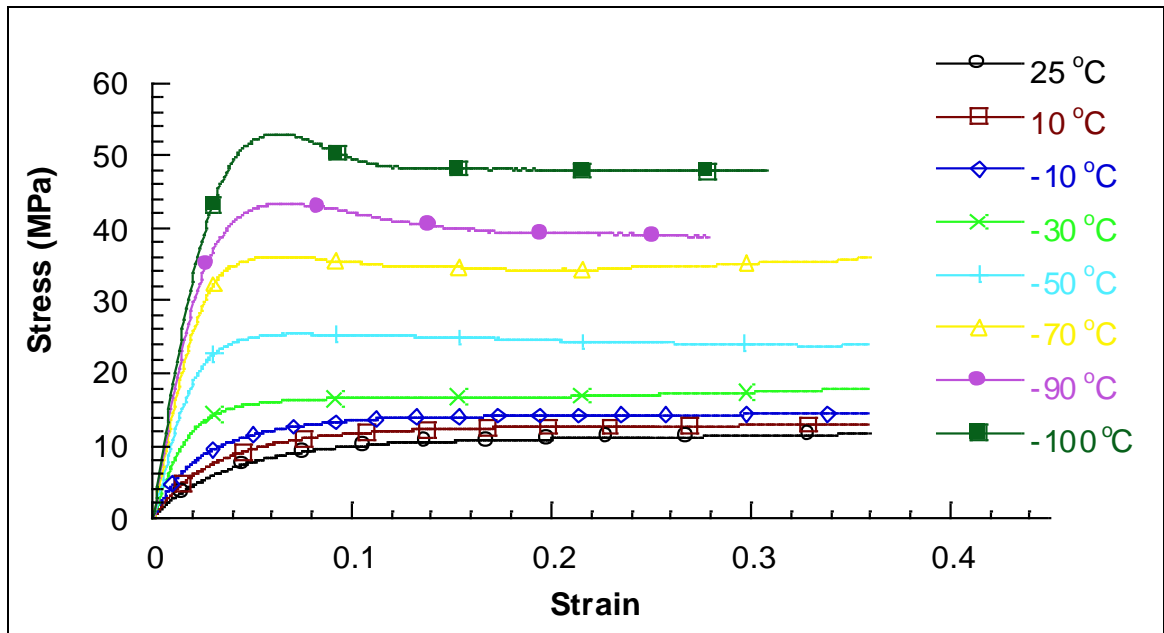
(d)

Figure 4.3. Stress-strain curve of (a) Pure LLDPE, (b) PE/1% MLS, (c) PE/1% amEP, (d) PE/1% amEP/1% MLS at different temperatures.

Temperature (^{o}C)	Sample	Yield stress (MPa)	UTS (MPa)	Elastic modulus E (GPa)
25	LLDPE	4.86	-	0.12
	PE/MLS 1	5.12	-	0.18
	PE/amEP 1	5.61	-	0.22
	PE/amEP 1/MLS 1	6.92	-	0.32
10	LLDPE	7.01	-	0.15
	PE/MLS 1	8.85	-	0.19
	PE/amEP 1	9.06	-	0.21
	PE/amEP 1/MLS 1	10.3	-	0.26
-10	LLDPE	11.38	-	0.26
	PE/MLS 1	10.84	-	0.32
	PE/amEP 1	11.67	-	0.38
	PE/amEP 1/MLS 1	12.15	-	0.42
-30	LLDPE	14.65	-	0.38
	PE/MLS 1	14.92	-	0.57
	PE/amEP 1	17.1	-	0.74
	PE/amEP 1/MLS 1	19.43	-	0.84
-50	LLDPE	17.86	18.8	0.52
	PE/MLS 1	19.87	21.52	0.77
	PE/amEP 1	22.34	23.62	0.98
	PE/amEP 1/MLS 1	24.3	25.4	1.04
-70	LLDPE	22.84	23.01	0.64
	PE/MLS 1	24.90	25.13	0.95
	PE/amEP 1	25.39	27.09	1.26
	PE/amEP 1/MLS 1	35.51	34.06	1.39
-90	LLDPE	21.18	27.54	1.15
	PE/MLS 1	29.57	31.61	1.24
	PE/amEP 1	30.34	40.4	1.31
	PE/amEP 1/MLS 1	37.1	43.3	1.54
-100	LLDPE	26.02	33.1	1.21
	PE/MLS 1	34.84	39.95	1.38
	PE/amEP 1	38.57	45.3	1.39
	PE/amEP 1/MLS 1	41.64	53.0	1.63

Table 4.3. Tensile test results of LLDPE nanocomposites at different temperatures.

Adding MLS to PE increased the yield stress and the elastic modulus. The addition of 1% amEP and 1% MLS gave the best performance. At room temperature, the material exhibited increased work hardening in all samples. As temperatures decreased,

the trends in mechanical properties were similar with the LLDPE < PE/MLS 1 < PE/amEP 1 < PE/amEP 1/MLS 1. A decreased work hardening, however, was evidenced by a drop in stress following UTS. This change in deformation mechanism occurred for tests below -50 ^{o}C. Below the β transition, an upper and lower yield deformation reflective of the relaxation processes in the matrix was evident in all samples.

4.3.3. Creep Test Results

Figure 4.4 shows the creep-recovery curves of LLDPE/amEP/MLS nanocomposites at room temperature. For an elastic material, complete recovery was obtained. All samples at room temperature showed an irrecoverable permanent deformation. This deformation explains the non-linear viscoelastic response of the material. The neat LLDPE showed the highest compliance and the highest permanent deformation.
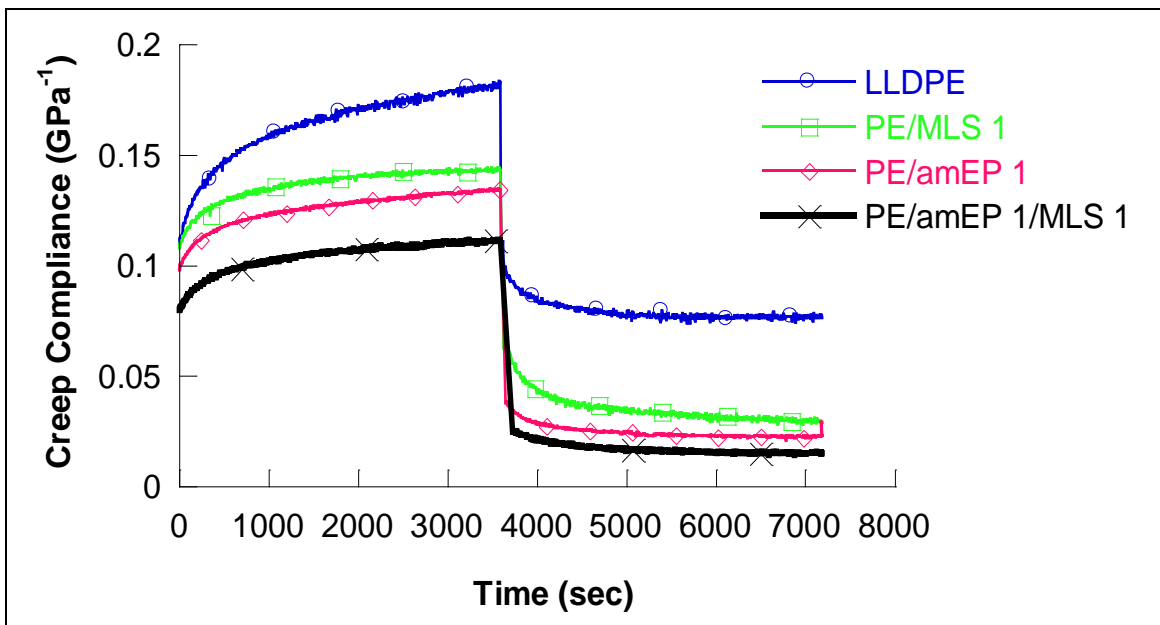
Figure 4.4. Creep-recovery curves of LLDPE nanocomposites at room temperature.

When 1% MLS was added, creep compliance decreased and the material showed more recovery. The addition of an elastic component (MLS) gave the matrix its stiffness (less creep) and elasticity (more recovery). The addition of the elastomeric amEP improved the recovery in the LLDPE/amEP 1 blend. When a combination of amEP/MLS was added to the PE matrix, the material showed the lowest creep compliance and the lowest unrecoverable deformation. This behavior mirrors the tensile test results where LLDPE/amEP 1/MLS 1 showed the highest modulus (lowest creep).

The effect of temperature on the creep properties is important in high- altitude balloons missions. Creep-recovery tests were performed on the LLDPE films at temperatures as low as -100 ^{o}C, which corresponds to high-altitude conditions. Figure 4.5 shows the creep-recovery curves of LLDPE nanocomposites at different temperatures. The results show the dependence of creep compliance on temperature.
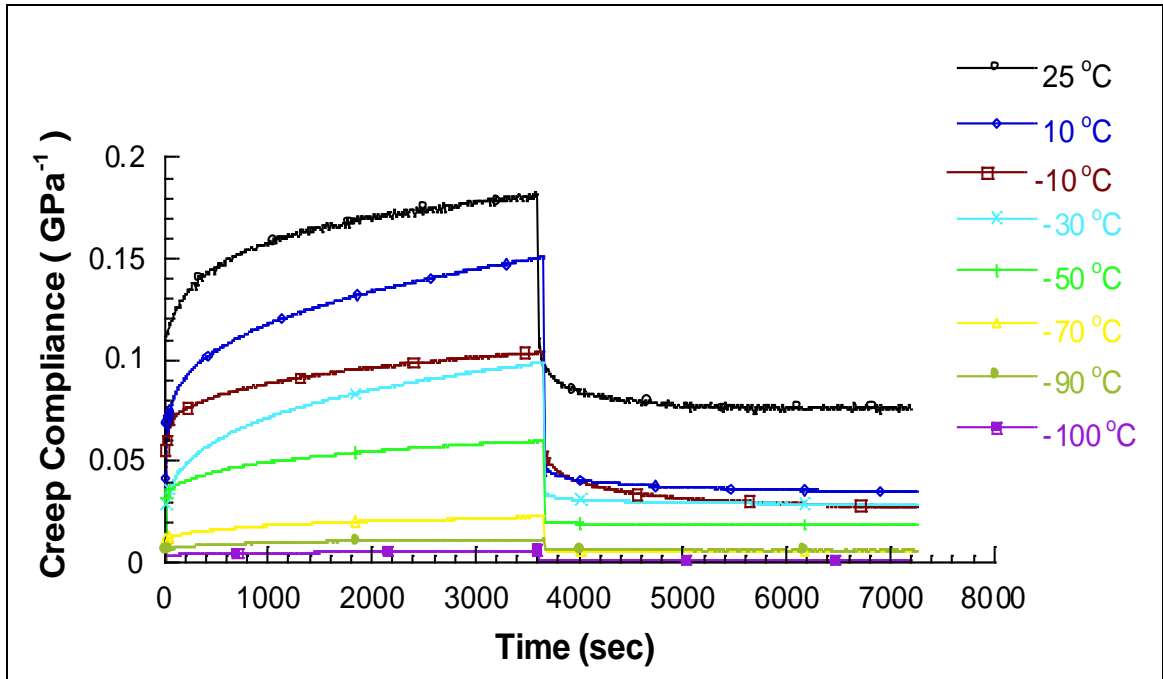
(a)
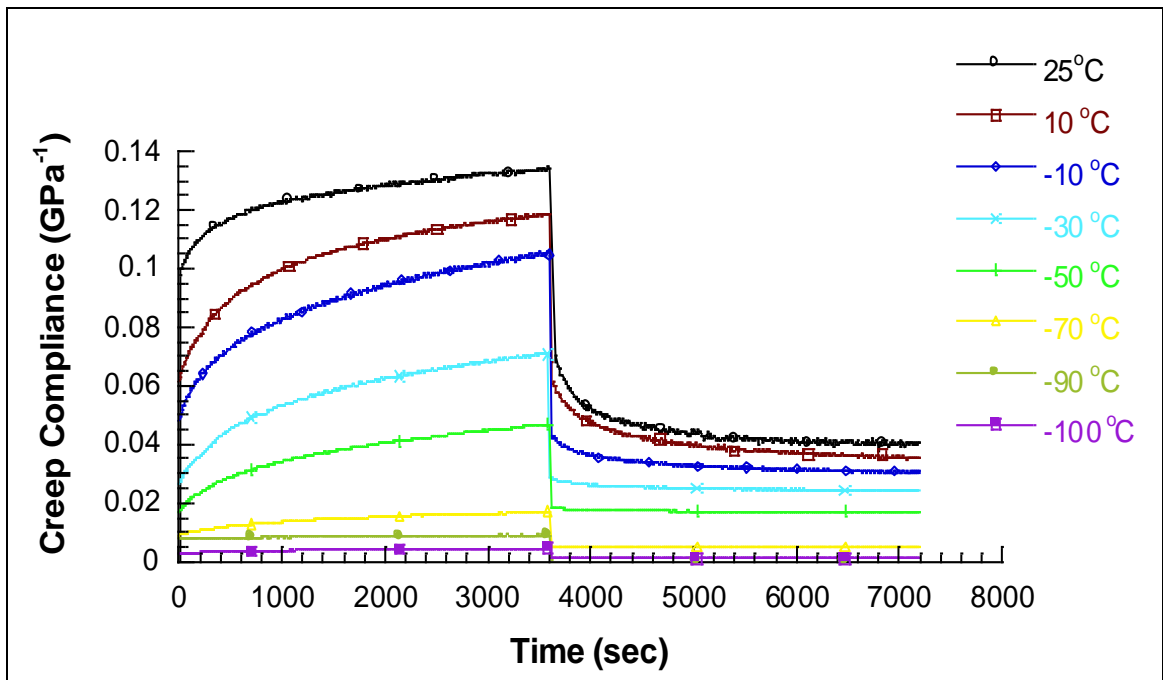
(b)
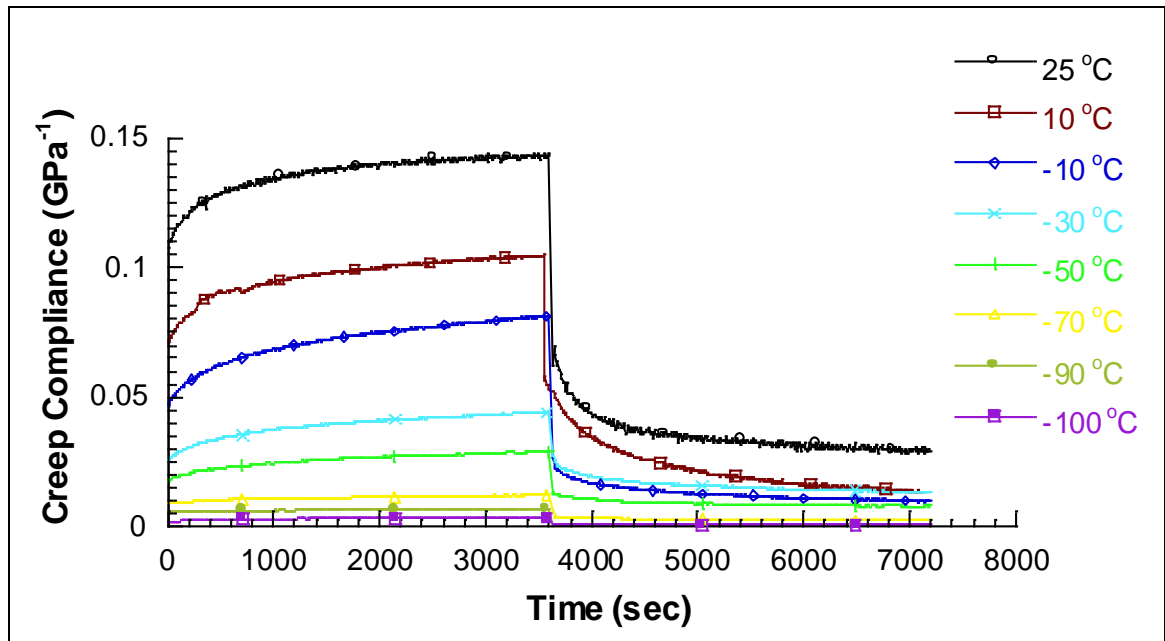
(c)
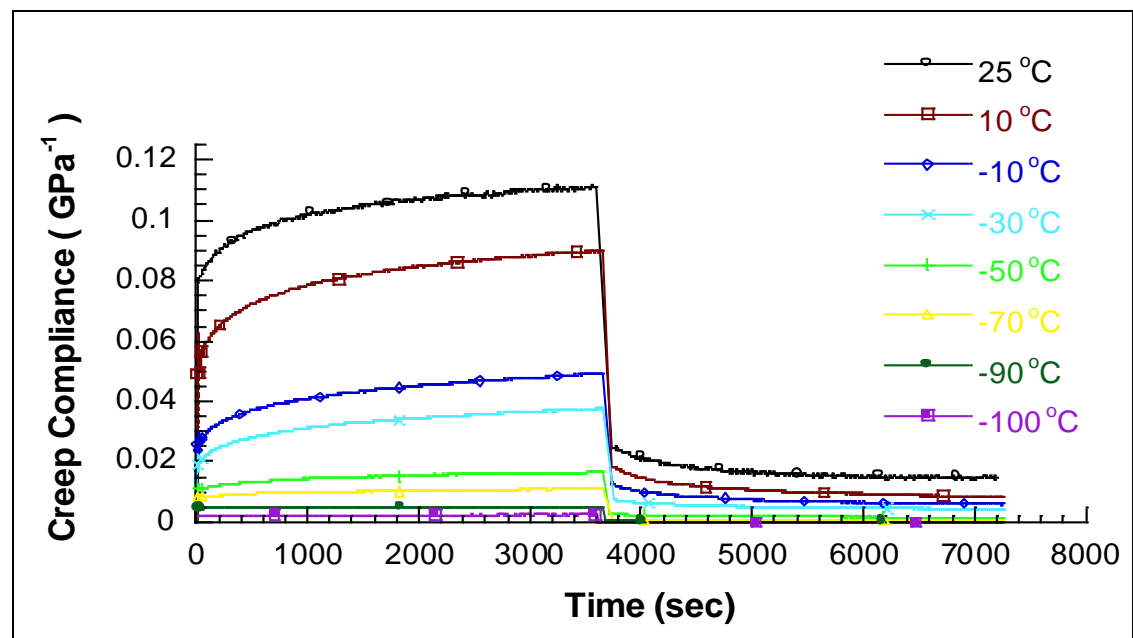
(d)

Figure 4.5. Creep-recovery of LLDPE nanocomposites: (a) pure LLDPE, (b) PE/1% MLS, (c) PE/1% amEP, (d) PE/1% amEP/1% MLS at different temperatures.

4.3.3.1. Creep-Recovery Analysis

In linear viscoelasticity,

$$\varepsilon_c(t - t_a) = \varepsilon_r(t - t_a)$$

where ε_c and ε_r are the creep and recovery strains, respectively; t_a is the time at unloading; and ε_p is the unrecovered plastic strain. If the strain is completely recoverable after removal of the applied load, the recovered strain will coincide with the recovered strain from the creep strain. However, if the material behaves in a non-linear viscoelastic manner, $\varepsilon_c(t-t_a)$ doesn't coincide with $\varepsilon_r(t-t_a)$ after the load is removed. Divergence of the creep strain from the creep strain shows that an irrecoverable plastic strain is produced by the applied load. Figure 4.6 shows a comparison of creep and recovery compliance of LLDPE nanocomposites at different temperatures.
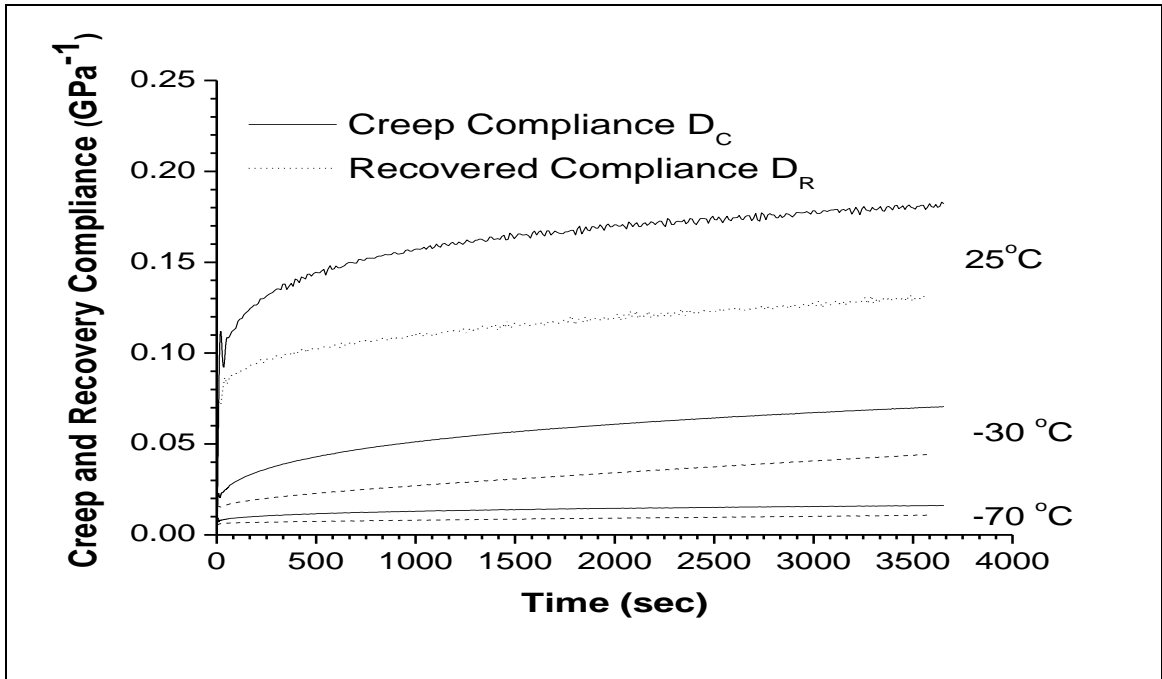
(a)
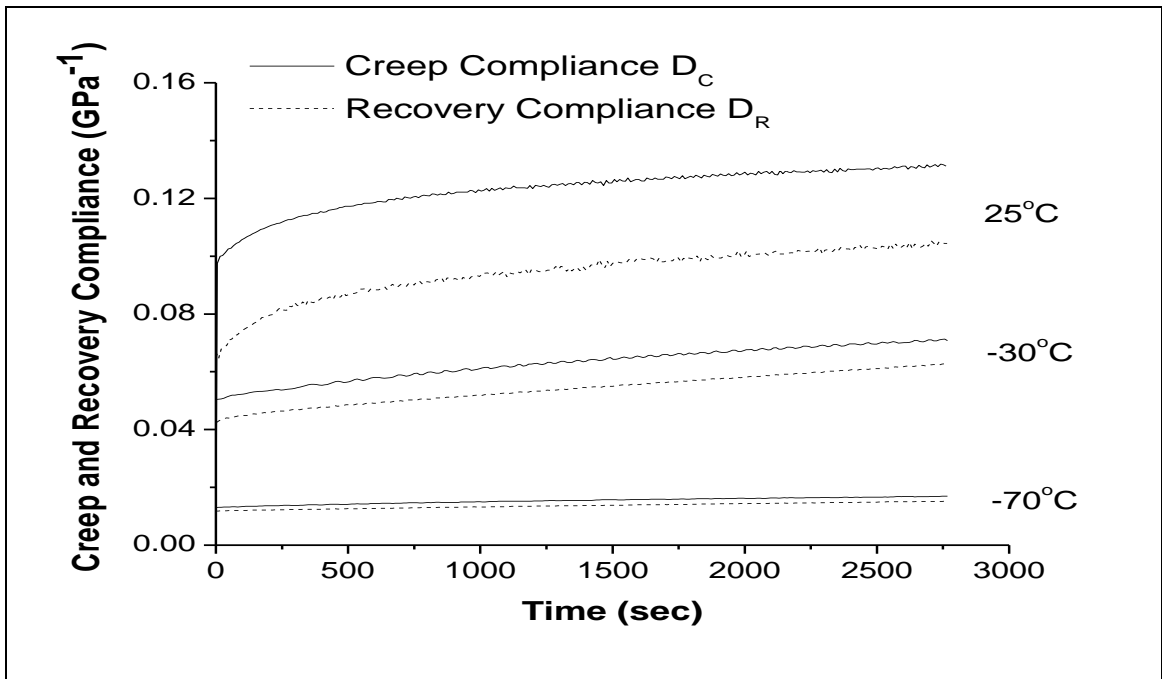
(b)
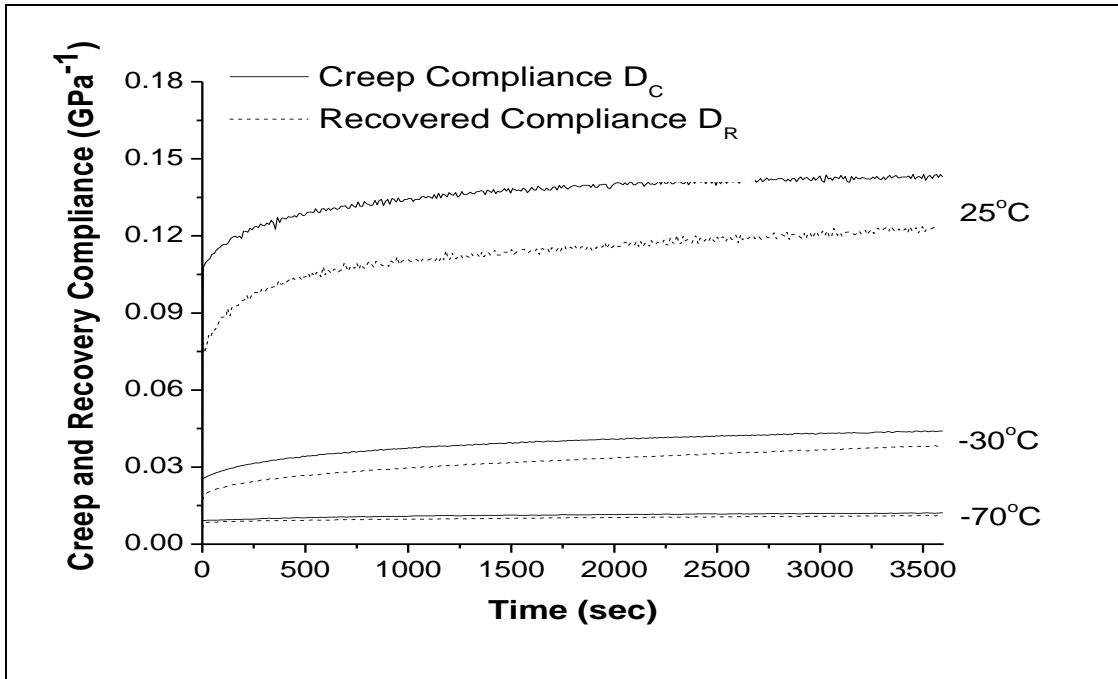
(c)
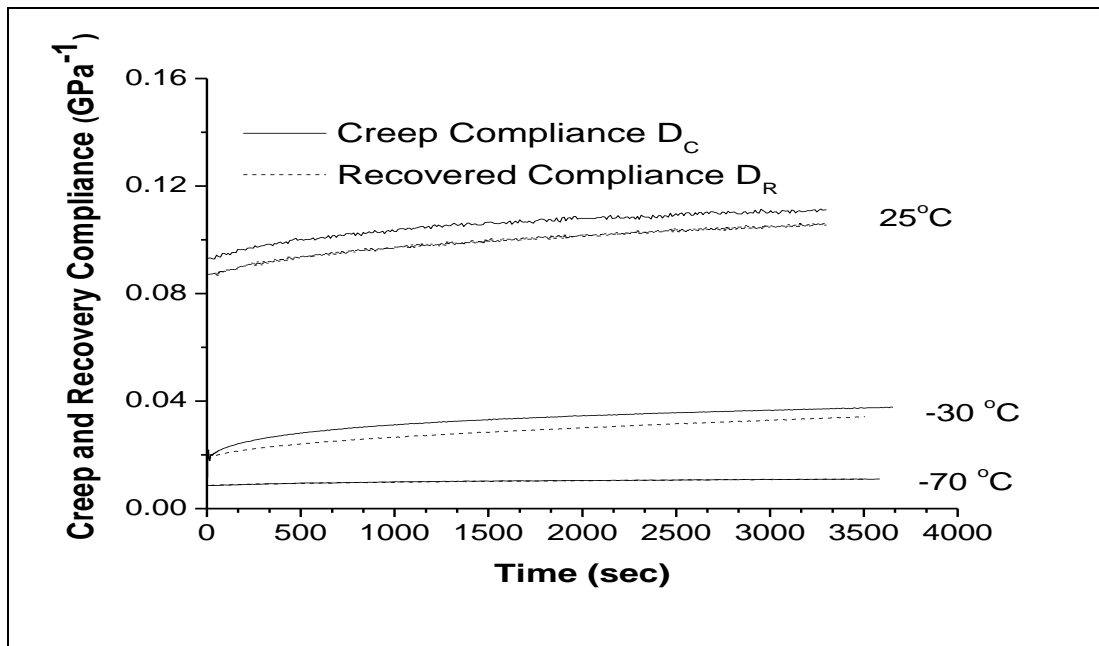
(d)

Figure 4.6. Creep-recovery analysis of LLDPE nanocomposites: (a) pure LLDPE, (b) PE/1% MLS, (c) PE/1% amEP, (d) PE/1% amEP/1% MLS at different temperatures.

At room temperature, creep compliance shows a reasonable divergence form the recovery compliance for all specimens. The addition of MLS with and without amEP to the neat PE matrix enhances the elasticity of the matrix and leads to a higher percentage of recovery (Table 4). This behavior suggests the role of MLS particles in the absence of crystallites. MLS particles act as hinges in the amorphous matrix; this action is reflected in higher modulus, higher yield strain, and more recovery. The same trend is observed at lower temperatures where the percentage of recovery of the nanocomposites is higher than that of the neat polymer matrix. This observation is supported by the dynamic mechanical data at low temperatures where the storage modulus E', which marks the elastic portion of deformation, increases with the addition of MLS.

4.3.3.2. Modeling Parameters of the Burgers Model

To evaluate the changes of the material properties with temperature, we used the Burgers model to fit the creep data at different temperatures. Figure 4.7 shows the experimental and theoretical creep results of pure LLDPE and LLDPE/amEP 1/MLS 1 at different temperatures. There is agreement between theoretical and experimental results at different temperatures. The results of the Burgers fit parameters for all temperatures are tabulated in Table 4.4.

(a)

(b)

103
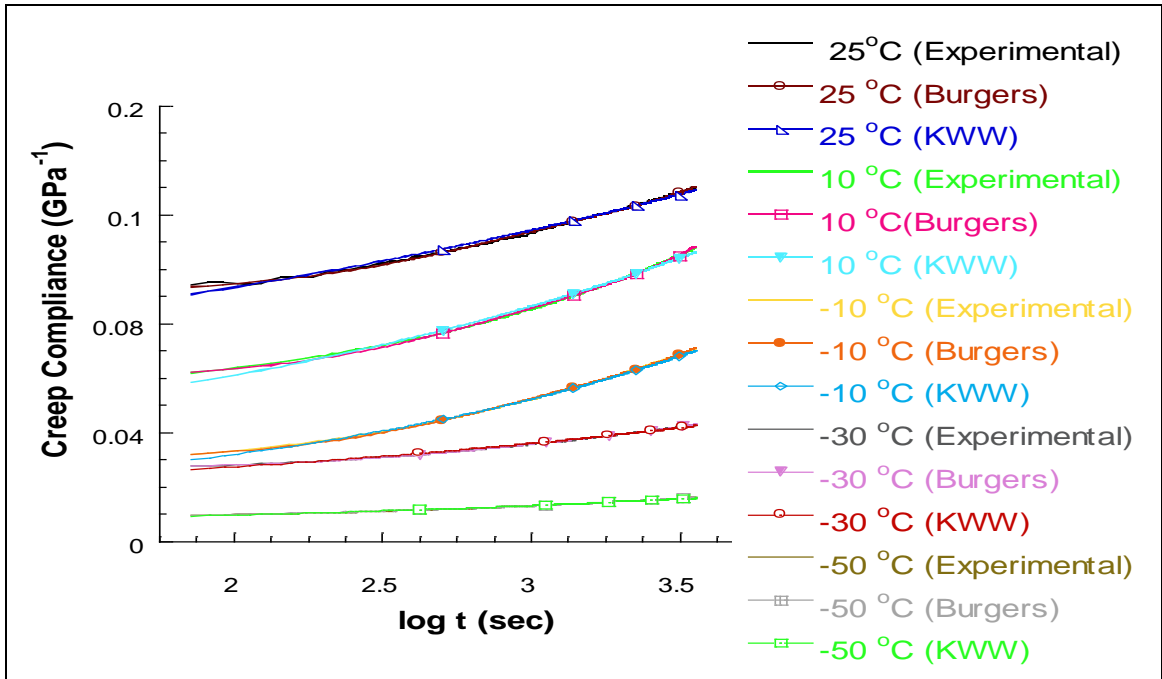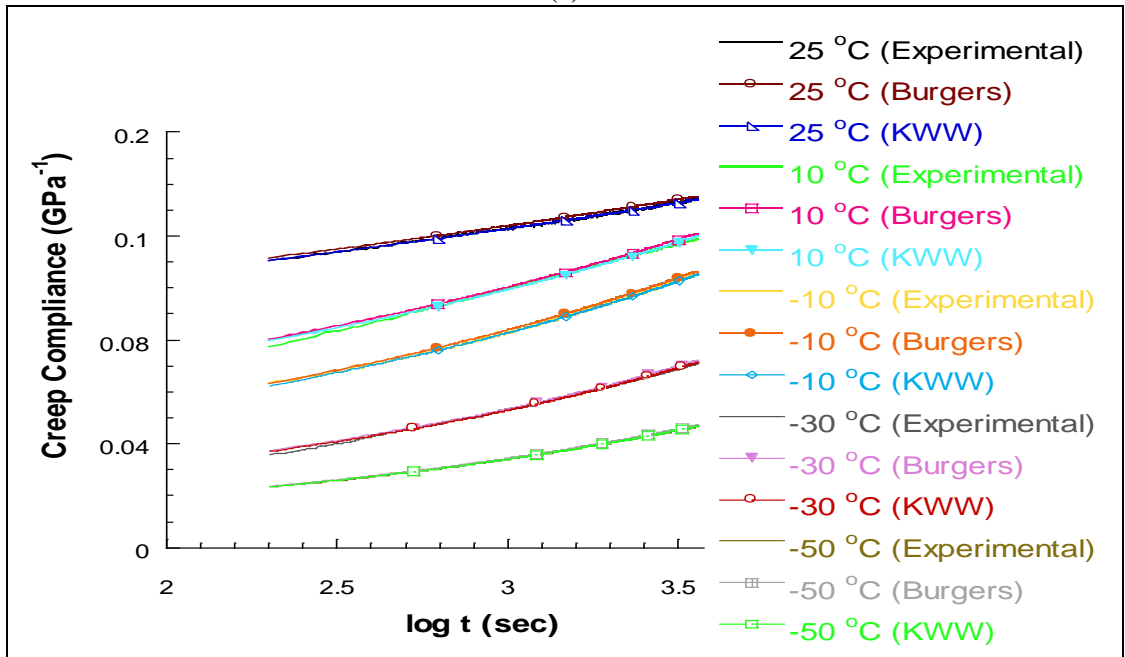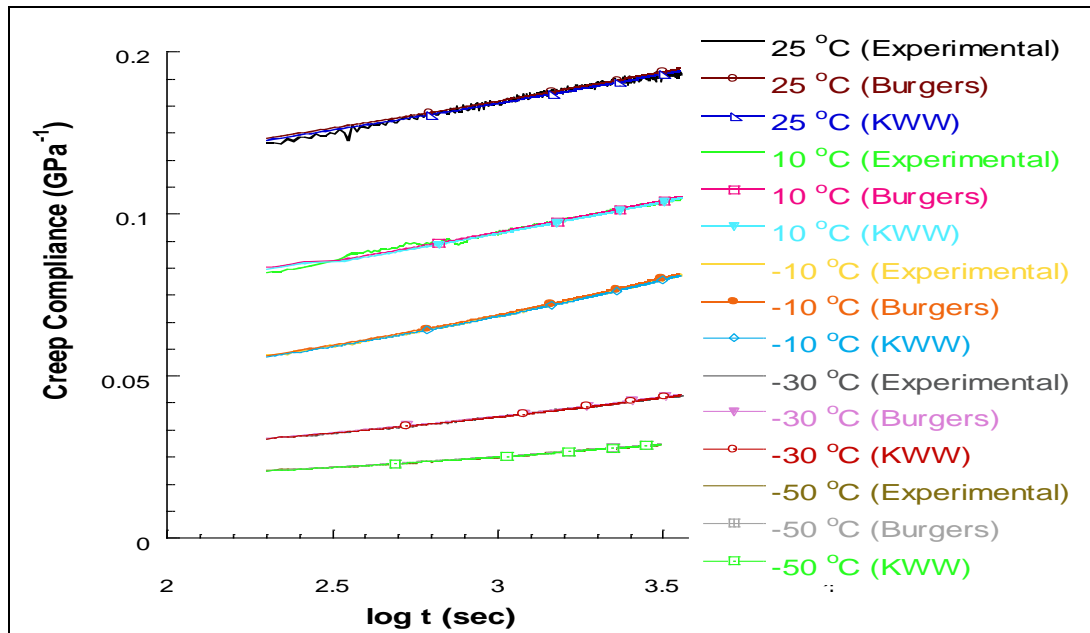
(c)
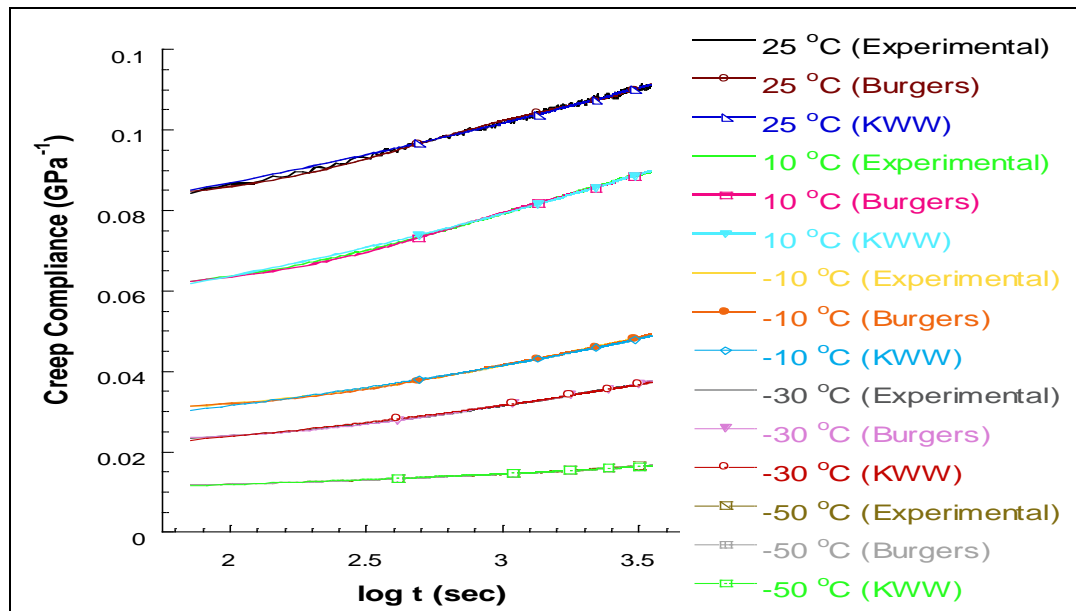
(d)

Figure 4.7. Experimental and theoretical (Burgers and KWW) results of LLDPE nanocomposites: (a) pure LLDPE, (b) PE/1% MLS, (c) PE/1% amEP, (d) PE/1% amEP/1% MLS at different temperatures.

| Temperature (^{o}C)	Sample	E_M (10^9 Pa)	E_K (10^9 Pa)	η_K (10^{11} Pa.s)	η_M (10^{12} Pa.s)	τ (sec)	% Recovery
25	LLDPE	0.09	0.29	1.52	1.32	528	72
	PE/MLS 1	0.08	0.31	1.54	2.75	493	95
	PE/amEP 1	0.09	0.52	2.64	3.39	482	88
	PE/amEP 1/MLS 1	0.12	0.66	3.53	4.83	472	95
10	LLDPE	0.11	0.47	2.35	2.45	512	76
	PE/MLS 1	0.11	0.31	1.46	2.96	498	95
	PE/amEP 1	0.12	0.52	2.57	3.92	467	88
	PE/amEP 1/MLS 1	0.13	0.74	3.86)	4.72	449	95
-10	LLDPE	0.13	0.52	2.36	3.35	476	76
	PE/MLS 1	0.15	0.43	1.95	3.61	461	95
	PE/amEP 1	0.21	0.66	3.27	3.86	446	89
	PE/amEP 1/MLS 1	0.28	1.09	4.92	4.84	436	96
-30	LLDPE	0.29	0.55	2.33	4.76	451	77
	PE/MLS 1	0.29	0.49	2.21	4.89	439	95
	PE/amEP 1	0.32	0.71	3.41	4.65	422	89
	PE/amEP 1/MLS 1	0.37	1.39	6.26	5.19	420	96
-50	LLDPE	0.30	1.34	6.23	4.78	538	78
	PE/MLS 1	0.45	1.16	5.93	5.62	529	95
	PE/amEP 1	0.48	1.00	5.06	4.56	518	90
	PE/amEP 1/MLS 1	0.75	1.49	7.07	8.49	505	97
-70	LLDPE	0.92	1.28	6.21	8.74	564	79
	PE/MLS 1	0.84	1.10	5.92	8.48	576	95
	PE/amEP 1	0.89	0.91	4.88	10.95	535	90
	PE/amEP 1/MLS 1	0.91	1.46	7.78	15.03	521	97
-90	LLDPE	1.28	1.22	5.96	9.44	487	79
	PE/MLS 1	1.39	1.09	5.91	11.29	541	96
	PE/amEP 1	1.47	0.90	4.84	15.57	538	91
	PE/amEP 1/MLS 1	1.66	1.38	7.39	25.82	526	98
-100	LLDPE	1.63	1.15	5.68	12.05	573	80
	PE/MLS 1	1.76	1.04	5.72	15.86	548	96
	PE/amEP 1	1.86	0.77	4.18	18.21	564	91
	PE/amEP 1/MLS 1	1.98	1.28	7.04	32.28	528	98

Table 4.4. Burgers modeling parameters of LLDPE nanocomposites at different temperatures.

4.3.3.2.1. Time-Independent Elasticity E_M

The Burgers constitutive equation shows that the modulus E_M of the Maxwell spring determines the instantaneous elastic creep strain, which can be immediately recovered on removal of stress. In general, the nanocomposites showed higher values of E_M than the neat matrix at each temperature. Among the nanocomposites, LLDPE/amEP 1/MLS 1 behaved with the highest elasticity. In the case of LLDPE/MLS systems, the nanoclay layers could bear load because of the large aspect ratio of individual platelets while discounted by the slippage of stacks and large amount of unexfoliated layers. Hence, the resulting E_M of LLDPE/amEP 1/MLS 1 was higher than that of the neat matrix.

The variations of E_M of the tested materials under various temperatures illustrated the reinforcing characteristics of the nanofiller. The E_M of each specimen showed an increasing tendency with decreasing temperature, which could be explained by the fact that the bulk materials became stiffer at lower temperatures and the stiffness was thus increased with a higher instantaneous modulus as depicted by the tensile test results (Table 4.3).
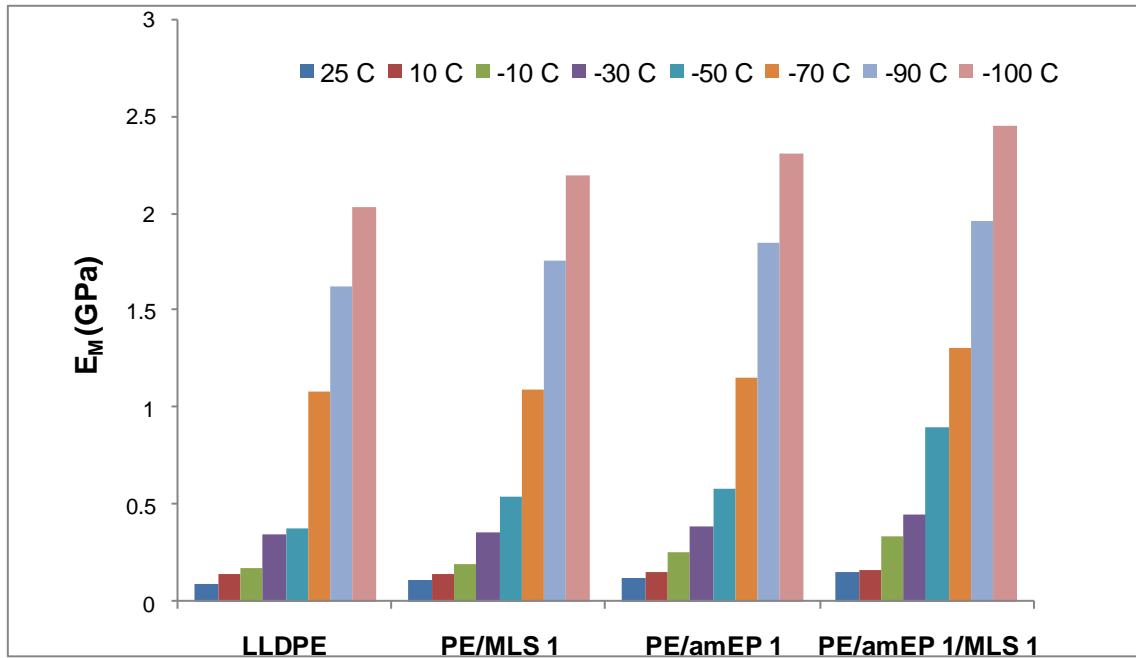
Figure 4.8. Temperature dependence of Burgers E_M.

At 25 ^oC, the E_M showed comparatively small changes between the neat PE matrix and the nanocomposites, and the instantaneous elasticity was not altered much by the addition of nanofiller. The instantaneous elasticity E_M corresponded reasonably to the elasticity of the crystalline part of the polymer, which took the immediate load because of the high stiffness compared to the amorphous polymer. The crystallinity of each specimen was not obviously altered with the addition of the MLS particles [14], which implied that the load bearing parts between the neat matrix and the nanocomposites were not greatly different.

As temperature was decreased to lower temperatures reaching -100 ^oC, E_M of each specimen increased. Among the observed specimens, the nanocomposites behaved with

much better elasticity than the pure matrix, showing an effective reinforcement by the addition of nanofiller.

At -100 $^{\circ}$C, E_M increased from 1.63 GPa for the pure LLDPE to 1.98 for the addition of 1% of amEP and MLS. These results depict the contribution of amEP and MLS to the elasticity of the bulk material. Below the β-transition temperature, polymer chains began to become less active. Consequently, the stiffness of bulk material increased, which resulted in the higher value of E_M compared to that at room temperature.

4.3.3.2.2. Retardant Elasticity E_K and Viscosity η_K

The retardant elasticity E_K and viscosity η_K of each specimen showed a similar dependency as the instantaneous elasticity E_M, increasing with decreasing temperature. The deformation of the Kelvin unit of each material also decreased with the decreasing temperature. The time-dependent E_K and η_K in the Kelvin unit are associated with the stiffness and viscous or oriented flow of amorphous polymer chains in the short term, respectively.

E_K and η_K of the nanocomposites increased considerably with decreasing temperature, showing high-temperature dependency. The materials with relatively higher bulk modulus deformed very little at lower temperatures, which showed that the Kelvin unit behaved with higher modulus and lower viscous flow. With decreasing temperature, the orientation movement of amorphous chains, including elastic deformation and viscous flow, became difficult, resulting in the higher E_K and η_K.

E_K and η_K were used to determine the retardation time $\tau = \eta_K/E_K$. Ideal elastic materials display an immediate recovery after loading and subsequent removal of the load. In the case of viscoelastic materials, there is a time delay for recovery. The retardation time is the delayed response to an applied force or stress. Figure 4.9 shows the temperature dependence of the retardation time obtained from Burgers fit. The consistent change of E_K and η_K with temperature led to a lower retardant time τ for the LLDPE/amEP 1/MLS 1 nanocomposite as illustrated in Table 4.4.
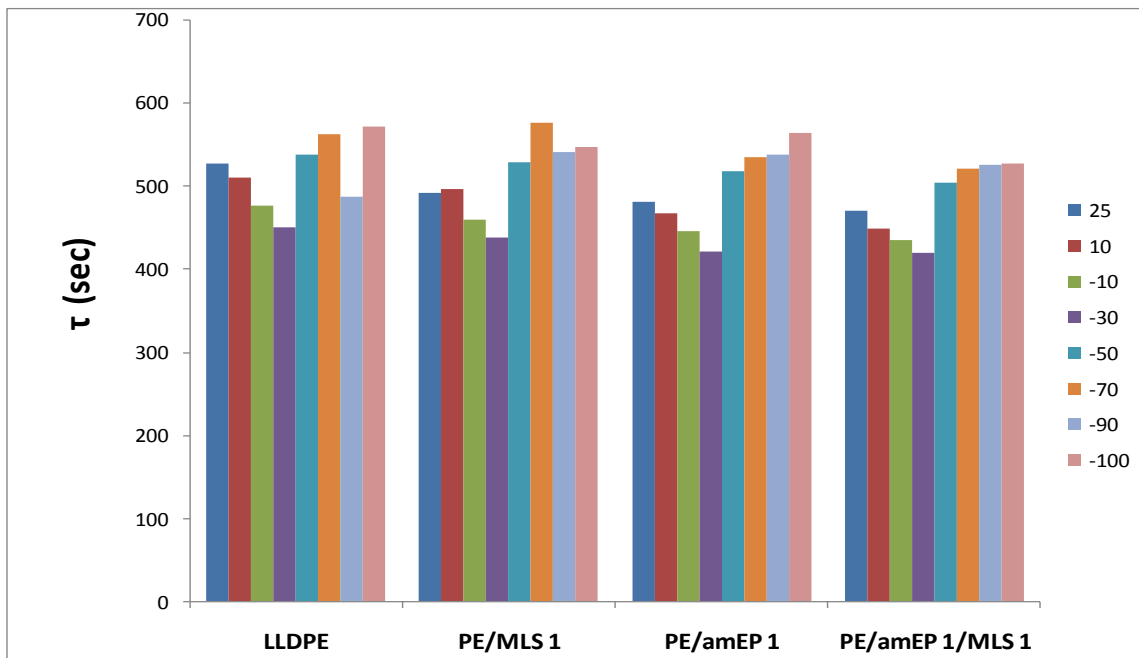
Figure 4.9. Temperature dependence of Burgers τ.

The nanofiller showed reinforcing effectiveness on the Kelvin unit. The nanoclay layers were the most effective in retarding the deformation of the Kelvin elements resulting in lower retardation times at temperature lower than room temperature.

At temperatures below the β-transition temperature, the amorphous polymer becomes less active. Thereafter, the polymer chains have restricted mobility. The Kelvin unit could not be deformed further; therefore, a higher retardant time τ is observed.

4.3.3.2.3.   Permanent Viscous Flow η_M

Following the discussion of the effect of the addition of amEP and MLS on the instantaneous and time-dependent recoverable parameters in the Burgers constitutive equation, it is of importance to provide an analysis of η_M which represents the irrecoverable creep in a creep-recovery experiment. The effect of temperature on such parameter is presented in Table 4.4.

From Table 4.4, it can be seen that η_M is strongly dependent on temperature. It can be considered that η_M is associated with the damage from crystallized polymer or oriented noncrystalline regions, such as the pulling out of chain folds by a crystal slip process and the breaking of an intercrystalline tie molecule or the irreversible deformation from amorphous regions, such as breaking of bridging segments between the clay particles and the polymer chains.

At room temperature, η_M of the pure LLDPE increases with the addition of 1% amEP and 1% MLS separately. The value of η_M increases from 1.32 for pure LLDPE to 4.83 with the addition of 1% amEP and 1% MLS as illustrated in Table 4. The results show that no damage of the crystallized polymer occurred due to the fact that the stress levels applied are still within the elastic limits of the crystallized part of the polymer. The enhanced deformation resistance was obtained to the presence of amEP and MLS in the

LLDPE nanocomposite which acted to form a stiff structure together with the crystallized molecules.

As temperature is decreased below the β-transition temperature, η_M significantly increases. The irreversible deformation is diminished by the addition of amEP and MLS to the LLDPE matrix, which enhanced the elasticity of the nanocomposites at lower temperatures. The results are supported by the higher % recovery obtained with the addition of amEP and MLS.

4.3.3.3. Viscoelastic Response

To compare the creep compliance obtained for the different compositions, creep compliance curves were fitted with the KWW stretched exponential function,

$$D(t) = D_0[1 - \exp(-t/\tau)^{\beta}]$$

where D(t) is the creep compliance, τ is the characteristic retardation time, and β is a creep shape parameter. The results of the curve fit parameters are tabulated in Table 4.5. OriginLab® nonlinear least-squares data analysis software was used for the numerical analysis of the creep compliance curve fits.

Temperature ($^{\mathrm{o}}$C)	Sample	τ_{KWW}	β_{KWW}
25	LLDPE	1.47	0.50
	PE/MLS 1	0.89	0.21
	PE/amEP 1	0.93	0.19
	PE/amEP 1/MLS 1	0.86	0.21
10	LLDPE	0.75	0.26
	PE/MLS 1	0.64	0.27
	PE/amEP 1	0.82	0.22
	PE/amEP 1/MLS 1	0.75	0.24
-10	LLDPE	0.64	0.31
	PE/MLS 1	0.61	0.31
	PE/amEP 1	0.68	0.27
	PE/amEP 1/MLS 1	0.69	0.27
-30	LLDPE	0.53	0.33
	PE/MLS 1	0.54	0.33
	PE/amEP 1	0.69	0.27
	PE/amEP 1/MLS 1	0.67	0.28
-50	LLDPE	0.68	0.28
	PE/MLS 1	0.53	0.34
	PE/amEP 1	0.72	0.27
	PE/amEP 1/MLS 1	0.80	0.26
-70	LLDPE	0.70	0.32
	PE/MLS 1	0.60	0.29
	PE/amEP 1	0.86	0.23
	PE/amEP 1/MLS 1	0.91	0.23
-90	LLDPE	0.66	0.26
	PE/MLS 1	0.64	0.24
	PE/amEP 1	0.90	0.22
	PE/amEP 1/MLS 1	0.95	0.22
-100	LLDPE	0.68	0.21
	PE/MLS 1	0.66	0.21
	PE/amEP 1	0.92	0.20
	PE/amEP 1/MLS 1	0.99	0.21

Table 4.5. KWW fit parameters of LLDPE nanocomposites at different temperatures.

Figures 4.10 and 4.11 compare the KWW fit parameters of LLDPE nanocomposites at different temperatures. A retardation time represents resistance offered by the microstructure to the elastic deformation of the system. As retardation time decreases (less resistance occurs), system response becomes more elastic.
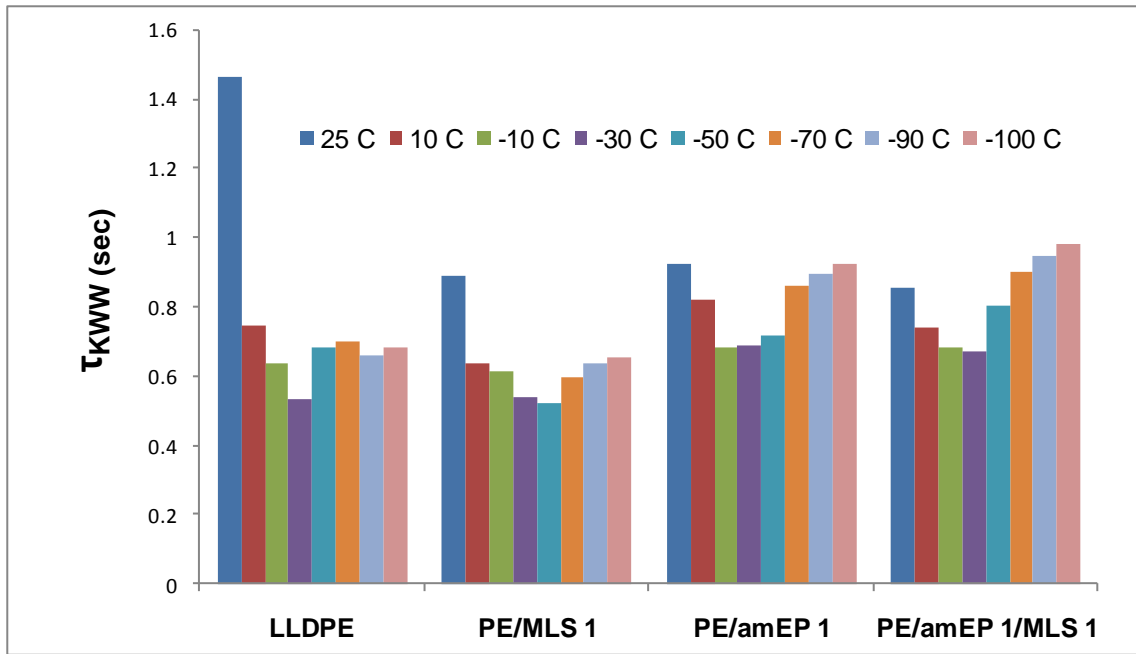
Figure 4.10. Temperature dependence of retardation time values obtained from the KWW fit.
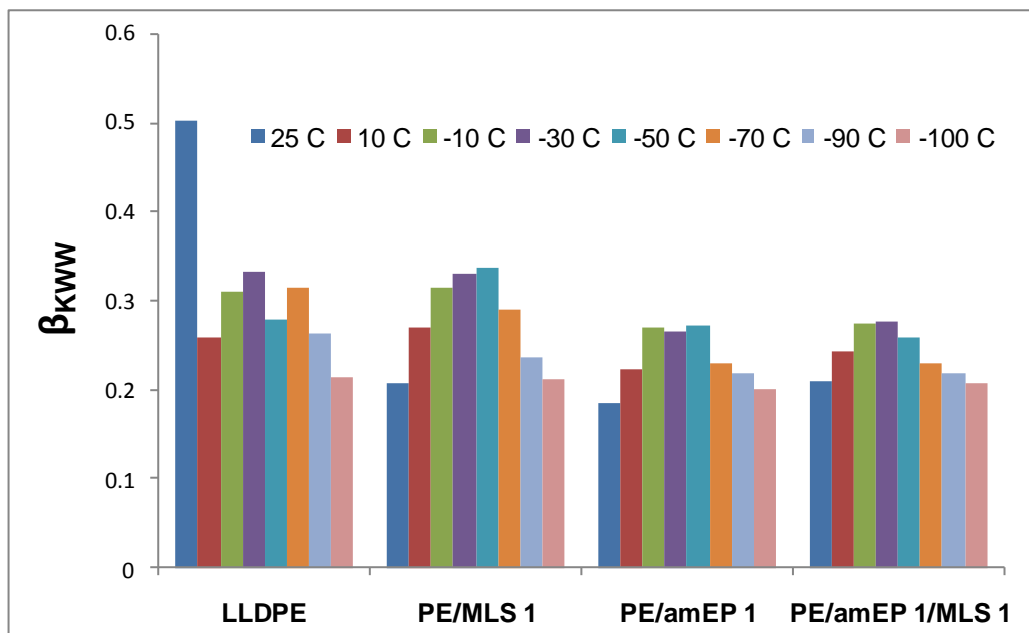
Figure 4.11. Temperature dependence of β values obtained from the KWW fit.

The general trend observed in the retardation time for the LLDPE nanocomposites can be summarized as follows: Retardation time decreases linearly with decreasing temperature above the β-transition temperature. Below the β-transition temperature, retardation time increases linearly with decreasing temperature. This behavior is exhibited because below the β-transition temperature, the material is in its glassy state where molecular mobility is hindered, reducing the polymer elasticity.

Comparing the retardation time among the different LLDPE compositions, we observed that the addition of MLS reduced the retardation time as compared to the neat PE. This reduction can be attributed to the addition of the rigid MLS platelets, which increases the matrix elasticity. Addition of amEP into the LLDPE matrix further increased retardation time. This increase can be related to the amorphous nature of the

compatibilizer. A combination of amEP and MLS seemed to reduce the retardation time above the β-transition temperature and to increase it below the β-transition temperature.

Figure 4.11 shows the variation of β at different temperatures of LLDPE nanocomposites. Considering pure LLDPE, as temperature decreases, β values increase, indicating a broader distribution of retardation times. β reaches a maximum at -30 ^{o}C (β-transition temperature). Below -30 ^{o}C, β decreases linearly with decreasing temperature.

The same trend is observed with the addition of amEP and MLS separately and combined with the LLDPE matrix. The values of β do not show a significant change with the addition of 1% MLS. Addition of 1% amEP reduces the β values; the values remain unchanged with the addition of 1% of amEP and 1% MLS. According to the coupling theory proposed by Ngai et al. [16], a decrease in the β parameter can be interpreted as a strengthening of the coupling between the relaxing species and the medium and is related to an overall decrease of the molecular mobility. It is known that the crystalline phase hinders the molecular mobility of the amorphous one [17]. A decrease of β measured by a differential scanning calorimeter (from 0.4 to 0.2) was detected for amorphous and semi-crystalline polyethylene terephthalate (PET), respectively [18].

4.4. Conclusions

The creep behavior of LLDPE nanocomposites at different temperatures was analyzed. Creep compliance decreased with the addition of MLS particles. This effect was related to the enhancement of the tensile properties. The reduction in creep compliance with the addition of the clay leads to a material with higher dimensional stability; the materials behaved with higher stiffness and lower deformability under long-term loading situations because of the addition of inorganic nanofiller.

For the Burgers model, the instantaneous modulus E_M, the retardant modulus E_K, and viscosity η_K showed an explicit dependence on temperature. They also increased with the addition of clay. E_M showed an increase with decreasing temperature, which was also reflected in an increase of the yield stress and modulus of the materials with decreasing temperature.

Above the beta transition temperature, a decrease in the retardation time and an increase in the β values were observed with decreasing temperature. Below this temperature, the trends were reversed. This behavior was explained by the hindered mobility of the amorphous region.

4.5. References

1. K.K. Maniar., *Polymer-Plastics Tech. and Eng.*, **43**, 427-443 (2004).

2. D. Martin, P. Halley, R. Truss, M. Murphy, O. Jackson, and O.Y. Kwon, *Polym.*, 1774-1779(2003).

3. G. Liang, J. Xu, S. Bao, and W. Xu, *J. Appl. Polym. Sci.*, **91**, 3974-3980 (2004).

4. G. Malucelli, S. Ronchetti, N. Lak, A. Priola, N.T. Dintcheva, and F.P. La Manta, *Eur. Polym. J.*, **43**, 328-335 (2007).

5. J.J. Aklonis and W.J. MacKnight. *Introduction to Polymer Viscoelasticity*, John Wiley & Sons: New York (1983).

6. C.J. Perez, V.A. Alvarez, and A. Vasquez, *Mat. Sci. and Eng. A*, **480**, 259-265 (2008).

7. J.L. Yang, Z. Zhang, A. Schlarb, and K. Friedrich, *Polym,* **47**, 6745-6758 (2006).

8. A. Ranade, K. Nayak, D. Fairbrother, and N.A. D'Souza, *Polym,* **46**, 7323-7333 (2005).

9. A.D. Nunez, N.E. Marcovich, and M.I. Aranguren, *Polym. Sci. and Eng.*, **44**, 1594-1603 (2004).

10. C. Marais and G. Villoutreix, *J. Appl. Polym. Sci.*, **69**, 1983-1991 (1998).

11. M.D. Alvarez, W. Canet, F. Cuesta, and M. Lamua, *Z Lebensm Unters Forsch A*, **207**, 356-362 (1998).

12. J. Beckmann and G.B. McKenna, *Polym. Eng. and Sci.*, **37**, 1459-1468 (1997).

13. J.M. Cheriere, L. Belec, and J.L. Gacougnolle, *Polym. Eng. and Sci.*, **37**, 1664-1671 (1997).

14. A. Shaito, D. Fairbrother, J. Sterling, N.A D'Souza, "*Nonlinear creep deformation in PE nanocomposites: effect of amorphous maleated PE compatibilizers on room temperature creep*", *Polym. Eng. and Sci*, submitted (2008).

15. M. Niaounakis and E. Kontou, *J. Polym. Sci.: Part B: Polym. Phys.,* **43**, 1712-1727 (2005).

16. K.L. Ngai, A.K. Rajagopal, and S. Teitler, *J. Chem. Phys.*, **88**, 5086 (1988).

17. N.G. McCrum, B.E. Read, and G. Williams, *Anelastic and Dielectric Effects in Polymeric Solids*, Dover, New York, (1991).

18. N.M. Alves, J.F. Mano, E. Balaguer, J.M. Meseguer Duenas, and J.L. Gomez Ribelles, *Polym.*, **43**, 4111-4122 (2002).

CHAPTER 5

EFFECT OF STRESS ON ROOM TEMPERATURE MOLECULAR RELAXATION

5.1. Introduction

Polymer nanocomposites (PNs) have generated significant interest in science and engineering over the past years [1-4]. The time independent mechanical properties of polymer nanocomposites have been well investigated [5-6]. In most practical applications, isothermal compliance of the polymeric material not only depends on stress but also on time, and hence the time-dependent response i.e. , creep behavior is of significant importance [7].

The theoretical background of creep behavior in solid polymers is well studied within the range of linear viscoelasticity [8]. In this region, the creep compliance is assumed to be a function of time only, and not of stress and strain. Beyond a certain strain limit, the isothermal creep compliance becomes a function of time and stress (or strain). This non-linear viscoelastic behavior plays an important role in most applications [9]. Liu et al. [10] studied the nonlinear viscoelastic creep of polyethylene (PE). They found the material response to be dependent on stress. The nonlinear time dependent response of the material was modeled using multiple Kelvin elements. The validation of the model is done by comparison with tensile test result. Yang et al. [11] modeled the long term performance of polyamide 66 nanocomposites using Burgers viscoelastic creep model. The variations in the simulating parameters were used to study the variation of the

material properties with stress. The predicting results showed the enhancement in the creep resistance even at extended long time scale.

Several mechanical models have been used to explain the creep, recovery, and stress relaxation aspects of polymeric materials of which the spring-dashpot model; Maxwell-Voigt model and Burger model, and models based on distribution functions like the Kohlrausch-Williams-Watts (KWW) function are commonly used. The KWW function, which is an empirically stretched exponential function, is mainly used to explain the time-dependent behavior of amorphous materials [12]. In this paper, the structure-property relationship is carried out by the parameters analysis of the Burgers model at different stress levels to account for the nonlinear behavior. The variations of these parameters illustrate the influence of the fillers on the creep resistance of the bulk LLDPE matrix. Also, the breadth of relaxation is considered by analyzing the fit parameters of the KWW exponential stretched function.

5.2. Experimental

5.2.1. Materials

LLDPE DOWLEX 2056G (Dow chemical company) was used to prepare the PE nanocomposite films (density = 0.92 g/cc; Melt index = 1.0 gm/10 min). Montmorillonite-layered silicate (MLS) (Cloisite 15A™), supplied by southern clay products, was used as the nanofiller. An amorphous maleic anhydride functionalized elastomeric copolymer, Exxelor VA 1803 (ExxonMobil corporation), was used as a compatibilizer between the MLS and the PE matrix. Exxelor VA 1803 has a nominal

density of 0.86 g/cm^3 and a melt index of 3 g/10 min (ASTM D1238, 230 $^{\circ}$C, 2.16 kg). The maleic anhydride (MA) level is in the range of 0.5 to 1%.

5.2.2. Sample Preparation

Nanocomposites were compounded with a Haake TW100 twin-screw extruder with a temperature profile of 200, 200, 205, and 210 $^{\circ}$C for zones 1 to 4, respectively. PE films 1.5 mil (0.04 mm) thick were processed with a Killion single-screw extruder (L/D = 24:1), fitted with a dual-lip air ring and a die diameter of 2 inches. Blends of PE+amEP+MLS were made, and the mixtures were compounded and pelletized. The compounded pellets were then processed into a blown film. Table 5.1 summarizes the concentrations used.

Sample	LLDPE (wt %)	Exxelor VA 1803 (wt %)	MLS (wt %)
LLDPE	100	0	0
PE/MLS 1	99	0	1
PE/amEP 1	99	1	0
PE/amEP 1/MLS 1	98	1	1

Table 5.1. Summary of concentrations used.

5.2.3. Tensile Testing

Yield stress and elastic modulus E were determined by using RSA III films fixture with an extension rate of 0.208 mm/min.

5.2.4. Creep Testing

Uniaxial tensile creep tests were performed by using RSA III with the films attachment. The desired constant stress to be applied for each measurement was calculated to be 10, 25, and 50% of the yield stress. The constant stress was applied for 1 hour of loading followed by 1 hour of unloading. A linear displacement transducer with a force capacity of 35 N was used to monitor the strain during the experiment. The creep compliance was calculated by the ratio of the measured creep strain to the initial applied stress.

5.3. Results and Discussion

5.3.1. Stress Dependence of Creep-Recovery Response

The experimental data of creep of LLDPE nanocomposites at various stress levels is shown in Figure 5.1, where the creep compliance D (t) is defined as the ratio of the measured time-dependent strain, ε (t), to the applied stress σ.
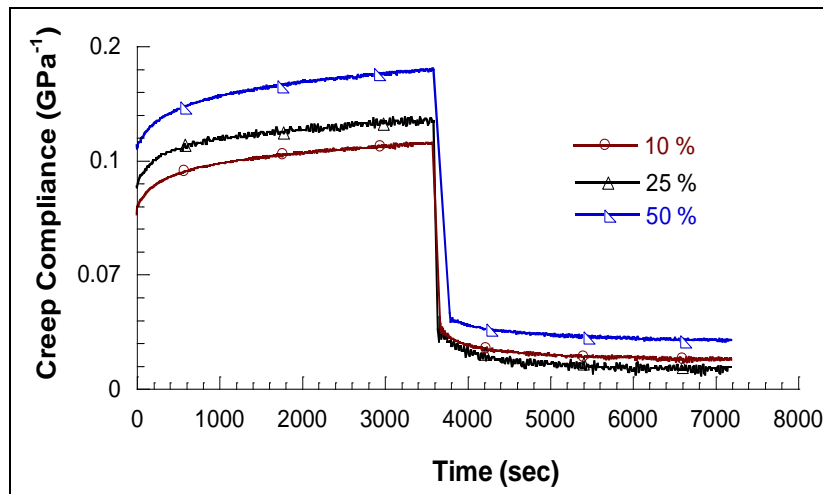
(a)
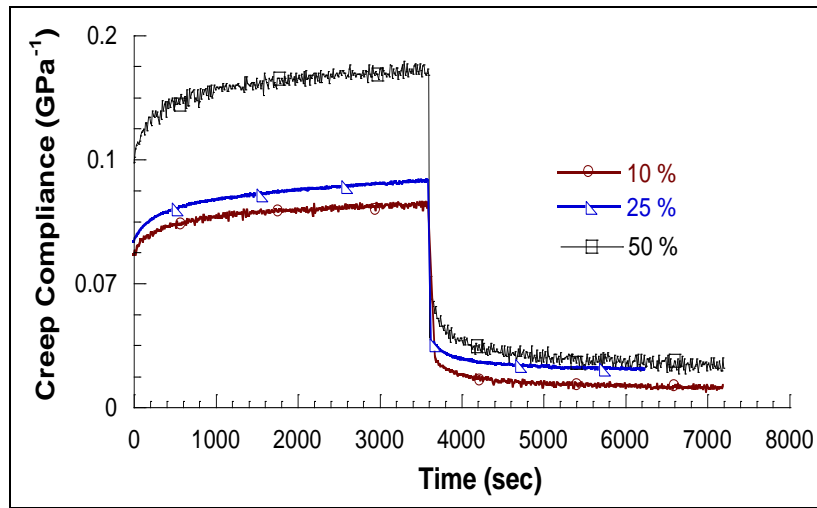
(b)
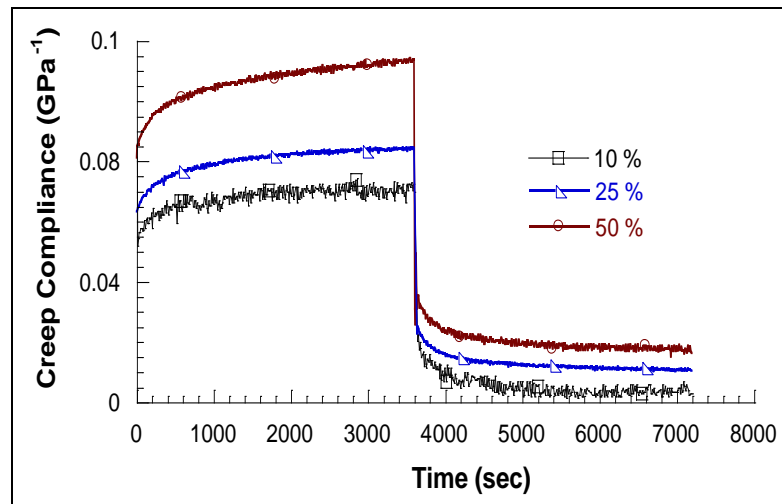
(c)
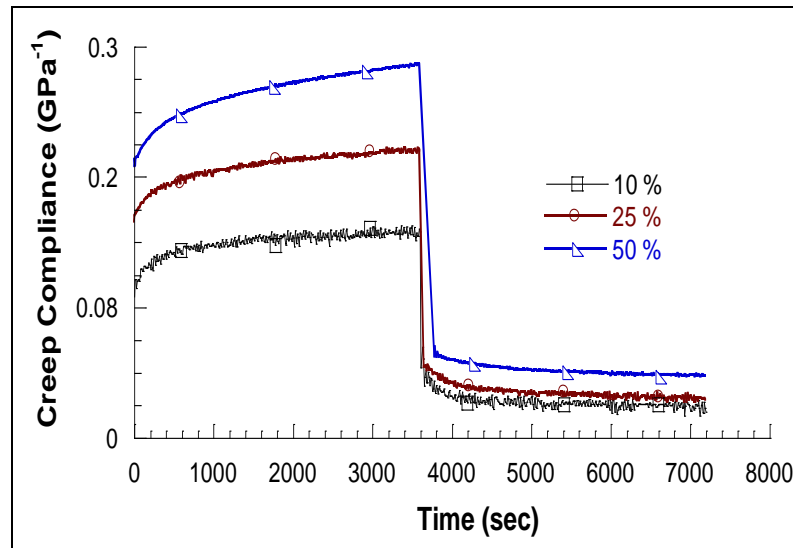
(d)

Figure 5.1. Creep compliance versus time plot of LLDPE nanocomposites: (a) pure LLDPE, (b) PE/1% MLS, (c) PE/1% amEP, (d) PE/1% amEP/1% MLS at room temperature.

Figure 5.1 shows that creep compliance is stress-dependent at all stress levels and that the creep compliance curve increases with the applied stress. This indicates that LLDPE exhibits a strong nonlinear behavior with the stress dependence and time dependence of creep compliance coupled. For most amorphous polymers, a linear viscoelasticity and a transition from linear to non-linear viscoelasticity exist. However, no linearity for LLDPE was observed as seen in Figure 5.1. The linearity of the materials seems to exist at relatively small stresses, possibly due to the structural features of the semicrystalline polymer.

5.3.2. Burgers Modeling Parameters

To evaluate the changes of the material properties with the addition of amEP and MLS, Burgers model was used to fit the creep data of LLDPE nanocomposites at the

123

different stress levels. The results of Burgers fit parameters for all samples are tabulated in Table 5.2. Figure 5.2 shows the good agreement between experimental results and model predictions.
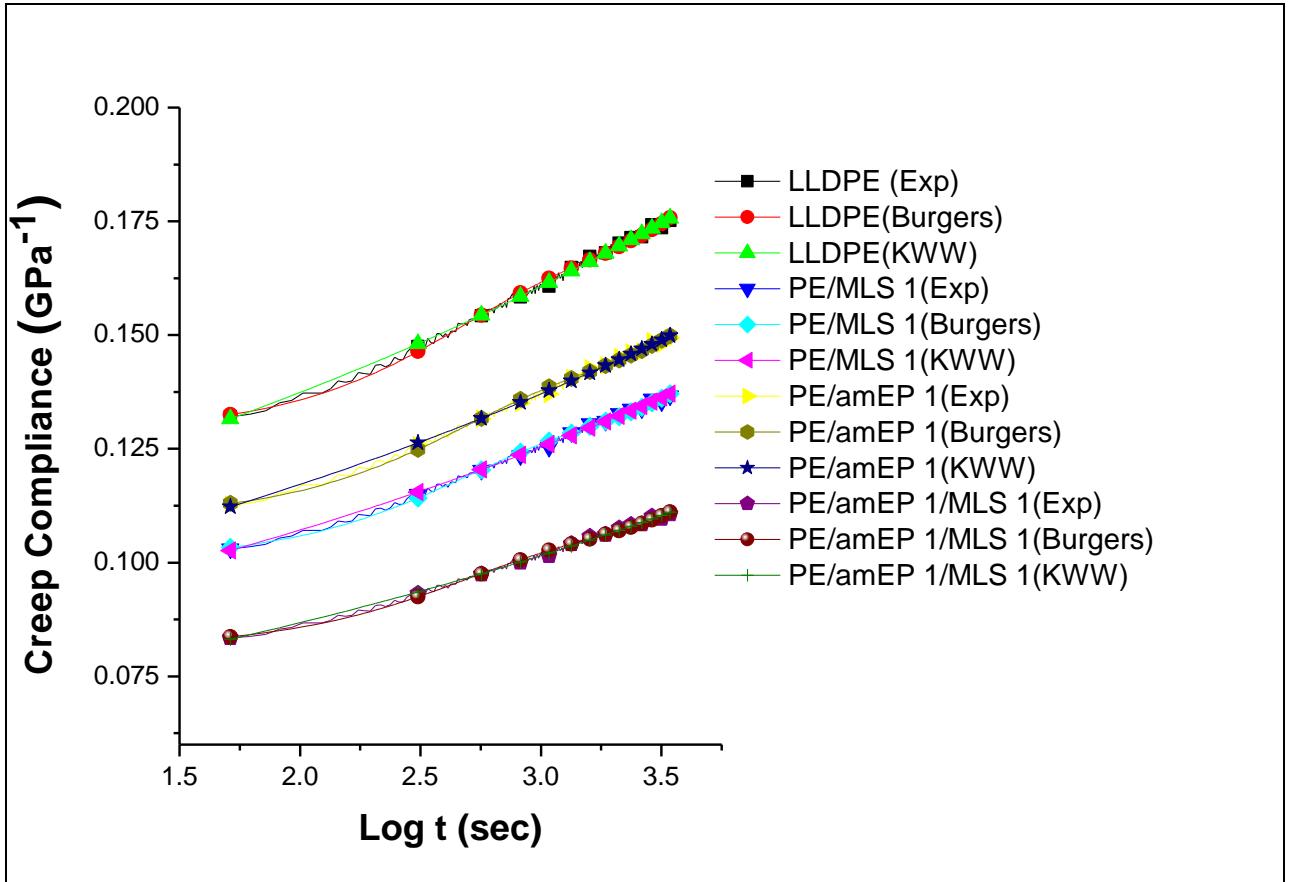
Figure 5.2. Comparison of experimental data to the Burgers model and the KWW function for 50% yield stress.

Sample	Applied Stress (% yield stress)	E_M $(10^9$ Pa)	E_K $(10^9$ Pa)	η_K $(10^{11}$ Pa.s)	η_M $(10^{12}$ Pa .s)	τ (sec)
LLDPE	10	0.08	3.02	2.10	5.24	490
	25	0.09	1.58	2.15	2.51	510
	50	0.09	0.29	1.52	1.32	528
PE/MLS 1	10	0.06	3.27	1.07	5.62	475
	25	0.08	1.29	1.45	2.27	486
	50	0.08	0.31	1.54	2.75	493
PE/amEP 1	10	0.10	3.85	2.57	6.04	459
	25	0.10	1.67	2.41	2.82	473
	50	0.09	0.52	2.64	3.39	482
PE/amEP 1/MLS 1	10	0.11	4.47	3.91	7.00	445
	25	0.12	1.71	4.01	3.36	466
	50	0.12	0.66	3.53	4.83	472

Table 5.2. Burgers fit parameters of LLDPE nanocomposites.

The modulus E_M of the Maxwell spring determines the instantaneous elastic creep strain, which could be immediately recovered on the removal of stress. The addition of 1% MLS did not show significant changes at all stress levels as compared to the neat PE matrix. Adding 1% amEP into LLDPE showed marginal changes. However LLDPE/amEP 1/MLS 1 showed 38% and 33% at 10 and 25% yield stress levels respectively. In the case of LLDPE/MLS systems, the nanoclay layers could bear load because of the large aspect ratio of the individual platelet while discounted by the slippage of stacks and large amount of unexfoliated layers. Hence, the resulting E_M of LLDPE/amEP 1/MLS 1 was higher than the neat matrix. This increase reflects the tensile test results in which the nanocomposites with amEP and MLS had higher yield stress and modulus. The increasing values of E_M with the applied stress provided the fact that the

elasticity of the nanocomposites was not altered with the addition of amEP and MLS to the LLDPE matrix.

The time-dependent parameters E_K and η_K were considerably decreased with increasing stress, showing high stress dependency. This indicated the fact that materials with a relatively higher bulk modulus deformed very little, and the Kelvin unit behaved with a higher modulus and very difficult viscous flow. With increasing stress, the orientation movement of the amorphous chains including elastic deformation and viscous flow became difficult resulting in lower E_K and η_K.

E_K and η_K were used to determine the retardation time $\tau= \eta_K/E_K$. Ideal elastic materials display an immediate recovery after loading and subsequent removal of the load. In the case of viscoelastic materials, there is a time delay for recovery. The retardation time is the delayed response to an applied force or stress. Figure 5.3 shows the stress dependence of the retardation time obtained from Burgers fit. The consistent change of E_K and η_K with stress led to a lower retardant time τ for the LLDPE/amEP 1/MLS 1 nanocomposite as illustrated in Table 5.2. The increase observed in retardation time with the applied stress for all samples can be explained by the orientational hardening of the polymer chains including plastic deformation and viscous flow of the crystalline and amorphous chains. The nanofiller showed reinforcing effectiveness on the Kelvin unit. The nanoclay layers were most effective in retarding the deformation of the Kelvin elements resulting in lower retardation times for the LLDPE nanocomposite.
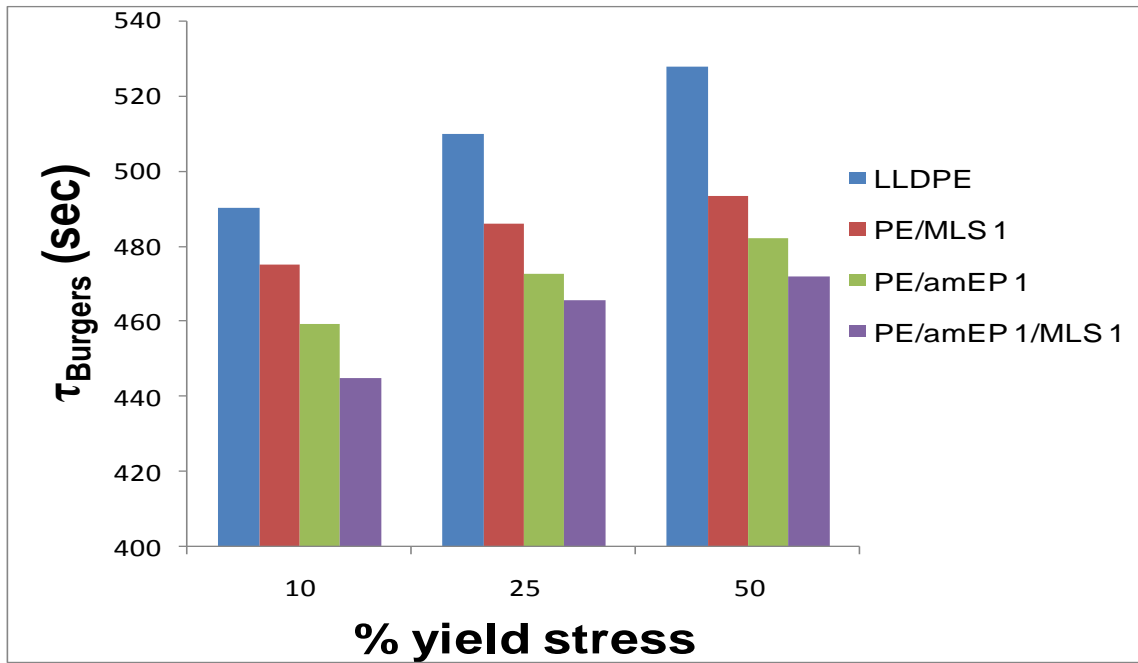
Figure 5.3. Burgers retardation time comparison of LLDPE nanocomposites.

5.3.3. Modeling Parameter from KWW Function

To assess both the retardation time and the breadth of relaxation times, creep compliance curves were fitted with the KWW [13-14] stretched exponential function,

$$D(t) = D_0[1 - \exp(-t/\tau)^{\beta}]$$

where D(t) is the creep compliance, τ is the characteristic retardation time, and β is a creep shape parameter. The results of the curve fit parameters are tabulated in Table 5.3. The numerical analysis of the creep compliance curve fits was performed using OriginLab™ nonlinear least-squares data analysis software.

Sample	Applied Stress (% yield stress)	τ_{KWW} (sec)	β_{KWW}
LLDPE	10	0.89	0.21
	25	0.93	0.19
	50	0.95	0.21
PE/MLS1	10	0.89	0.19
	25	0.91	0.21
	50	0.95	0.19
PE/amEP 1	10	0.88	0.20
	25	0.90	0.19
	50	0.92	0.20
PE/amEP/MLS1	10	0.85	0.21
	25	0.89	0.20
	50	0.92	0.20

Table 5.3. KWW curve fitting parameters.

Figures 5.4 and 5.5 compare the KWW fit parameters of LLDPE nanocomposites. A retardation time represents resistance offered by the microstructure to the elastic deformation of the system. As the retardation time decreases (i.e., as less resistance occurs), the system response becomes more elastic. The results of the samples investigated are tabulated in Table 4.
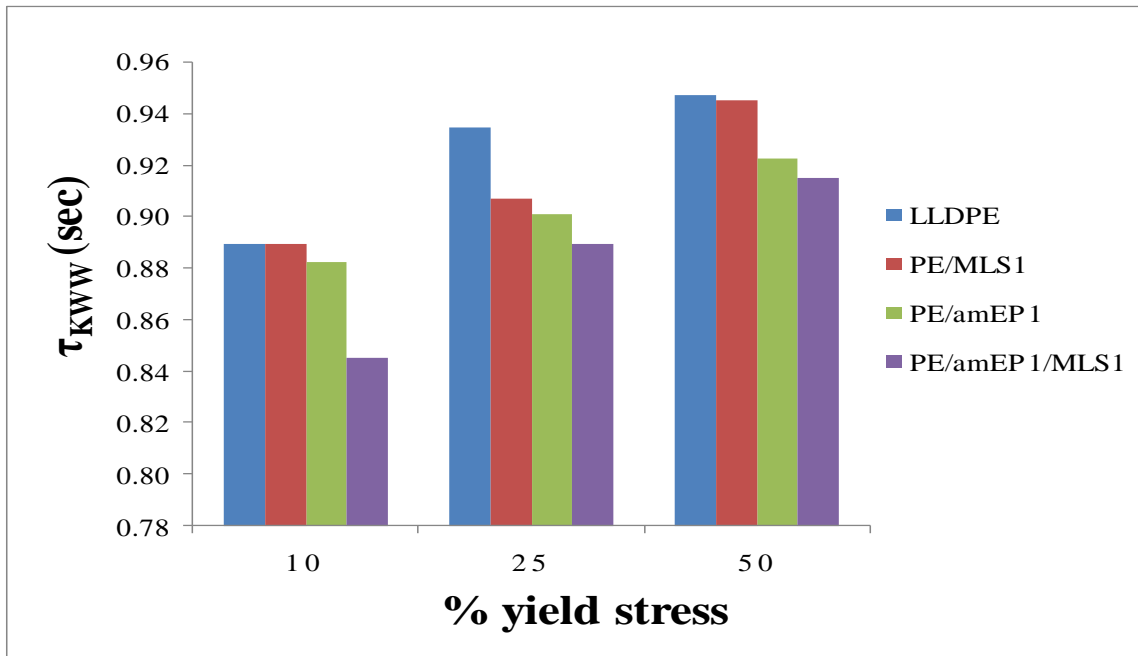
Figure 5.4. KWW retardation time comparison of LLDPE nanocomposites.
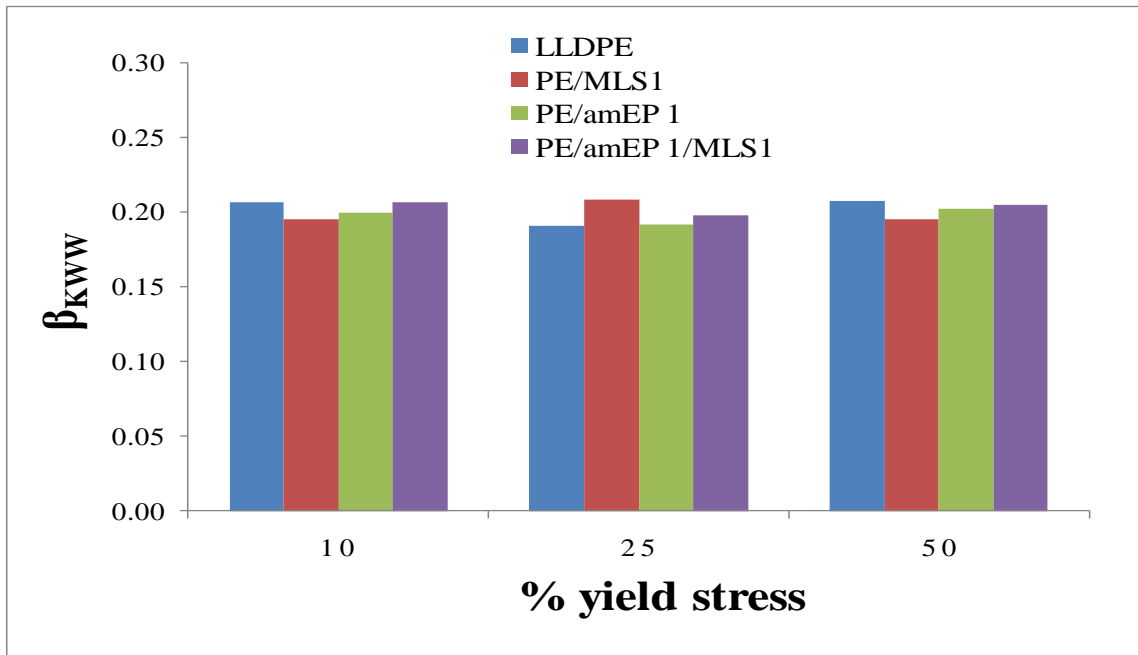
Figure 5.5. Comparison of β_{kww} for the different LLDPE nanocomposites.

In the analysis of the parameters, stress effects and materials effects are to be considered. At a stress of 10 % yield stress, the addition of 1% MLS decreases the retardation time. The results can be explained by the addition of the rigid MLS particles, which act to increase the elasticity of the matrix and hence reduce the retardation time.

The corresponding effect on the breadth of relaxation, which is inversely related to β, is to increase it substantially. A minimum in the values of retardation time is obtained when a combination of 1% MLS and 1% amEP is used The values of β remained constant ($\beta = 0.20 \pm 0.01$) despite the different amounts of MLS and amEP that have been added into the PE matrix.. The results obtained for LLDPE nanocomposites suggest that a combination of 1%MLS and 1% amEP gives the lowest retardation time. A similar behavior is observed at 25 and 50 % yield stress.

5.4. Conclusion

The modeling of the creep response of LLDPE nanocomposites was successfully conducted by using Burgers model and KWW stretched exponential function. The simulating parameters helped to comprehensively understand the improvement of the creep resistance by the addition of amEP and MLS and suggested the structure-property relationship representatively.

From Burgers model, the instantaneous modulus E_M showed an explicit dependence on stress which indicated that the materials behaved with higher stiffness and lower deformability under long-term loading. The addition of amEP and MLS contributed to the lower retardation time and thus resulted in reduced creep deformation.

The results of retardation time from KWW function at all stress levels matched Burgers prediction for the different materials.

5.5   References

1.K.K. Maniar., *Polymer-Plastics Tech. and Eng.*, **43**, 427 (2004).

2.D. Martin, P. Halley, R. Truss, M. Murphy, O. Jackson, and O.Y. Kwon, *Polym.,* 1774 (2003).

3.G. Liang, J. Xu, S. Bao, and W. Xu, *J. Appl. Polym. Sci.*, **91**, 3974 (2004)

4.G. Malucelli, S. Ronchetti, N. Lak, A. Priola, N.T. Dintcheva, and F.P. La Manta, *Eur. Polym. J.*, **43**,

   328 (2007).

5.S.C. Tjong, *J. Matr. Sci. Eng.*, **53**, 73 (2006).

6.J.N. Coleman, U. Khan, K. Friedrich, W.J. Blau, Y.K. Gun'ko, *Carbon,* **44,** 1624 (2006).

7.J. Raghavan, M. Meshii, *Compos. Sci. Technol.,* **57,** 1673 (1997).

8.J.J. Aklonis and W.J. MacKnight. *Introduction to Polymer Viscoelasticity*, John Wiley & Sons: New York (1983).

9.J. Kolarik, A. Pergoretti, *Polym. ,* **47,** 346 (2006).

10.H Liu, MA Polak, 33rd Annual General conference of the Canadian Society for Civil Engineering 2005.

11.J.L. Yang, Z. Zhang, A. Schlarb, and K. Friedrich, *Polym.*, **47**, 6745-6758 (2006).

12.K.S. Fancey, *J. Mater. Sci.,* **40,** 4827 (2005).

13. F. Kohlrausch, Pogg. Ann Physics, **12**, 393 (1847).

14.G. Williams, D.C. Watts, Trans Faraday Soc, **66**, 80 (1970).

CHAPTER 6

SEPARATION OF STRUCTURAL TIME DEPENDENT DEFORMATION DUE TO
STRESS MAGNITUDE

6.1   Introduction

Viscoelastic behavior exhibits various properties. Creep under constant stress, stress relaxation under constant strain, time-dependent recovery of strain after constant load is removed, time-dependent creep rupture, and frequency dependence of fatigue strength are a few examples. If a material does not recover completely after the removal of the constant load in a creep test and if an unrecoverable strain persists, the material is said to have a residual viscoplastic strain. Nonlinearities may be due to intrinsic behavior, local nonlinear stress-strain behavior, or macro-stress-strain equations that are large to be modeled with local continuum mechanics models. Although linear viscoelastic principles are useful for describing the long-term properties, they are not adequate when the stresses are so high that non-linearity is observed in the response of the material.

Recent studies have focused on polymer nanocomposites as novel materials [1]. The mechanical properties of polymer nanocomposites have been extensively studied; and enhanced performances, such as strength, stiffness, and toughness, have been achieved to extend the different applications such as load-carrying components [2]. Important factors such as filler concentration, dispersion state, and interfacial bonding are considered to be able to significantly influence the properties of bulk materials. Because of their nanoscale size and the huge interfacial area of the nanoparticles, a low

concentration of these nanoparticles is usually used. Many researchers have reported that the incorporation of these nanoparticles can cause a significant improvement in mechanical and thermal properties. Even though their strength and elastic properties have been studied in recent years [3-6], data on the time-dependent behavior of these materials is still lacking. Consequently, studies on creep of these new promising nanocomposites are very important and necessary. Pegoretti et al. [7] studied the creep resistance of polyethylene terephthlate (PET)/MLS nanocomposites. A decrease in creep compliance was observed in the nanocomposites when compared to the neat matrix. Vlasveld et al. [8] also studied the effects of physical aging and moisture on the creep performance of polyamide 6 (PA6) filled with layered silicates. Creep compliance was found to be reduced by the addition of the layered silicates.

A previous work by our laboratory focused on the improvement of the creep resistance of LLDPE/MLS nanocomposites for potential use in stratospheric balloons [3]. Stratospheric balloons are large aerospace structures with the primary bearing material being linear low-density polyethylene (LLDPE) that is 10 to 20 μm in thickness. The viscoelastic behavior of these structures has been studied extensively [9-11]. Of particular importance is the analysis of the state of stress in such structures. Several studies showed the good ability of Schapery model to predict the stress response in a broad class of materials. Papanicolaou et al. [12] studied the non-linear viscoelastic response of unidirectional carbon-fiber-reinforced polymer matrix. Creep and recovery measurements in tension with different stress levels were made for this purpose. A modified Schapery model was used to describe the non-linear viscoelastic response and determination of

non-linear parameters. A viscoplastic term was added for the description of the total strain response in the system. The viscoplastic strain was revealed as a remaining strain at the end of recovery. Good agreement between experimental data and theoretical results was obtained. Papanicolaou et al. [13] further developed the technique suggested by Zaoutsos [12] by means of an analytical prediction of nonlinearity parameters as a function of the applied stress. The prediction takes into account certain characteristic properties, such as linear and nonlinear stress threshold and the ultimate tensile strength of the material. The validity of the model is confirmed by creep-recovery tests on a 90° unidirectional carbon-fiber/epoxy-matrix composite. A decrease in the values of g_o with respect to the applied stress level was mostly due to the hardening of the specific material. The values of both g_1 and g_2 increased with increasing applied stress. Touatl et al. [14] proposed a method to predict non-linear relaxation behavior from creep experiments. For a given nonlinear creep properties and creep compliance, the Schapery creep model could be transformed into a set of first-order nonlinear equations. The solution of these equations enables obtaining the nonlinear stress relaxation curves. The method was demonstrated on test data for polyurethane and showed good agreement with the experimental results. Luna et al. [15] studied the nonlinear behavior of polypropylene (PP) nanocomposites. The Schapery model was used to determine the overall mastercurve from the behavior of the material at different load levels. The material showed nonlinear behavior below the yield point and referred that to a change in the structure of the material. Lai and Bakker [16] modeled the time-dependent behavior of high-density polyethylene (HDPE) with a one-dimensional integral

representation. The total strain in the material could be decomposed into a recoverable viscoelastic strain and an irrecoverable plastic strain. The viscoelastic deformation is represented by the Schapery creep model. Rand et al. [11] studied the nonlinear behavior of LLDPE. Stress-time-temperature superposition principles similar to time-temperature superposition principles were used to form a "mastercurve."

It is thus very common to account for the linear viscoelastic behavior of some polymers when analyzing their short- and long-term performance. The assumption of linearity is often used, even when the nonlinearity is significant because the nonlinearities are not well understood and/or useful experimental and theoretical data are not available for nonlinear characterization and analysis. The rapid growth of computing power and the availability of advanced finite element software that allows for the use of customized material models account for the computational aspects. The experimental characterization of the mechanical aspects of the material remains a need. In this chapter, experimental data are collected for LLDPE nanocomposites, and the results are used to study the nonlinearities in the behavior of the material. Schapery's nonlinear model is used to describe the nonlinear effects.

6.2   Experimental

6.2.1   Sample Preparation

Nanocomposites were compounded by using a Haake TW100 twin-screw extruder with a temperature profile of 200, 200, 205, and 210 $^{\circ}$C for zones 1 to 4, respectively. PE films 1.5 mil (0.04 mm) thick were processed with a Killion single-screw extruder (L/D = 24:1), fitted with a dual-lip air ring and a die diameter of 2 inches.

Blends of PE + amEP+ MLS were made and the mixtures were compounded and pelletized. The compounded pellets were then extruded into blown films. Table 6.1 summarizes the concentrations used.

Sample	LLDPE (wt %)	Exxelor VA 1803 (wt %)	MLS (wt %)
LLDPE	100	0	0
PE/MLS 1	99	0	1
PE/amEP1	99	1	0
PE/amEP1/MLS 1	98	1	1

Table 6.1. Summary of composition used.

6.2.2   Tensile Testing

Yield stress, ultimate tensile strength (UTS), and elastic modulus E were determined by using RSA III film fixture with an extension rate of 0.208 mm/min.

6.2.3   Creep Testing

Uniaxial tensile creep tests were performed by using RSA III with the films attachment. The desired constant stress to be applied for each measurement was calculated to be 10, 25, and 50% of the yield stress. The constant stress was applied for 1 hour of loading followed by 1 hour of unloading. A linear displacement transducer with a force capacity of 35 N was used to monitor the strain during the experiment. The creep compliance was calculated by the ratio of the measured creep strain to the initial applied stress.

6.3 Results and Discussion

6.3.1 Stress Effects on Creep

The experimental data of creep of LLDPE nanocomposites at various stress levels is shown in Figure 6.1, where the creep compliance D(t) is defined as the ratio of the measured time-dependent strain, ε (t), to the applied stress σ.

$$D(t) = \frac{\varepsilon(t)}{\sigma}$$
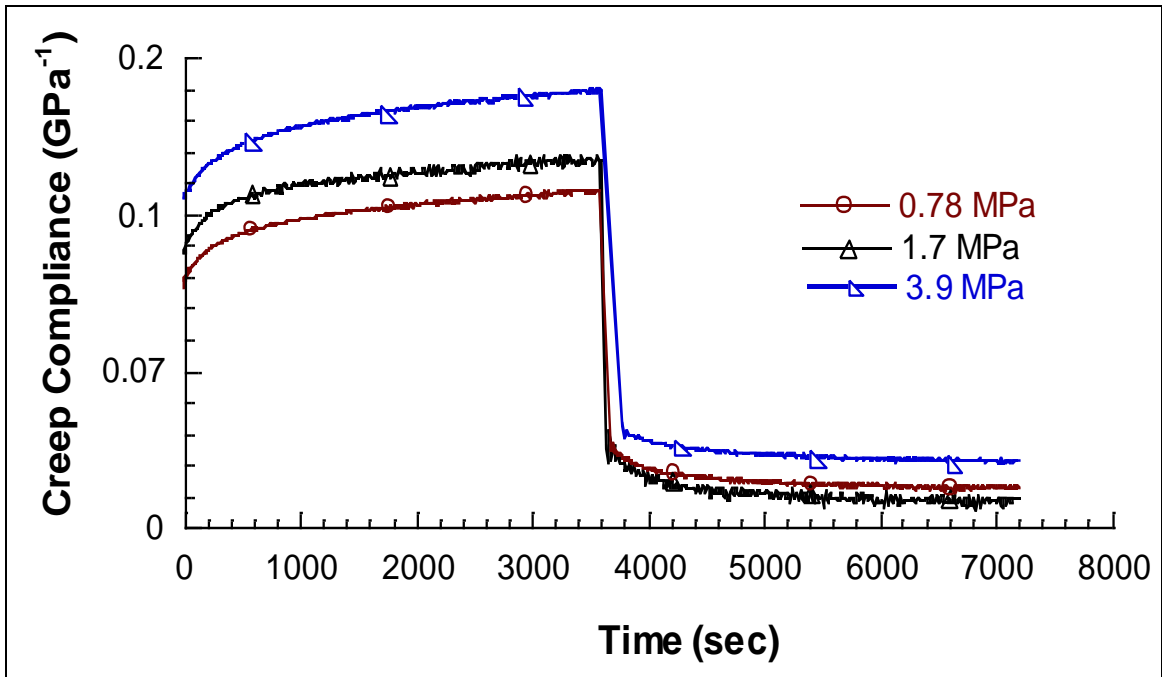
(a)
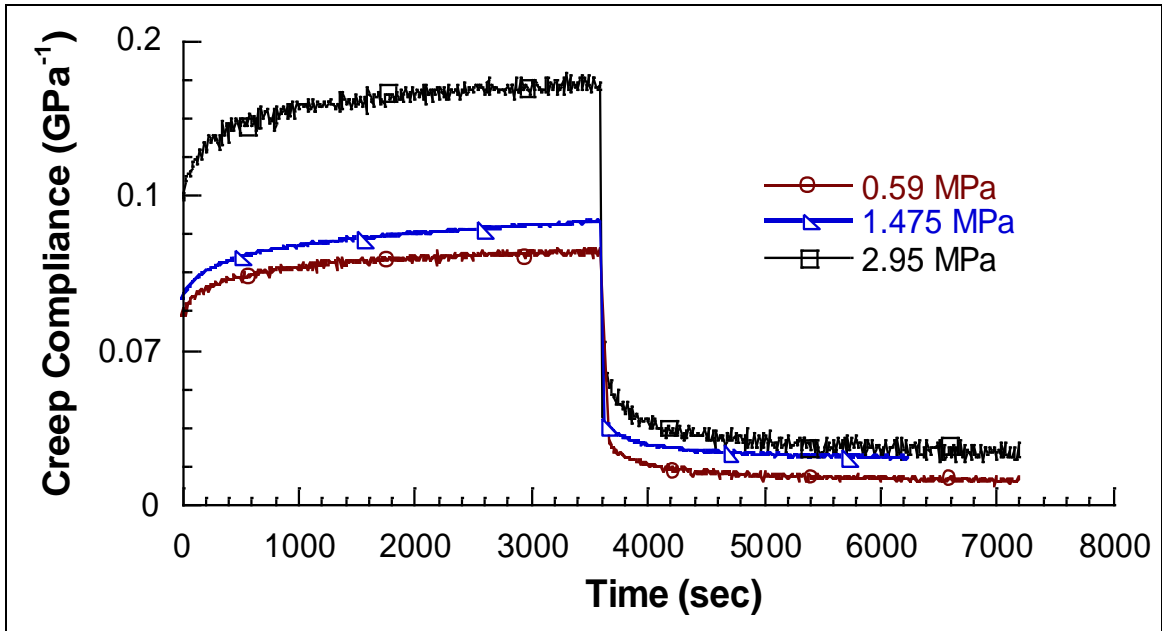
(b)
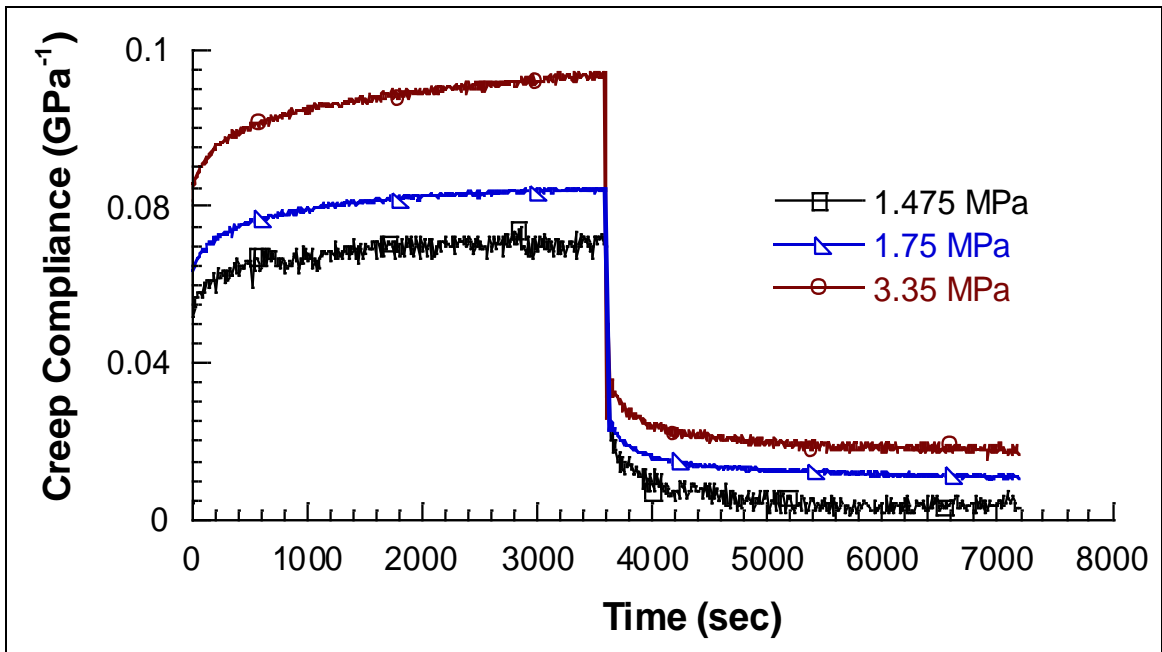
(c)
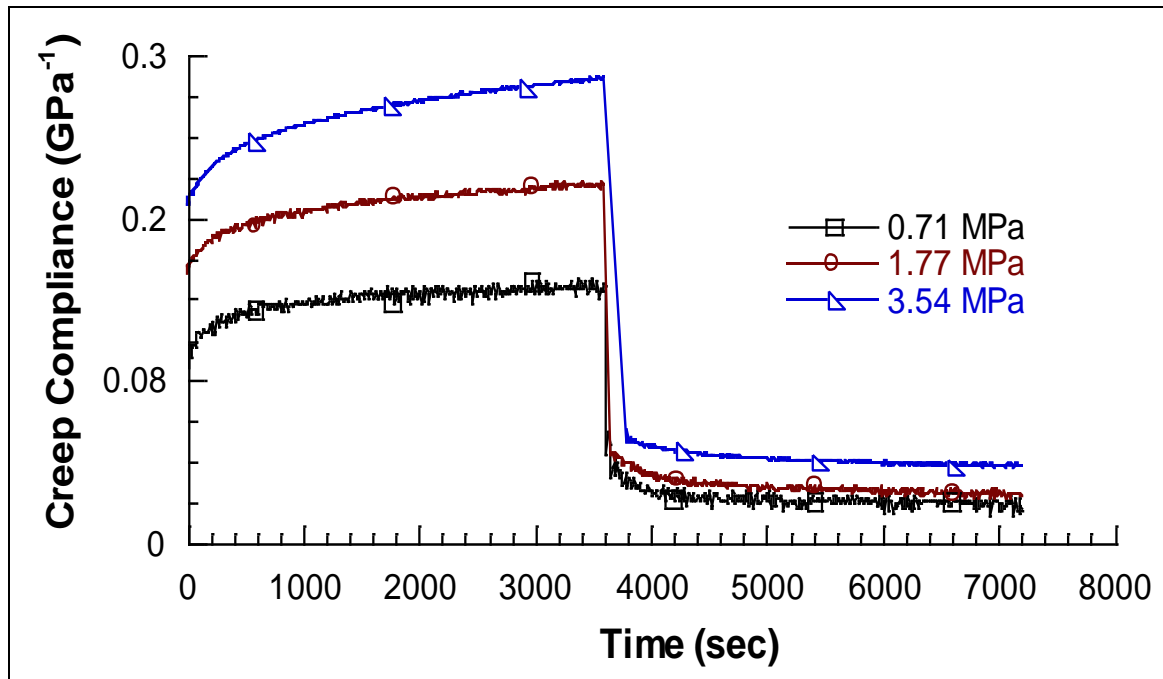
(d)

Figure 6.1.Creep compliance versus time plot of LLDPE nanocomposites: (a) pure LLDPE, (b) PE/1% MLS, (c) PE/1% amEP, (d) PE/1% amEP/1% MLS at room temperature.

Figure 6.1 shows that creep compliance is stress-dependent at all stress levels and that the creep compliance curve increases with the applied stress. This indicates that LLDPE exhibits a strong nonlinear behavior with the stress dependence and time dependence of creep compliance coupled. For most amorphous polymers, a linear viscoelasticity and a transition from linear to non-linear viscoelasticity exist. However, no linearity for LLDPE was observed as seen in Figure 6.1. The linearity of the materials seems to exist at relatively small stresses, possibly due to the structural features of semicrystalline polymers. Struik [17] proposed that in semicrystalline polymers, polymer crystals reduce the segmental mobility of amorphous regions close to them. Amorphous

regions far from these crystals remain undisturbed and hence are more mobile. For PE, above its glass transition temperature, the amorphous regions far from the crystals are in their rubbery state, whereas those near the crystals are still in their glassy state and hence behave elastically. The amorphous region far from the crystals exhibits a non-linear behavior induced by the applied stress accompanied by a change in the free volume typical of amorphous polymers above their glass transition temperature.

The strong nonlinearity exhibited by LLDPE nanocomposites and the increase of the creep compliance with the applied stress suggests the applicability of the time-stress superposition principle. According to this principle, if the creep compliance curves are plotted in logarithmic scale, then different curves at different stress levels can be superposed by a horizontal shift. For thermorheologically complex materials such as semicrystalline material, a vertical shift factor of the data plots along the y-axis should be considered [18]. The concept of the vertical shift factor has been used by many authors [19-21]. Although the real cause of the vertical shift is not clear, it is thought that it is a representation of the change in crystallinity [22].

To obtain the mastercurve of the creep compliance curve, the reference stress σ_0 is chosen to be the lowest stress applied. The corresponding mastercurves of LLDPE nanocomposites are shown in Figure 6.2.
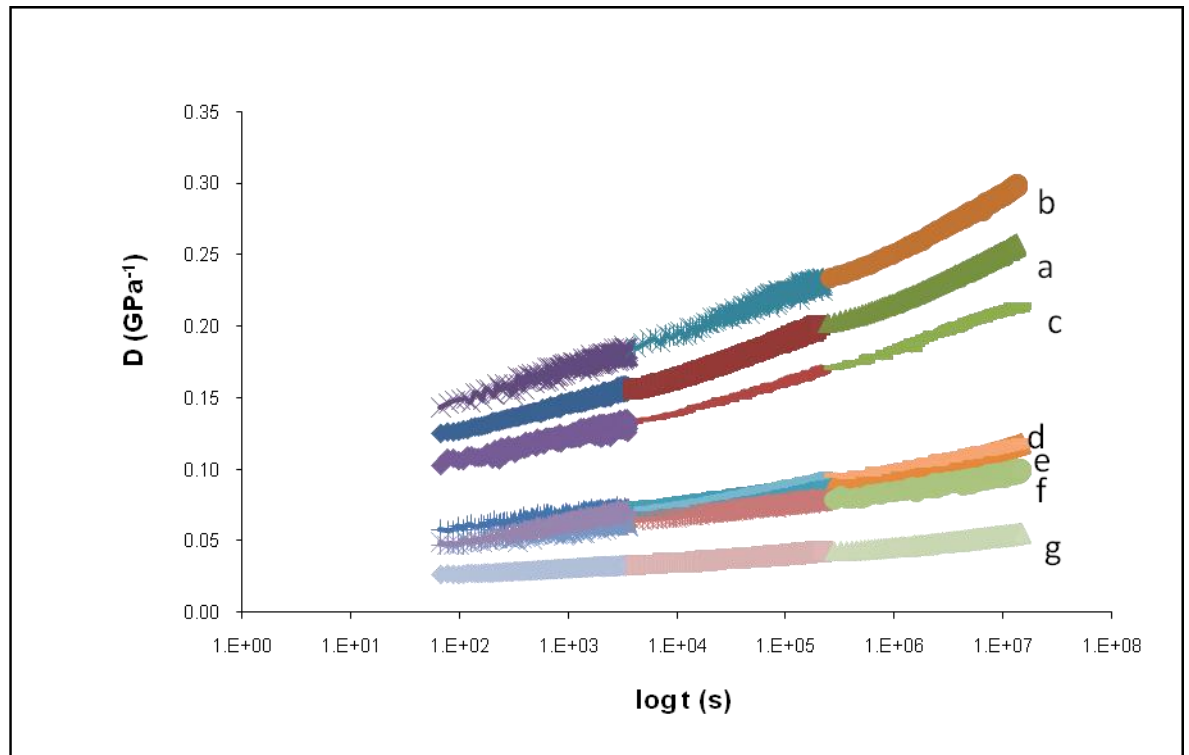
Figure 6.2. Mastercurve of linear transient compliance at 25 °C of (a) LLDPE, (b) PE/MLS 1, (c) PE/amEP1, (d) PE/amEP1/MLS 1, (e) PE/amEP1/MLS 2, (f) PE/amEP2/MLS 1, and (g) PE/amEP2/MLS 2.

The addition of low concentrations of MLS increases the stiffness of the matrix and shows higher compliance in comparison with the PE and PE + amEP samples. The creep compliance decreases with the addition of amPE, which can be explained by the addition of an elastomeric component to the PE matrix which acts to increase its elastic behavior. The creep compliance further decreases with the addition MLS and amEP with different ratios to the PE matrix .This behavior is attributed to strong compatibility between the PE matrix and MLS.

The average creep compliance curves for amEP and amEP/MLS nanocomposites at different stress levels are presented in Figure 6.3. The different shapes of the compliance curves with increasing stress show the nonlinearity of the viscoelastic behavior of the material. It is noted that the creep compliance curves are lower for amEP/MLS nanocomposites than for the neat amEP. The lower curves indicate an enhancement in creep resistance with the addition of MLS into the amEP matrix.
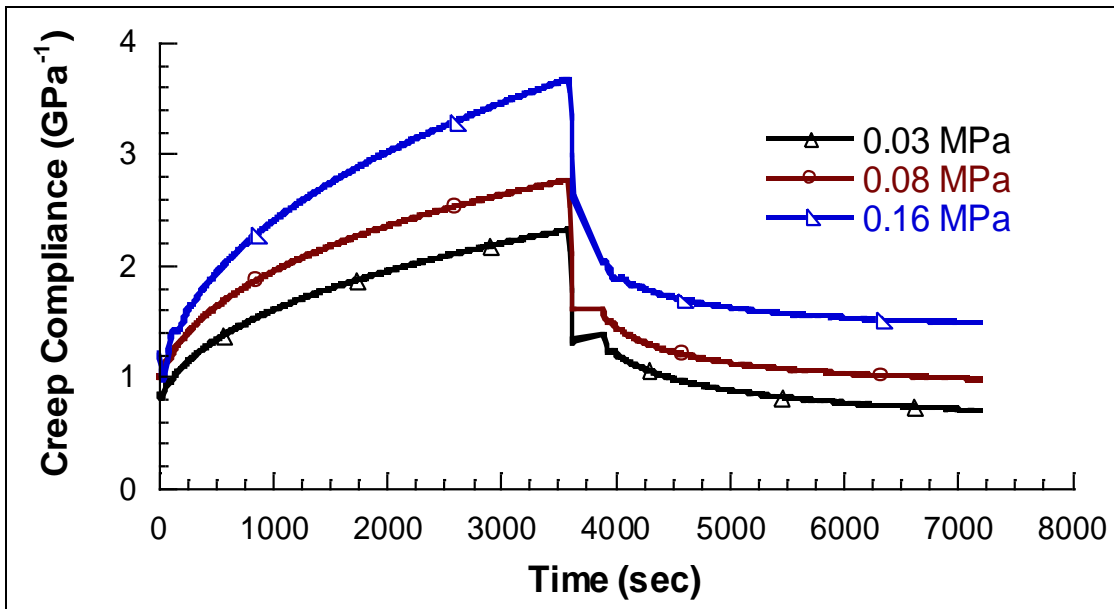
(a)
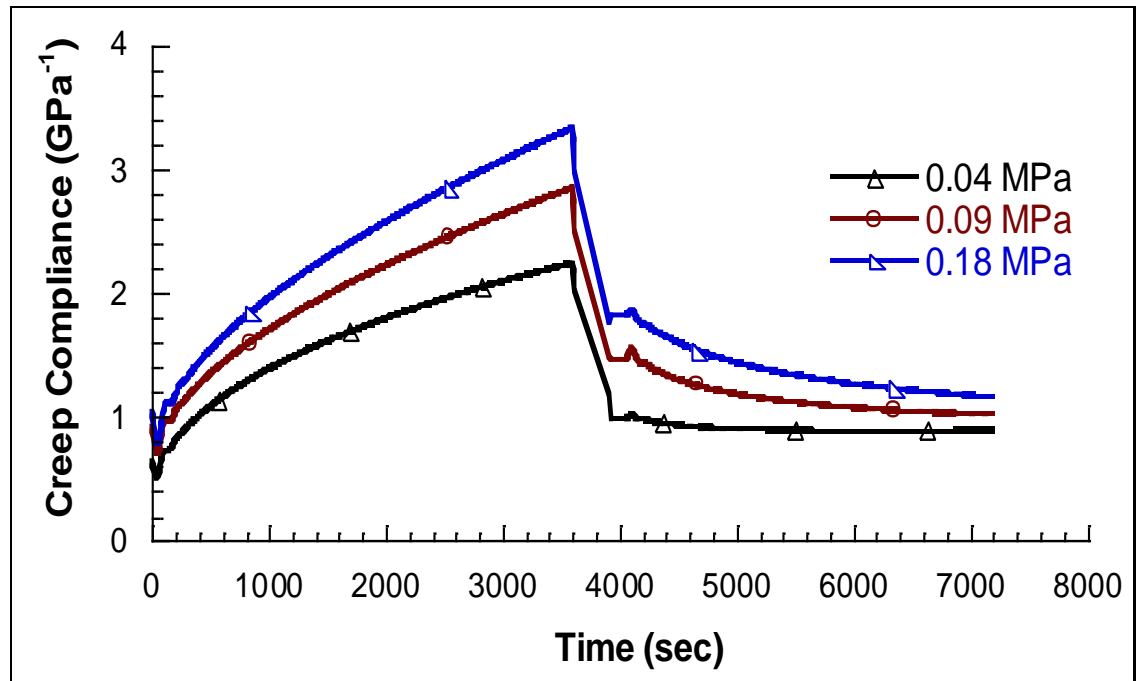
(b)
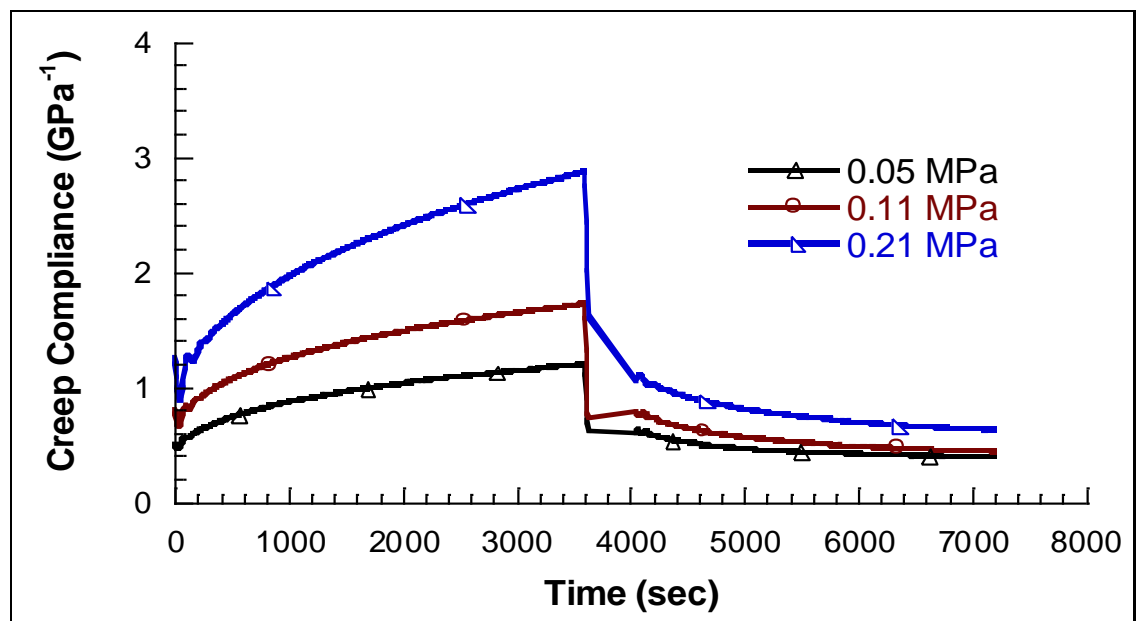
(c)

Figure 6.3. Creep compliance versus time plot of LLDPE nanocomposites: (a) amEP, (b) amEP/1% MLS, (c) amEP/3% MLS at room temperature.

The nonlinear creep model based on the time-stress superposition principle was also applied for the description of the creep data of the amEP nanocomposites. The creep compliance curves at the different stress levels were shifted horizontally to obtain the smooth mastercurves shown in Figure 6.4. As expected, no vertical shifting was applied because of the amorphous nature of amPE. As seen from Figure 6.4, the addition of 1% MLS into amEP led to a significant enhancement in the material creep resistance. The highest creep resistance was obtained for the addition of 3% MLS.
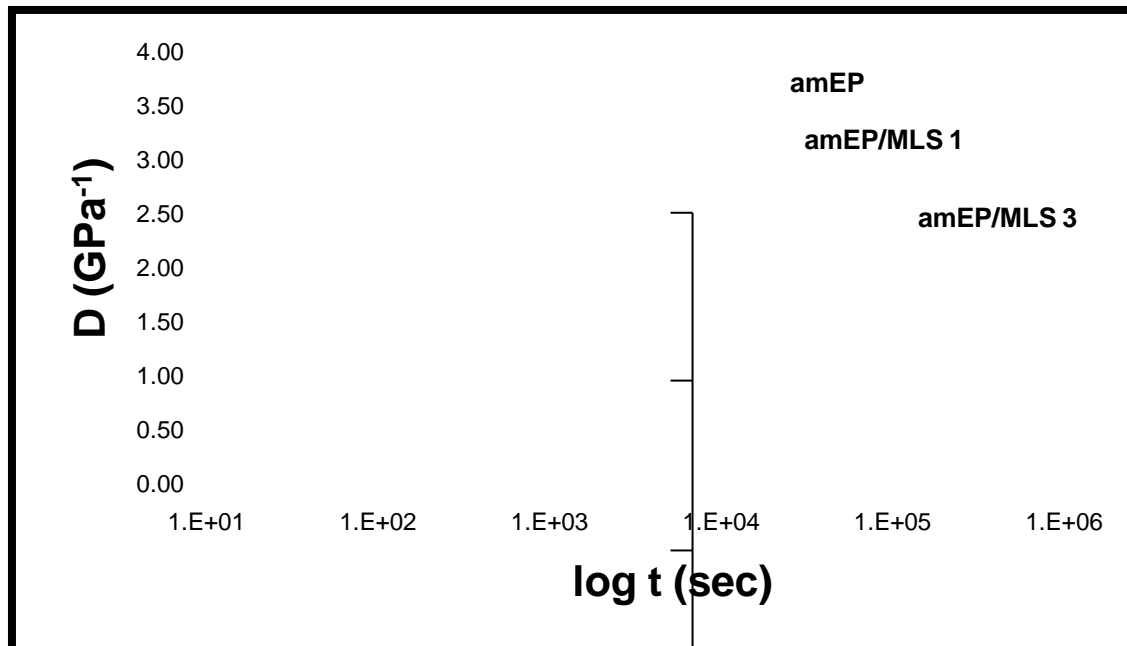
Figure 6.4. Mastercurve of linear transient compliance at 25 $^{\circ}$C of amEP/MLS nanocomposites.

6.3.2   Schapery Modeling Parameters

The successful superposition of a mastercurve of the LLDPE nanocomposites indicates that the creep tests of LLDPE nanocomposites can be accelerated by increasing

the stress level applied during the test. The time-stress superposition principle can be related to the Schapery thermodynamic theory. Experimental creep-recovery tests for the various LLDPE nanocomposites are shown in Figure 6.5. The stress related constants g_0, g_1, g_2, and a_σ in the Schapery model were determined by using the numerical method outlined before. Creep-recovery data were used to evaluate these constants, which are summarized in Table 6.2.
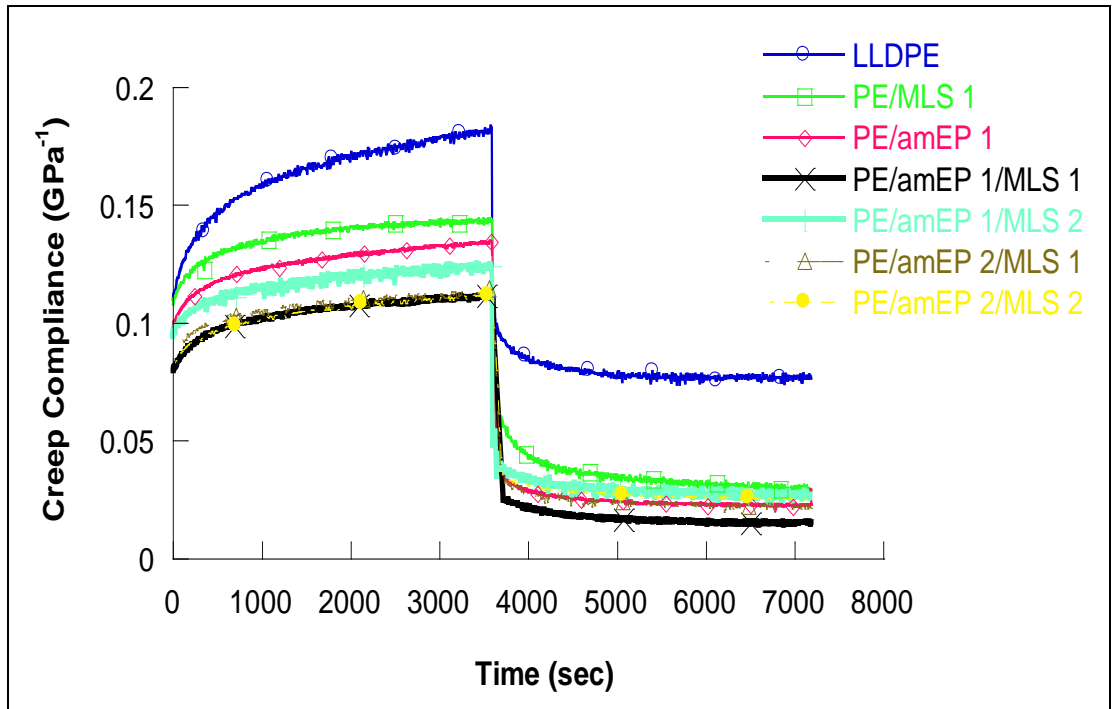
Figure 6.5. Creep-recovery curves of LLDPE nanocomposites at room temperature.

Sample	Applied Stress σ (MPa)	g_0	g_1	g_2	a_σ
LLDPE	0.78	0.97	1.16	0.97	0.67
	1.7	0.86	1.23	1.11	0.15
	3.9	0.42	1.48	2.31	0.04
PE/MLS 1	0.59	0.93	1.39	0.96	0.52
	1.47	0.92	1.39	1.17	0.14
	2.95	0.52	1.87	1.84	0.02
PE/amEP1	1.475	0.90	1.68	0.99	0.69
	1.75	0.89	1.72	1.20	0.11
	3.35	0.41	1.96	2.70	0.05
PE/amEP1/MLS 1	0.71	0.92	1.02	0.94	0.78
	1.77	0.94	1.56	1.19	0.13
	3.54	0.42	2.33	2.45	0.03
PE/amEP1/MLS 2	0.65	0.96	0.83	0.98	0.64
	1.48	0.93	1.16	1.26	0.12
	2.45	0.47	1.41	2.25	0.04
PE/amEP2/MLS 1	0.85	0.95	1.17	0.96	0.74
	1.73	0.96	1.20	1.19	0.12
	3.15	0.47	1.19	2.28	0.03
PE/amEP2/MLS 2	0.89	0.98	1.72	0.98	0.78
	1.85	0.95	1.30	1.16	0.11
	3.35	0.46	1.32	2.21	0.02
amPE	0.03	0.96	0.95	0.95	0.95
	0.08	0.69	1.08	1.11	0.36
	0.16	0.49	1.21	1.35	0.03
amPE/MLS 1	0.04	0.99	0.99	0.98	0.98
	0.09	0.63	1.06	1.33	0.30
	0.18	0.27	1.27	2.18	0.03
amPE/MLS 3	0.05	0.96	0.96	0.98	0.96
	0.11	0.44	1.24	1.67	0.25
	0.21	0.21	1.38	2.45	0.05

Table 6.2. Values of the nonlinear factors g_0, g_1, and a_σ for LLDPE nanocomposites.

The stress shift factors g_0 and g_1 are determined from the creep data by fitting the creep strain to Schapery's equations derived in chapter 2. Figure 6.6 shows the comparison between creep and recovery experimental data and the Schapery model predictions. The values of g_2 and a_σ were determined by fitting the recovery data to Schapery's recovery equation for each stress level applied. It is worth mentioning that the resulting n-values were more reliably obtained from creep rather than recovery data as proposed by Augl [23]. The n values were then used to analyze the others parameters by using recovery the Equation.
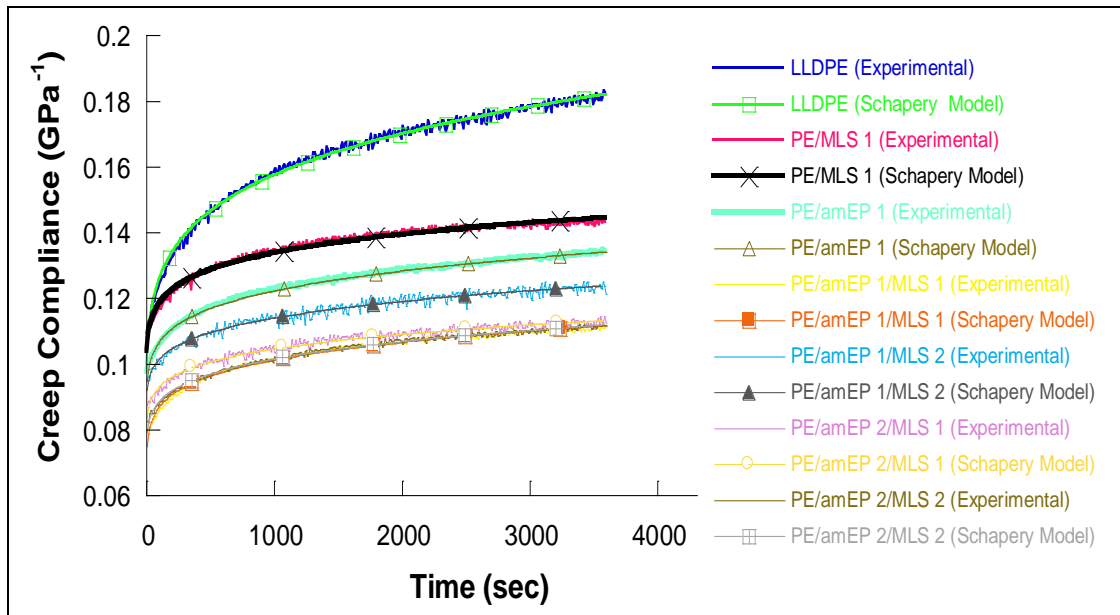
(a)
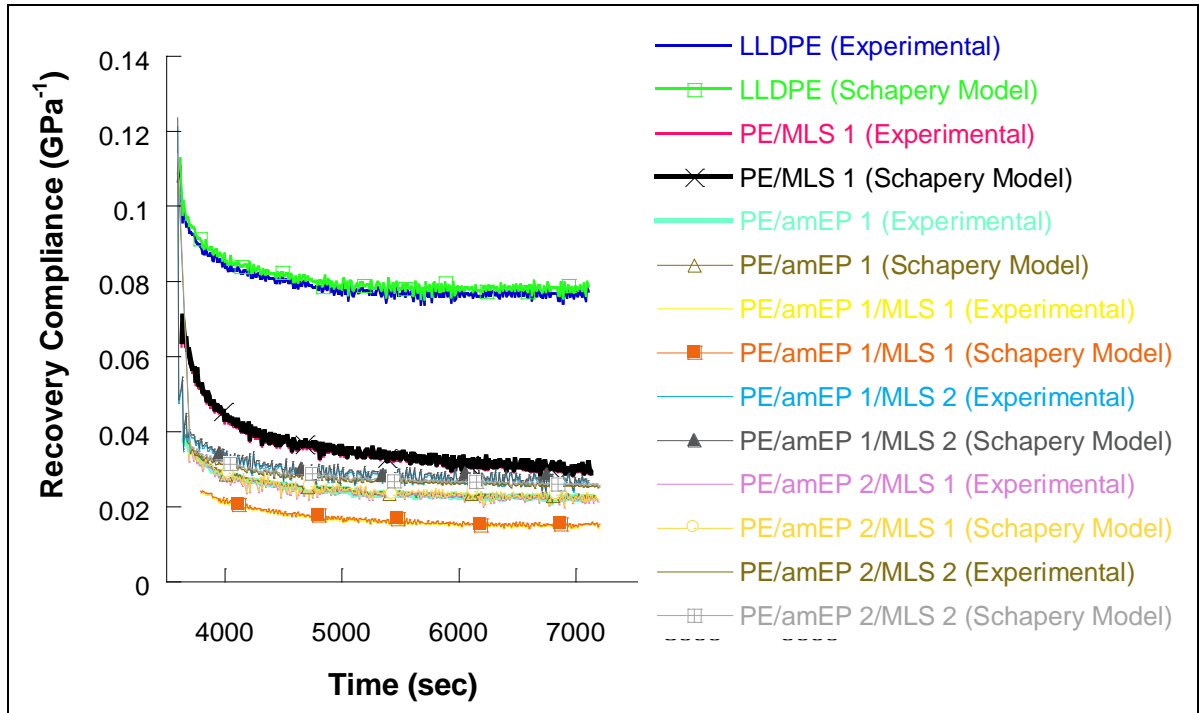
(b)

Figure 6.6. Experimental and theoretical (Schapery model) comparison of (a) creep compliance and (b) recovery compliance.

Following the steps described, each of the Schapery nonlinear parameters was separately estimated. Each of the parameters has a specific physical meaning. The parameter g_0 is a measure of the stress dependence of the initial *time-independent* component of the compliance D_0. Parameter g_1 expresses the stress dependence of the *transient, time dependent* component of the compliance ΔD (ψ- ψ'). Parameter g_2 reflects the effect of loading rate on the time-dependent response of the material and depends on both stress and temperature, and a_σ is a shift factor superimposing the creep curves on a general master curve.

A graphical representation of the g_0 variation versus the applied stress is shown in Figure 6.7. The decreasing values of g_0 with increasing stress levels denote a material hardening occurring because of the application of load. The values of g_0 are lower in samples containing a combination of amEP and MLS. This indicates a material reinforcing effect with the addition of amEP and MLS which is reflected in higher modulus and strength for LLDPE nanocomposites as compared to the pure LLDPE matrix. The values have noticeable variations at higher stresses, where the applied stress values are close to the elastic limit.
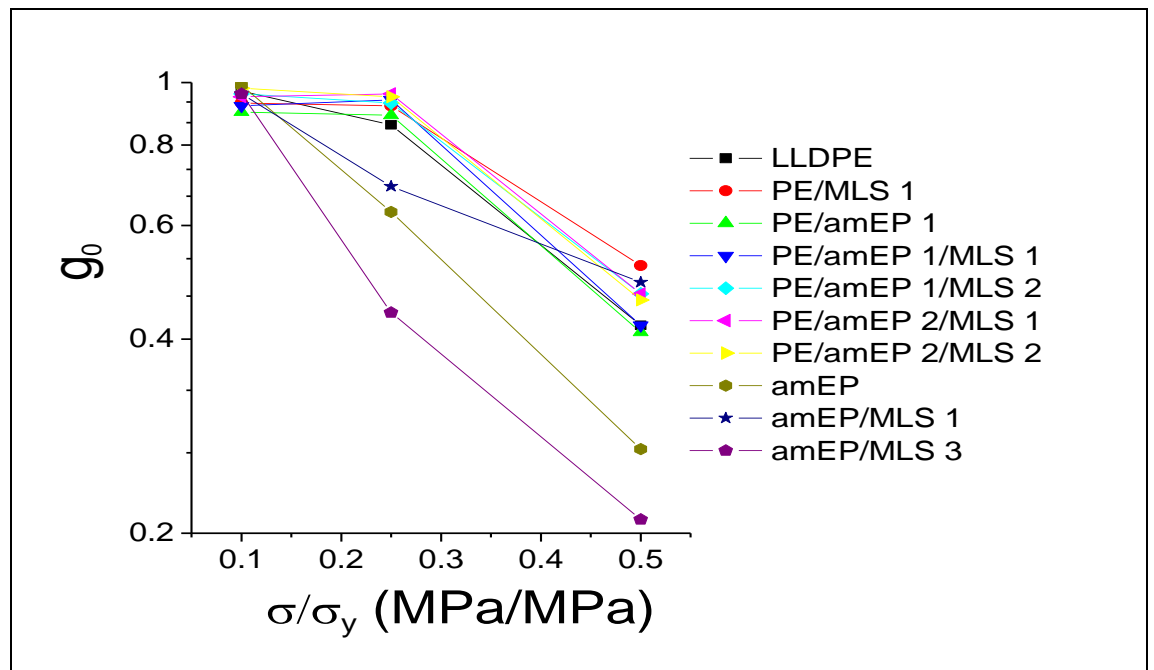
Figure 6.7. Stress dependence of the stress shift factor g_0.

The g_1 values represent the part of creep that is recoverable after the load has been removed. In that sense, it is a stress-dependent factor. A high value of g_1 suggests quickness in recovery. It is observed that the values of g_1 increase with the applied stress for all compositions as shown in Figure 6.8. The relative increase is higher when MLS is added compared to pure LLDPE. The g_1 value is further increased with the addition of amPE. This increase can be related to the addition of an elastic matrix which acts to improve the elastic recovery of the material. The maximum increase in g_1 is seen for compositions containing a 1:1 ratio of amEP and MLS. For amEP nanocomposites, the addition of 1% MLS shows a small increase in g_1 values. The addition of 3% MLS into amEP shows a further increase with respect to amEP at all stress levels. The results support the previous observations in which the addition of MLS acts to increase the g_1 values of LLDPE nanocomposites. The lower values of g_1 values for amEP as compared to LLDPE are explained by the amorphous nature of the matrix.
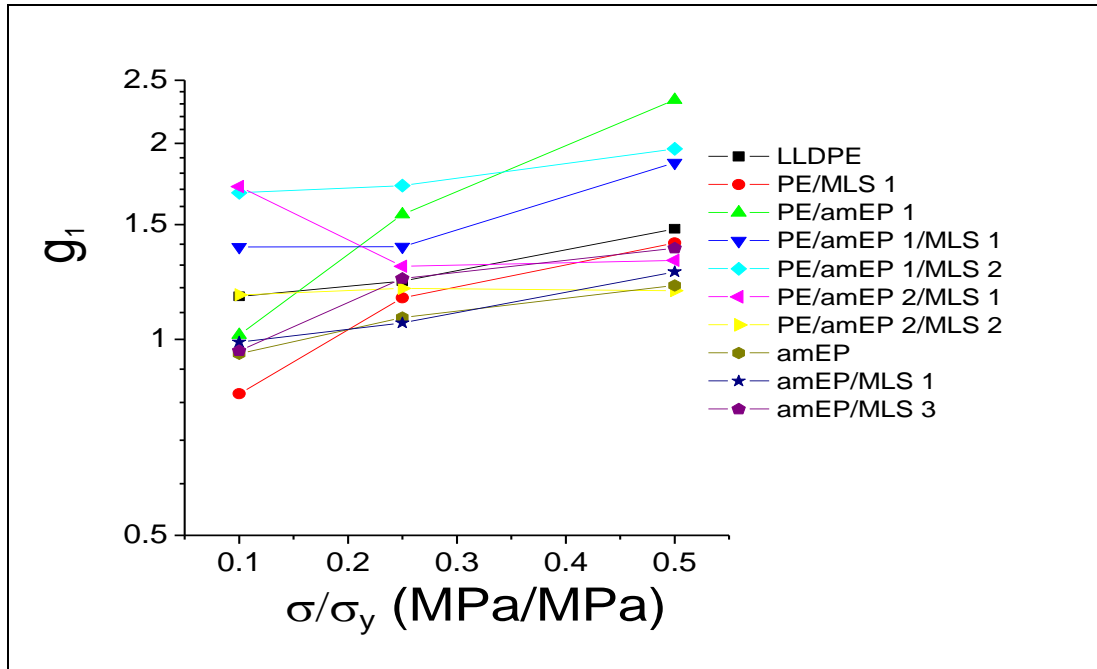
Figure 6.8. Stress dependence of the stress shift factor g_1.

Using the recovery equation in Schapery's model, the recovery test data for each recovery experiment were fitted in order to obtain the values of a_σ. The values of a_σ are plotted as a function of the applied stress in Figure 6.9. The values are less than 1, indicating that the reduced time is greater than the real time. This finding suggests that higher stress will cause the material to accelerate its creep behavior. Figure 6.9 shows that the values of a_σ are largely material dependent. These factors are structure dependent and are obtained from analyzing experimental results. Since they are material dependent, they will change from one sample to another. Also, due to their correspondence with the structure of the material, they can indicate the degree of linearity and non-linearity of the system. The addition of a combination of amEP and MLS shows lower values indicating

151

a decrease in the non-linear dependence of the creep of the material and hence improvement of the creep resistance.
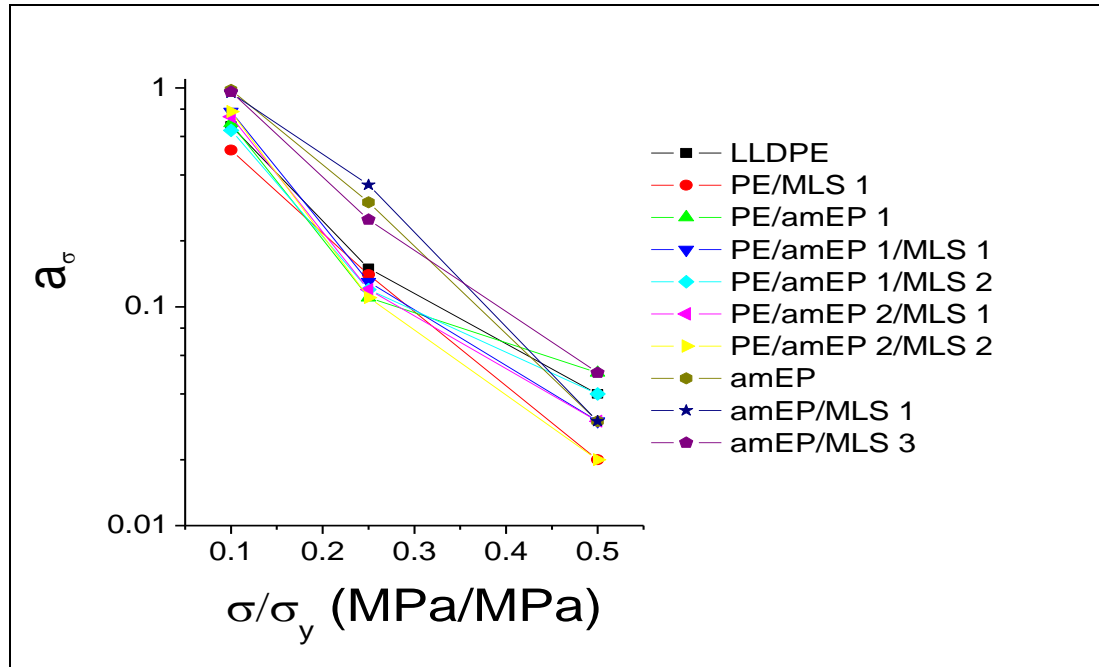
Figure 6.9. Stress dependence of the stress shift factor a_σ.

The values of g_2 represent the response of the material with no stress applied (recovery). Comparing g_2 and the product of g_1 and g_2 allows the separation of stress effects during creep from material effects during recovery. Figure 6.10 shows the variation of g_2 for LLDPE nanocomposites with the applied stress. It can be seen that the magnitude of g_2 increases with the applied stress for all LLDPE samples. This shows that the behavior the specimens during recovery with no stress applied is material dependent .It is observed that the values of g_2 are higher when MLS is added as compared to pure LLDPE. The addition of amEP serves to increase the values. The values of g_2 for all compositions containing a combination of amEP and MLS are higher than these

containing amEP and MLS separately. For amEP nanocomposites, the same trend is observed in g_2 values. For compositions containing 1% MLS, the g_2 values are higher than for the neat amPE. The addition of 3% MLS further increases the g_2 values for all stress levels. This implies that the addition of low concentrations of amEP and MLS leads to a different structure in recovering. The results can be explained by structural differences induced with the addition of amEP and MLS, and reinforces the initial theory about addition of amEP and MLS. The addition of amEP increases the strength of the system, leading to a more ductile material that will undergo a higher degree of deformation. This has been noted at all the stages of the mechanical testing. The addition of low concentrations of MLS increases the stiffness of the matrix and shows lower compliance in comparison with the PE and PE + amEP samples.
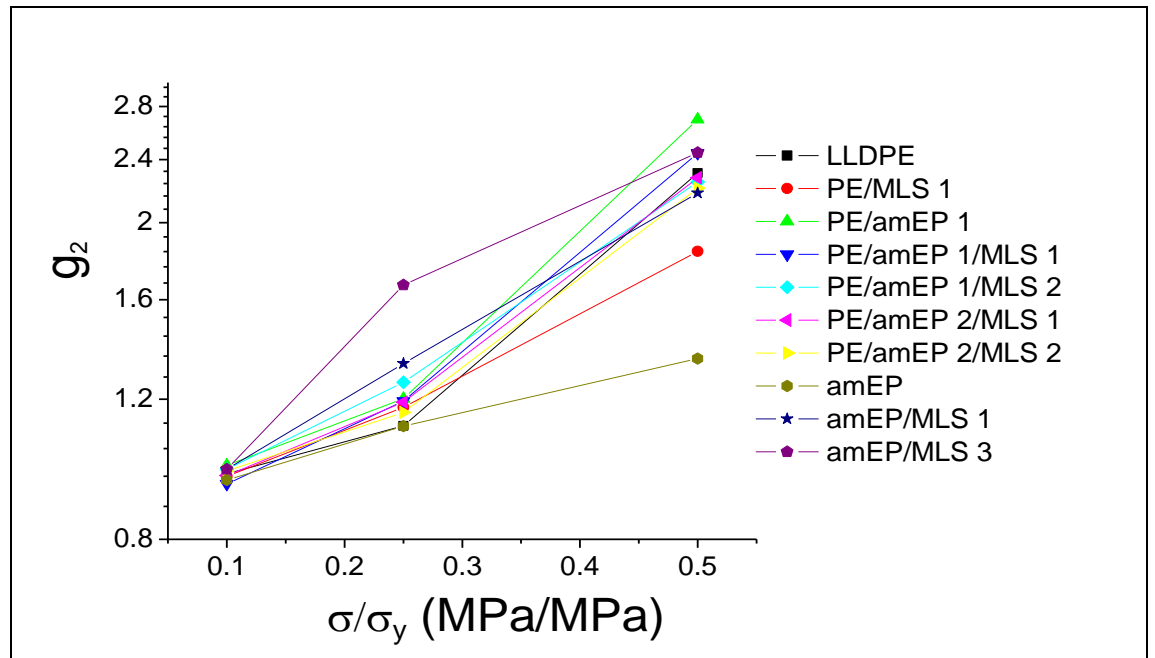
Figure 6.10. Stress dependence of the stress shift factor g_2.

6.4   Conclusions

The tensile behavior and long-term creep of LLDPE nanocomposites were investigated. The creep behavior of the polymer was viscoelastic, and the nonlinearity in stress was revealed by investigating the creep compliance of the material at different stress levels. The creep compliance mastercurves can be used to predict the long-term creep behavior of the nanocomposites.

A considerable enhancement in the creep resistance was obtained with the addition of amEP and MLS when compared with the pure LLDPE and was revealed by comparing the stress-dependent mastercurves. The Schapery nonlinear model was used to model the creep behavior of the nanocomposites with respect to stress. The absolute

values of the stress factors indicated an enhanced creep resistance in the nanocomposites as compared with the neat PE and amEP matrix.

6.5. References

1. J.L. Yang, Z. Zhang, A. Schlarb, and K. Friedrich, *Polymer*, **47**, 2791-2801 (2006).

2. K.Maniar, *Polymer-Plastics Technology and Engineering*, **43**, 427-443 (2004).

3. A. Ranade, K. Nayak, D. Fairbrother, and N.A. D'Souza, *Polymer*, **46**, 7323-7333 (2005).

4. J.L. Yang, Z. Zhang, A. Schlarb, and K. Friedrich, *Polymer*, **47**, 2791-2801 (2006).

5. M. Niaounakis and E. Kontou, *J. Polym. Sci.: Part B: Polymer Physics,* **43**, 1712-1727 (2005).

6. G. Liang, J. Xu, S. Bao, and W. Xu, *J. Appl. Polym. Sci.*, **91**, 3974-3980 (2004).

7. A. Pegoretti, J. Kolarik, C. Peroni, C. Migliaresi, *Polymer*, **4**, 2751-2759 (2004).

8. D. Vlasveld, H. Bersee, and S.J. Picken., Polymer, **46**, 10279-10289 (2005).

9. J. Sterling and J. Rand, Biaxial Stress Limit for ULDB Film. AIAA 5th Aviation, Technology,

   Integration, and Operations Conference, Arlington, Virginia (2005).

10. J. Sterling and J. Rand, *Advances in Space Research*, **37,** (2006).

11. J. Rand, J. Henderson, and D. Grant. *Polym. Eng. and Sci.*, **36**, 1058-1064 (1996).

12. G. Papanicolaou, S. Zaoutsos, and A. Cardon, *Composites Science and Technology*, **58**, 883-

    889 (1998).

13. G. Papanicolaou, S. Zaoutsos, and A. Cardon, *Composites Science and Technology,* **59**,

    1311-1319 (1999).

14. D. Touatl and G. Cederbaum, *J. Eng. Mat. and Tech.,* 119: 121 (1997).

15. A. Luna and N. D'Souza. ANTEC 2000: Plastics, the Magical Solution: Conf. Proc., May 7-11, Orlando, Florida (2000).

16. J. Lai and A. Bakker, *Polym. Eng. and Sci.,* **36,** 1058-1064 (1995).

17. L.C.E. Struik , *Physical aging in amorphous polymers and other materials*, Elsevier: New

   York (1978).

18. M. Tajvidi, R. Falk, and J. Hermanson, *J. Appl. Polym. Sci.,* **97**, 1995-2004 (2005).

19. M Elahi and Y. Weitsman, *Mechanics of Time-Dependent Material*, **3**, 219–244 (1999).

20. D. Pooler and L. Smith, *J. Thermoplastic Composite Mat.*, **17,** 427-445 (2004).

21. A Pramanick and M Sain, *J. Thermoplastic Composite Mat.,* **19,** 35-59 (2006).

22. S. Onogi, T. Sato, T. Asada, and Y. Fukui, *J. Polym. Sci., Part A-2 (Polymer Physics),* **8,**

   1195-1209 (1970).

23. J. Augl, *J. Rheol.,* **31,** 1-36 (1987).

CHAPTER 7

SEPARATION OF STRUCTURAL TIME DEPENDENT DEFORMATION DUE TO TEMPERATURE

7.1.   Introduction

Polymer nanocomposites reinforced with montmorillonite layered silicate (MLS) have generated enormous interest in science and engineering in the last years. The time-independent mechanical properties of polymer–MLS nanocomposites have been well investigated [1-3] .In most practical applications, compliance of the polymeric material not only depends on stress but also on time and temperature and hence the time-temperature dependent response, i.e., creep behavior, is of immense significance [4,5] The theoretical background for creep behavior of solid polymers is well studied within the framework of linear viscoelasticity [3,6] .This theory assumes that the creep compliance is only a function of time and not of strain and stress. But beyond a certain strain limit compliance became a function of time and stress (or strain). This non-linear viscoelastic behavior plays a key role in most applications and the data analysis in this region is more difficult than in the linear region, which has a direct relation to the deeper understanding of the micromechanical processes controlling the mechanical response [7].

In the past decade, the nonlinear viscoelastic creep behavior of polyethylene nanocomposites has been studied. [8-10]. Although the time dependent linear and nonlinear response of polyethylene nanocomposites has been investigated in a number of publications, the effect of temperature on the mechanical properties of LLDPE

nanocomposites has not yet been studied in detail. Tajvidi et al. [11] studied the nonlinear creep behavior of high density polyethylene (HDPE)/Kenaf fiber composites under varying temperature. The time–temperature superposition principle was applied to investigate the viscoelastic properties of a composite of 50% kenaf fibers, 48% HDPE, and 2% compatibilizer. Creep data were shifted horizontally and vertically, and a master curve was constructed. The results indicated that the composite material was thermorheologically complex, and a single horizontal shift was not adequate to predict the long-term performance of the material. Pramanick et al. [12] studied the temperature-stress equivalency in nonlinear viscoelastic creep characterization of high density polyethylene (HDPE) composites. The combined effect of temperature and stress on creep strain was accommodated in a single analytical function where the interaction was shown to be additive.

In our previous work, we investigated the nonlinear creep compliance of LLDPE nanocomposites at room temperature using Schapery nonlinear model [13]. A considerable enhancement in the creep resistance was obtained with the addition of amEP and MLS when compared with the pure LLDPE and was revealed by comparing the stress dependent mastercurves. Schapery nonlinear equation was used to model the creep behavior of the nanocomposites with respect to stress. The absolute values of the stress factors indicated an enhanced creep resistance in the nanocomposites as compared with the neat PE and amEP matrix. In this paper, we investigate the temperature dependence of the nonlinear creep compliance of LLDPE nanocomposites. Time-temperature-stress superposition principles (TTSSP) similar to time-temperature superposition principles

(TTSP) were used to form a "master curve". The amplitude of compliance was found to be a function of both stress and temperature which implies that the material is not "thermorheologically simple".

7.2.   Calculation of Temperature-Related Creep Variables

D_0: The initial compliance value can be determined from the instantaneous deflection data of the creep/time curve in the linear region.

h_0: According to Equation 38 in chapter 2, h_0 could be calculated from creep plot when t is equal to zero. The following equation can be used to calculate the compliance

$$\varepsilon(0) = D(0)\sigma = D_0 h_0 \sigma \Rightarrow h_0 = \frac{\varepsilon(0)}{\sigma D_0}$$

h_1: h_1 can be calculated by curve fitting of recovery strain data to Equation 41 in chapter 2 and using the following equation

$$A = \frac{\Delta\varepsilon_a}{h_1} \Rightarrow h_1 = \frac{\Delta\varepsilon_a}{A}$$

a_T: The numerical estimation of aT can be done by fitting the recovery strain data to Equation 38 in chapter 2.

h_2: h_2 can be calculated from the following equation where the assumption is that $h_2=1$ in the linear region:

$$\frac{\Delta\varepsilon_1 a_T^n \sigma}{C_1 h_1} = h_2$$

7.2.1. Temperature Shift Factor

Temperature may influence compliance in a similar way as stress. Temperature effects can be described by changing the timescale of the viscoelastic response. Thus, if D is the compliance at a temperature T_1 and time t, the creep compliance at a temperature T_2 can be described as follows:

$$D(t,T_1) = gD(t/a_T,T_2)$$

Where aT is the temperature shift factor.

For thermorheologically complex materials such as semicrystalline material, a vertical shift factor of the data plots along the y-axis should be considered [14]. The concept of the vertical shift factor has been used by many authors [15-17]. While the real cause of the vertical shift is not clear, it is thought it is a representation of the change in crystallinity [18]. Furthermore, the temperature dependent shift factor a_T is related to the activation energy Ea as follows

$$\log a_T = \frac{E_a}{2.303R}\left(\frac{1}{T} - \frac{1}{T_{ref}}\right)$$

where R is the universal gas constant. The activation energy can be obtained from the slope of the curve of a_T against 1/T.

7.3.   Experimental

7.3.1. Materials

LLDPE DOWLEX 2056G (Dow chemical company) was used to prepare the PE nanocomposite films (density = 0.92 g/cc; Melt index = 1.0 gm/10 min). Montmorillonite-layered silicate (MLS) (Cloisite 15A™), supplied by southern clay products, was used as the nanofiller. An amorphous maleic anhydride functionalized elastomeric copolymer, Exxelor VA 1803 (ExxonMobil corporation), was used as a compatibilizer between the MLS and the PE matrix. Exxelor VA 1803 has a nominal density of 0.86 g/cm3 and a melt index of 3 g/10 min (ASTM D1238, 230 $^{\circ}$C, 2.16 kg). The maleic anhydride (MA) level is in the range of 0.5 to 1%.

7.3.2. Sample Preparation

Nanocomposites were compounded with a Haake TW100 twin-screw extruder with a temperature profile of 200, 200, 205, and 210 $^{\circ}$C for zones 1 to 4, respectively. PE films 1.5 mil (0.04 mm) thick were processed with a Killion single-screw extruder (L/D = 24:1), fitted with a dual-lip air ring and a die diameter of 50 mm (2 inches). Blends of PE+amPE+MLS were made, and the mixtures were compounded and pelletized. The compounded pellets were then processed into a blown film. . Table 7.1 summarizes the concentrations used.

Sample	LLDPE (wt %)	Exxelor VA 1803 (wt %)	MLS (wt %)
LLDPE	100	0	0
PE/MLS 1	99	0	1
PE/amEP1	99	1	0
PE/amEP1/MLS 1	98	1	1

Table 7.1. Summary of compositions used.

7.3.3. Creep Testing

Uniaxial tensile creep tests were performed using RSA III with the films attachment. The desired constant stress to be applied for each measurement is calculated to be 50% of the yield stress. The constant stress is applied for 1 hour of loading followed by 1 hour of unloading. A linear displacement transducer with a force capacity of 35 N is used to monitor the strain during the experiment. Creep tests were performed at the same set of temperatures as the tensile tests. The effect of temperature on creep was studied by running experiments at different temperatures of 25, 10, -10, -30, -50, -70, and -90 ^{o}C. A convection oven with a temperature range of -150 ^{o}C to 600 ^{o}C was used for this purpose.

7.4. Results and Discussion
7.4.1. Time/Temperature Equivalence

The effect of temperature on the nonlinear creep behavior of the LLDPE nanocomposites was investigated. The temperature was varied from -90 to 25 ^{o}C with a 20 ^{o}C interval. Figure 7.1 shows the creep behavior of LLDPE nanocomposites at different temperatures. The stress levels in the creep tests were chosen based on the results of the tensile tests and did not exceed 0.5 of the ultimate yield point. Since the

162

stress region is far from the yield point, it is assumed that the primary deformation mechanism for the materials in creep was of viscoelastic nature, while the contribution of plastic strains was insignificant in the stress and time ranges considered.
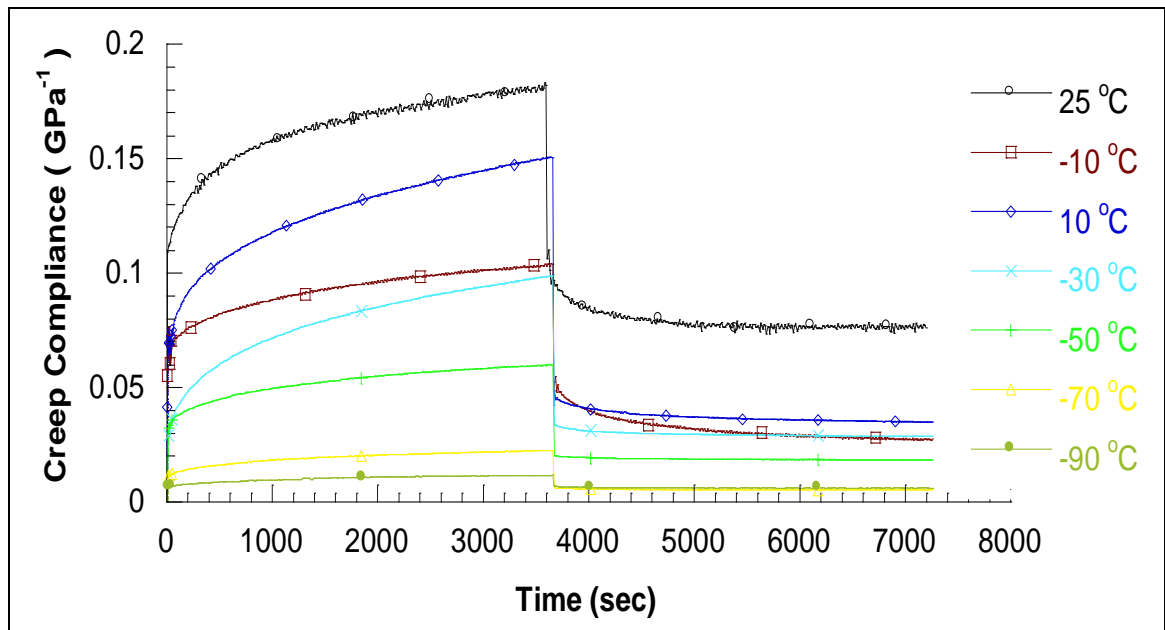
(a)
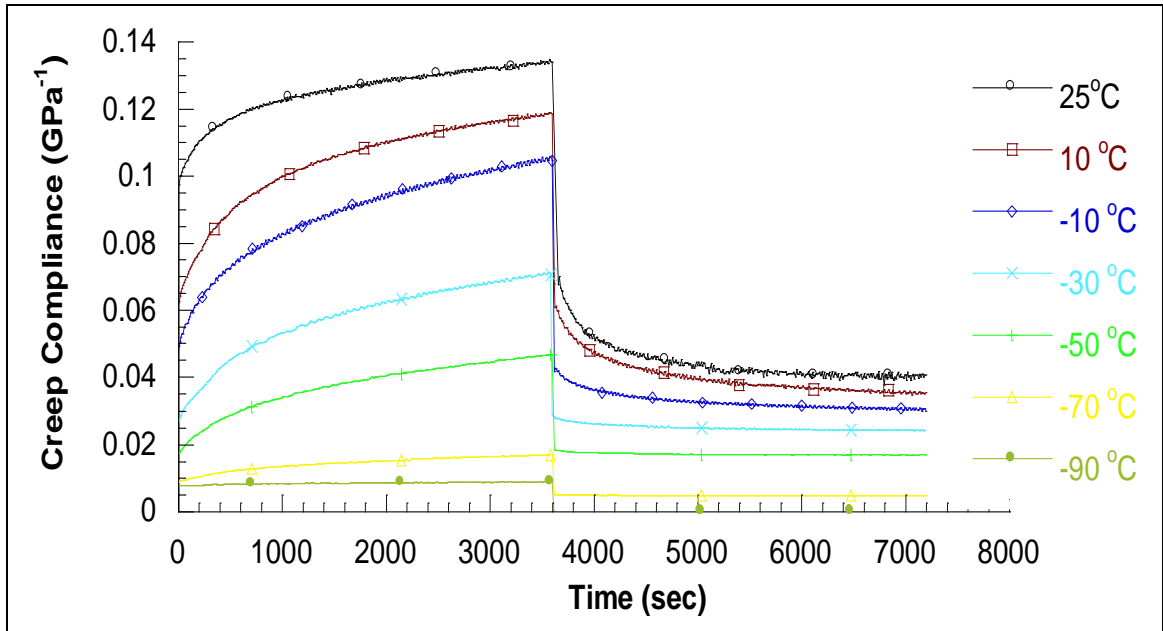
(b)
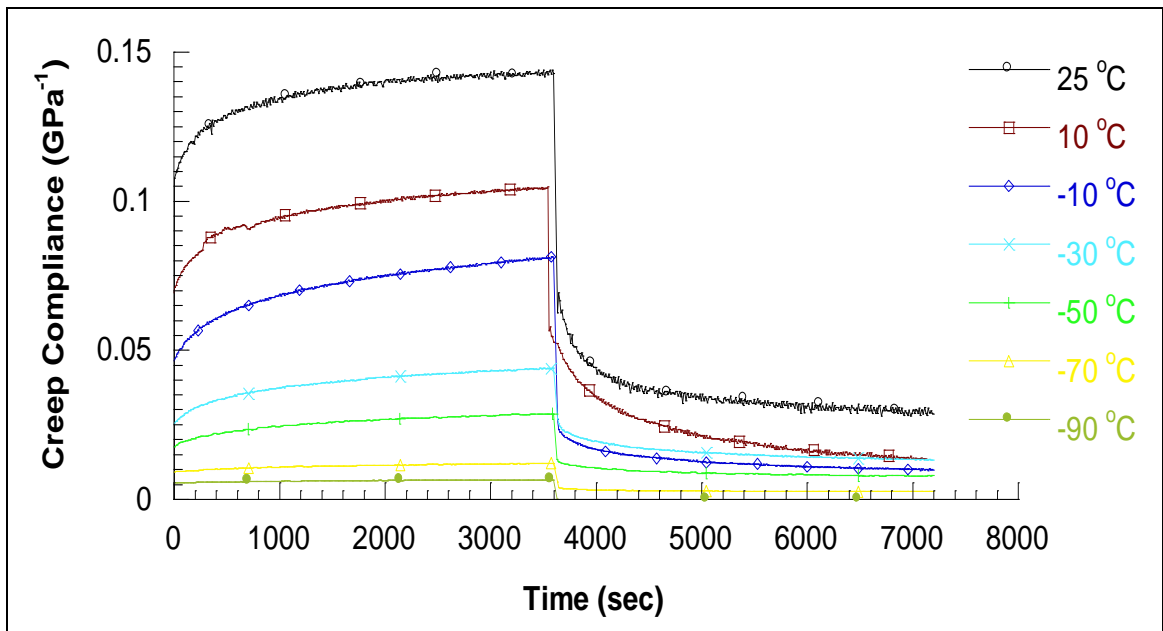
(c)
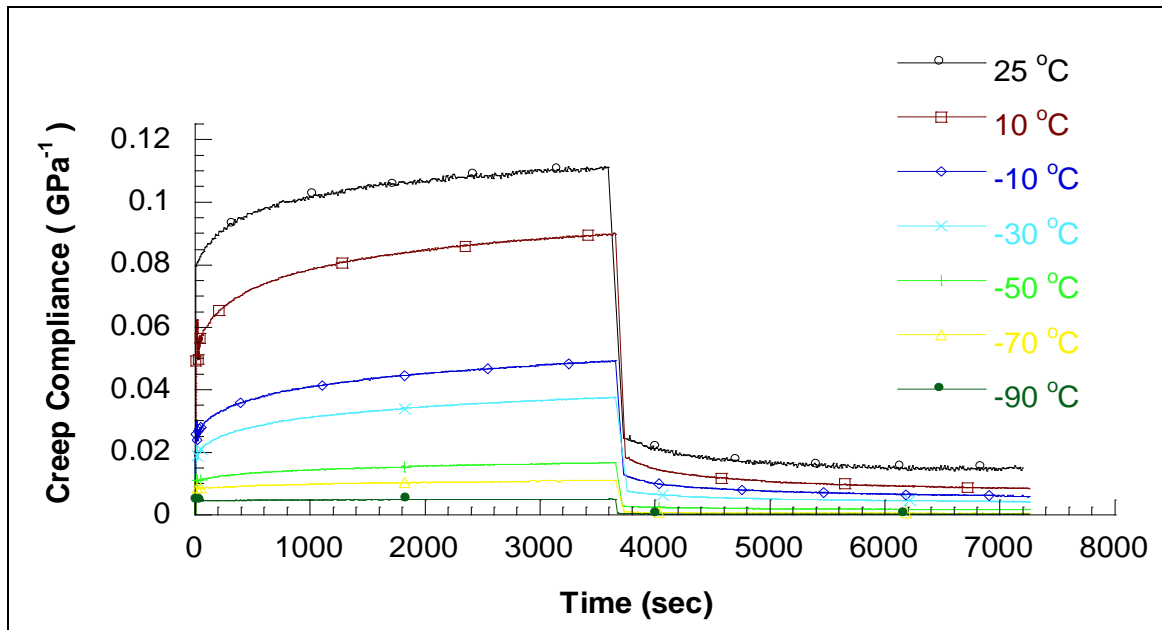
(d)

Figure 7.1. Creep-recovery of LLDPE nanocomposites (a) pure LLDPE (b) PE/1% MLS (c) PE/1% amEP (d) PE/1% amEP/1% MLS at different temperatures.

From Figure 7.1, it can be seen that the creep compliance of LLDPE nanocomposites is temperature dependent. The creep compliance curves increase with increasing temperature. This indicates that LLDPE nanocomposites exhibit a strong non-linear behavior with temperature similar to the stress dependence discussed in our previous study [13]. The non-linearity observed in temperature suggests that the time-temperature-stress-superposition principle (TTSSP) can be applied to LLDPE nanocomposites. According to this principle, long term creep deformation can be predicted based on short-term creep data at different temperatures and stress levels by a time-shifting method. It should be noted that at isothermal conditions, the TTSSP reduces to the time-stress-superposition principle (TSSP) used before. Horizontal and vertical

shifting was applied to construct the temperature dependent mastercurve of the LLDPE nanocomposites.

Figure 7.2 shows the temperature-dependent mastercurves of all samples. The mastercurves obtained could predict the creep behavior of the materials for a period of time more than 60 times exceeding the test time. From Figure 7.2, it can be seen that the creep compliance decreases with the addition of MLS. The addition of amEP further decreases the creep compliance. Strikingly, the nanocomposite with 1% amEP and 1% MLS exhibited the lowest compliance, i.e., the highest creep resistance. These observations led to a fundamental aspect for understanding the creep behavior of LLDPE nanocomposites. The creep response is controlled by the good interaction between amEP and MLS in the LLDPE nanocomposite.
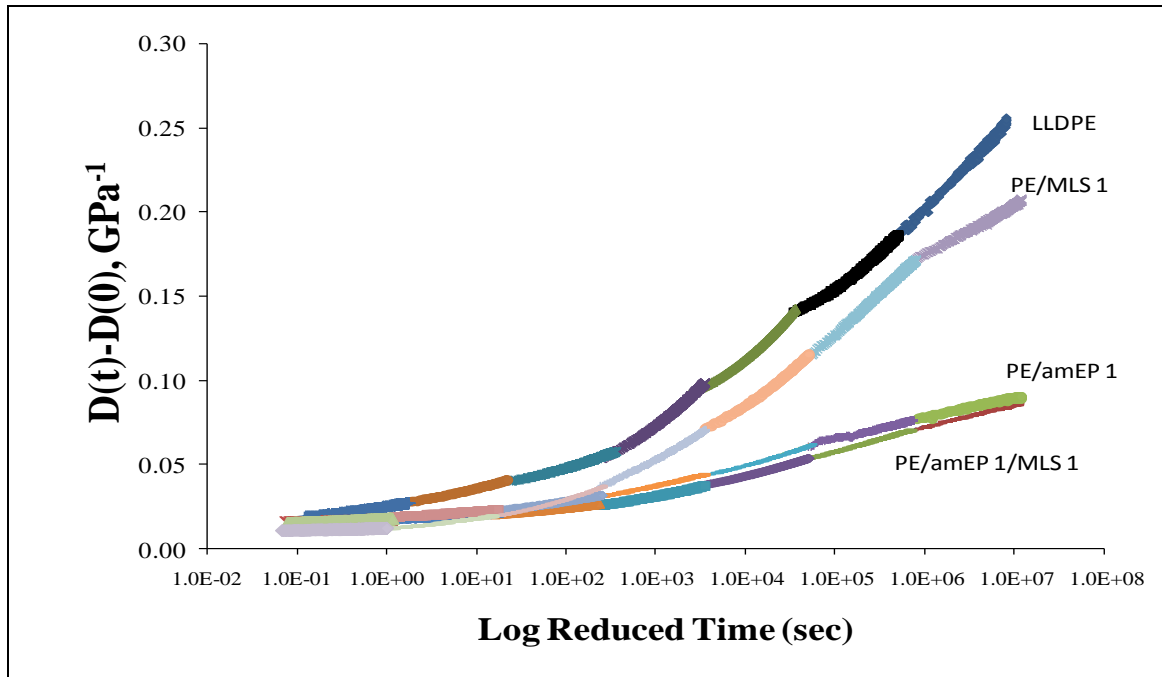
Figure 7.2. The temperature dependent creep compliance mastercurve.

7.4.2. Modeling Parameters of Schapery Model

The successful superposition of a mastercurve of the LLDPE nanocomposites indicates that the creep tests of LLDPE nanocomposites can be accelerated by increasing/decreasing the temperature/stress during the creep test. The time-temperature-stress superposition principle can be related to the Schapery thermodynamic theory. The temperature related constants h_0, h_1, h_2, and a_T in the Schapery model were determined by using the numerical method outlined before. Creep-recovery data were used to evaluate these constants, which are summarized in Table 7.2.

167

Sample	Temperature (^{o}C)	Applied Stress (MPa)	h_o	h_1	h_2	a_T
LLDPE	10	1.69	0.96	0.54	0.88	0.243
	-10	3.16	0.96	0.78	1.26	0.135
	-30	4.66	0.95	1.39	1.40	0.069
	-50	6.34	0.96	1.47	1.50	0.005
	-70	7.71	0.96	1.57	1.75	0.002
	-90	13.5	0.96	1.98	2.10	0.001
PE/MLS 1	10	4.85	0.95	1.11	0.93	0.129
	-10	5.08	0.94	1.12	1.23	0.059
	-30	6.58	0.96	1.23	1.33	0.008
	-50	9.80	0.95	1.25	1.52	0.002
	-70	9.80	0.95	1.3	1.68	0.001
	-90	11.84	0.96	1.3	2.21	0.001
PE/amEP1	10	2.34	0.96	1.08	0.89	0.622
	-10	2.61	0.95	1.26	1.31	0.251
	-30	4.64	0.96	1.3	1.39	0.109
	-50	8.14	0.95	1.38	1.52	0.088
	-70	14.23	0.95	1.57	1.76	0.058
	-90	24.67	0.96	1.58	2.05	0.008
PE/amEP1/MLS 1	10	5.35	0.95	0.92	0.98	0.405
	-10	6.85	0.95	1.05	1.30	0.248
	-30	8.50	0.95	1.1	1.42	0.064
	-50	12.25	0.95	1.16	1.68	0.026
	-70	17.35	0.96	1.24	1.76	0.005
	-90	22.77	0.94	1.49	2.27	0.001

Table 7.2. Values of the nonlinear factors h_0, h_1, and a_T for LLDPE nanocomposites at different temperatures.

Following the steps described, each of the Schapery nonlinear parameters was separately estimated. Each of the parameters has a specific physical meaning. The parameter h_0 is a measure of the stress dependence of the initial time-independent component of the compliance D_0. Parameter h_1 expresses the stress dependence of the transient, time dependent component of the compliance ΔD. Parameter h_2 reflects the effect of loading rate on the time-dependent response of the material and depends on both stress and temperature, and a_T is a shift factor superimposing the creep curves on a general master curve.

Figure 7.3 shows the variation of h_0 with temperature. It can be seen that the value of h_0 does not show significant change with temperature for all compositions tested. This implies a linear temperature dependent creep behavior of LLDPE nanocomposites.
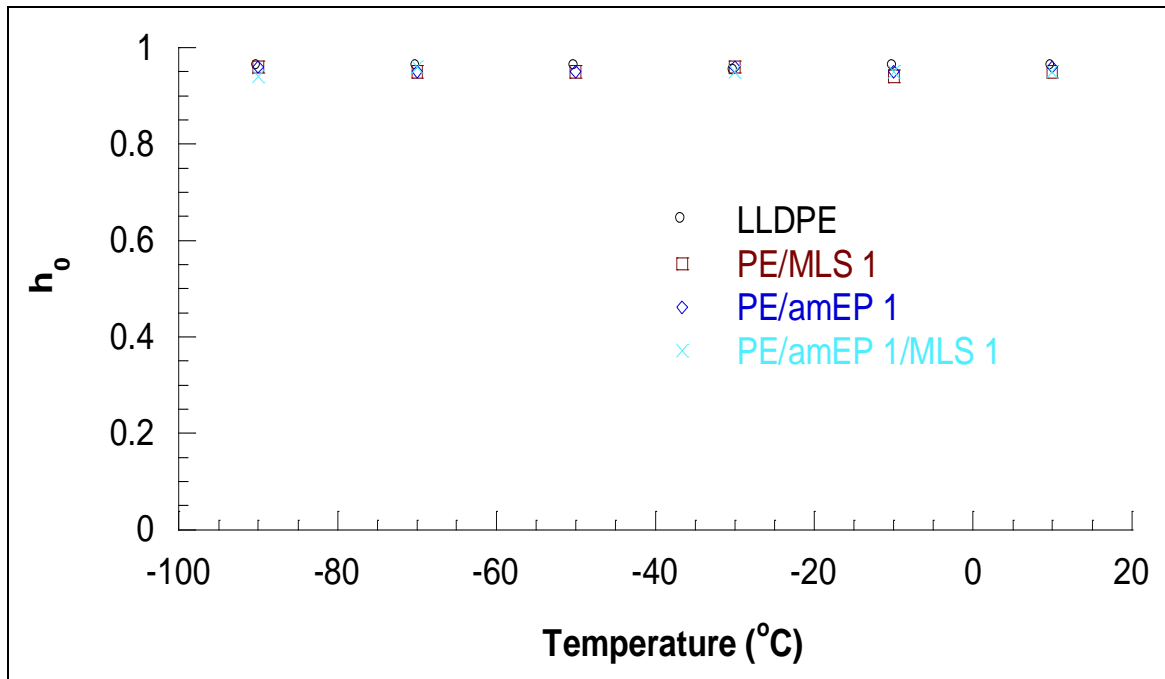
Figure 7.3. Variation of temperature dependent creep constant h_0 with temperature.

The h_1 values represent the part of creep that is recoverable after the load has been removed. In that sense, it is a stress dependent factor. A higher value of h_1 suggests quickness in recovery. It is observed that the values of h_1 increase with temperature for LLDPE as shown in Figure 7.4. The same relative increase with temperature is observed when MLS is added to pure LLDPE. The h1 value is further increased with the addition of amEP. This can be related to the addition of an elastic matrix which acts to improve the elastic recovery of the material at lower temperatures. The h_1 values for compositions containing a 1:1 ratio of amEP and MLS also show an increase suggesting an improvement in the creep resistance with decreasing temperature.
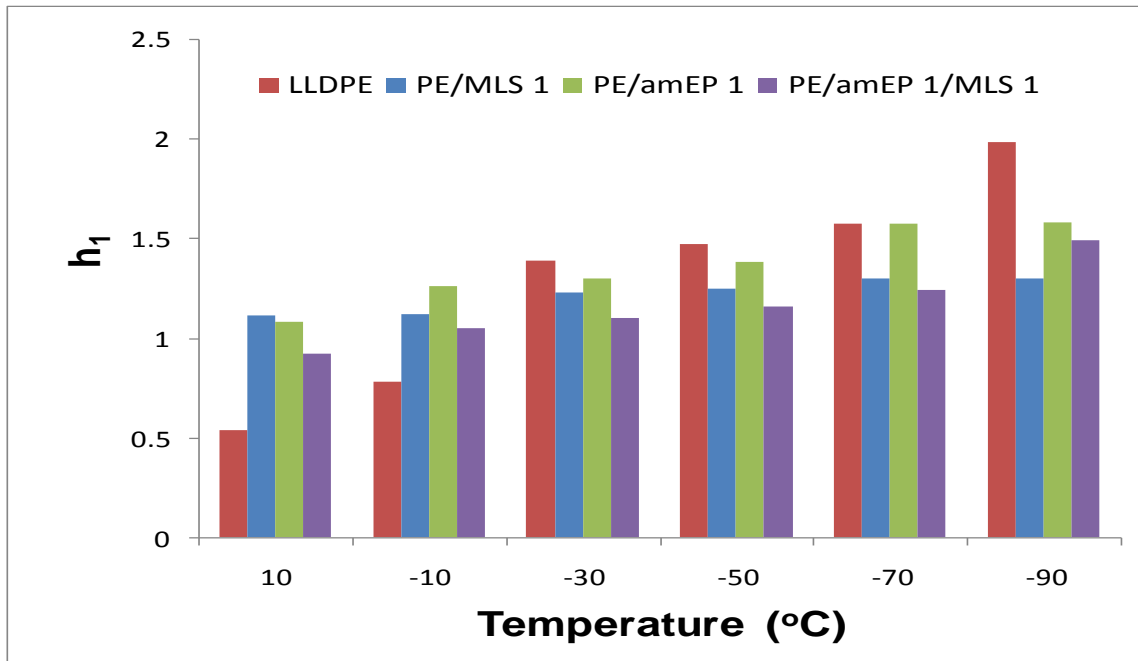
Figure 7.4. Variation of temperature dependent creep constant h_1 with temperature.

The values of h_2 represent the response of the material with no stress applied (recovery). This allows the separation of stress effects during creep from material effects during recovery. Figure 7.5 shows the variation of h_2 for LLDPE nanocomposites with temperature. It can be seen that the magnitude of h_2 increases with temperature for all LLDPE samples. It is observed that the values of h_2 are higher when MLS is added as compared to pure LLDPE. The addition of amEP serves to increase the values. The values of h_2 for all compositions containing a combination of amEP and MLS are higher than these containing amEP and MLS separately. This implies that the addition of low concentrations of amEP and MLS leads to a different structure in recovering. The results can be explained by structural differences induced with the addition of amEP and MLS, and reinforces the initial theory about addition of amEP and MLS. The addition of amEP

increases the strength of the system, leading to a more ductile material that will undergo a higher degree of deformation. This has been noted at all the stages of the mechanical testing. The addition of low concentrations of MLS increases the stiffness of the matrix and shows lower compliance in comparison with the PE and PE + amEP samples.

Figure 7.5. Variation of the temperature dependent shift factor h_2 with temperature.

Using the Schapery's recovery equation, test data for each recovery experiment were fitted in order to obtain the values of a_T. The values of a_T are plotted as a function of temperature for all LLDPE samples in Figure 7.6. The values are less than one indicating that the reduced time is greater than the real time. This suggests that lower temperatures will cause the material to accelerate its creep behavior. The shift factor showed a good linear dependence on temperature as shown in Figure 7.6. The activation energy was

obtained by the slope of a plot of log a_T against $1/T$. The calculated values are listed in Table 7.3.
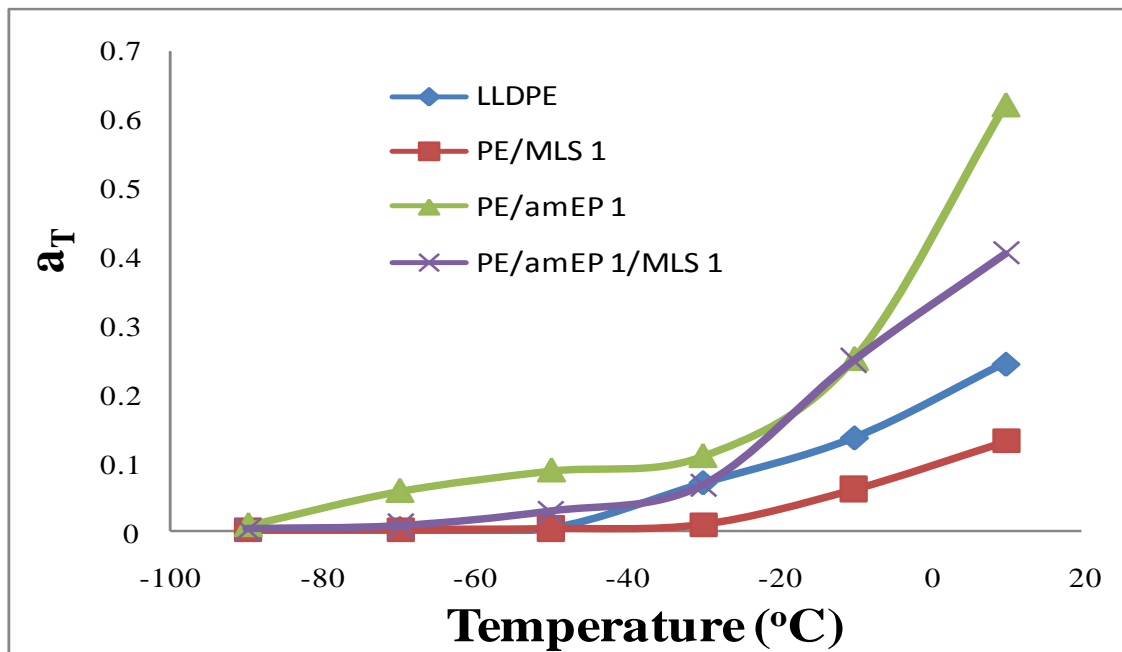
Figure 7.6. Variation of the shift factor a_T with temperature.

Sample	E_a (kJ/mol)
LLDPE	99.13
PE/MLS 1	93.56
PE/amEP1	99.18
PE/amEP1/MLS 1	92.8

Table 7.3. Activation energy of LLDPE nanocomposites obtained from the mastercurves.

The activation energy of the nanocomposites was lower than that of LLDPE, indicating that mobility of the polymer chains became easier with the addition of MLS.

The results are in agreement with dynamic mechanical measurements which show a decrease in the glass transition temperature with the addition of MLS [19].

7.5.   Conclusions

The tensile behavior and long-term creep of LLDPE nanocomposites was investigated .The creep behavior of the polymer was viscoelastic and the nonlinearity in temperature was revealed by investigating the creep compliance of the material at different temperatures. The creep compliance mastercurves can be used to predict the long term creep behavior of the nanocomposites. A considerable enhancement in the creep resistance was obtained with the addition of amEP and MLS when compared with the pure LLDPE and was revealed by comparing the temperature dependent mastercurves.

Schapery nonlinear model was used to model the creep behavior of the nanocomposites with respect to temperature. The absolute values of the temperature factors also indicated an enhanced creep resistance in the nanocomposites as compared with the neat PE matrix. The addition of 1:1 ratio of amEP and MLS shows to have the highest creep resistance among the materials investigated.

7.6. References

1. JL Yang, Z Zhang, A Schlarb, K Friedrich, *Polymer*, **47**, 2791-2801 (2006)

2. A Pegoretti, J Kolarik, C Peroni, Cilgiaresi, *Polymer*, **4**, 2751-2759 (2004)

3. Z Zhang, JL Yang, K Friedrich, *Polymer*, **45**, 3481-3485(2004)

4. JL Yang, Z Zhang, A Schlarb, K Friedrich, *Polymer*, **47**, 6745-6758(2006)

5. J Lai, W Findley, Transactions of the Society of Rheology, **17**, 63-87 (1973)

6. LCE Struik , *Physical aging in amorphous polymers and other materials*; Elsevier: New York (1978)

7. J Kolarik, A Pegoretti, *Polymer*, **47**, 346-356 (2006)

8. G Liang, J Xu, S. Bao, W. Xu, *J. of Appl. Polym. Sci*, **91**, 3974-3980 (2004)

9. D Martin, P Halley, R Truss, *Polym Int.*, **52,** ,1774–1779 (2003)

10. RW Truss, TK Yeow, *J. of Appl. Polym. Sci.*, **100**, 3044-3049 (2006)

11. M Tajvidi, R Falk, J Hermanson, *Appl. Polym. Sci.*, **97**, 1995-2004 (2005)

12. Pramanick, M Sain, *J. of Thermoplastic Composite Mat.,***19,**35-59 (2006)

13. A Shaito, D Fairbrother, J Sterling, N.A D'Souza, *"Nonlinear creep deformation in polyethylene nanocomposites: Temperature effects"*, Polym. Eng. and Sci, submitted (2008).

14. M Tajvidi, R Falk, J Hermanson, *J. Appl. Polym. Sci.*, **97**, 1995–2004 (2005)

15. M Elahi, Y Weitsman, *Mechanics of Time-Dependent Material*, **3**,219–244 (1999)

16. D Pooler, L Smith, *J. Thermoplastic Composite Mat.*,**17,**427-445 (2004)

17. A Pramanick, M Sain, *J. Thermoplastic Composite Mat.,***19,**35-59 (2006)

18. S Onogi, T Sato, T Asada, Y Fukui, *J. of Polym. Sci., Part A-2 (Polymer Physics),***8,**1195-1209 (1970)

19. A Shaito, D Fairbrother, J Sterling, N.A D'Souza, *"Nonlinear creep deformation in polyethylene nanocomposites: stress effects"*, Polym. Eng. and Sci, submitted (2008).

CHAPTER 8

CONCLUSIONS

The investigation of creep response in polyethylene nanocomposites and correlation to component contributions, synergistic advantages of their combinations and their stress and temperature dependent response have been investigated.

In the first section of the study, the tensile and creep properties of the materials were investigated at room temperature. Tensile results showed the reinforcing effects of MLS on both LLDPE and amPE. A noticeable increase in elastic modulus (166%) and yield stress (42%) was obtained with the addition of amEP and MLS to LLDPE. For the amEP matrix, a 35% increase in yield stress and 90% increase in elastic modulus was obtained with the addition of 3% MLS. The results suggest MLS to be a good reinforcement in both the amorphous amEP and the semicrystalline PE. The observed results from the tensile testing suggest a synergistic effect obtained with the addition of both amEP and MLS to LLDPE. To assess this, it was important to sort out the possible effect of different factors on such behavior. These factors include: composition of the matrix, crystallinity of the matrix, and dispersion of the filler within the matrix. To study the effect of the composition of the matrix, the ratio of the compatibilizer to the filler was varied and a set of composition were processed. Among the different compositions, the 1:1 ratio showed the best performance with the highest yield stress and modulus. The same composition showed the synergistic effects in a previous study by our laboratory. The yield stress and modulus generally increase with an increase in crystallinity. The

crystallization behavior of the nanocomposites was probed using DSC. No change in crystallinity was observed with the addition of amEP and MLS which negates the possibility that the observed reinforcement is due to a change in crystallinity. XRD showed that although no change in crystallinity was obtained with the addition of amEP and MLS, a thickening of the lamella was observed indicating a change in the morphology of the matrix.

XRD was then used to study the possible effect of the dispersion of the filler on the improvement in the tensile properties. The diffractograms of the different composition showed that increasing the MLS content from 1 % to 2% while keeping the amEP content at 1% decreased the interaction between MLS and the matrix, whereas increasing the degree of maleation from 1% to 2% causes a collapse of the intergallery chains of the surfactant. An intercalated/exfoliated system was obtained with the 1:1 ratio sample which suggests that this composition can be considered as the optimum composition to be used. The XRD of the pure amorphous amEP showed the disappearance of the MLS characteristic peak which suggested an intercalated/exfoliated system. To confirm the XRD observations, FIB was uniquely used to obtain a high resolution image of the dispersed clay platelets. The micrographs of the PE and amEP nanocomposites showed the good dispersion caused by the addition of amEP when compared withtheaddition of MLSalone.

Creep test results showed the same behavior observed in the tensile test. The different compositions were analyzed. A first qualitative analysis of the creep compliance plots showed the creep resistance improvement caused by the addition of MLS and amEP separately and combined to the PE matrix. The addition of MLS to the pure amorphous amEP matrix showed an interesting phenomenon. The MLS acts as a reinforcing agent in

amEP as well. Among the different composition, the 1:1 ratio showed the lowest creep compliance and the lowest unrecoverable deformation. Another qualitative comparison of the results was done by comparing the creep and recovery plots. The creep plots did not coincide with the recovery plots indicating a nonlinear viscoelastic behavior which is attributed to the "undisturbed" amorphous as explained by Struik's model. The % recovery was calculated to evaluate the degree of divergence and was found to increase in the nanocomposites samples.

The dependence of the material properties on structure is defined by considering Burgers nonlinear viscoelastic model. The structure-property relationship was carried out by analyzing the fit parameters in this model, since the variations of these parameters illustrate the influence of the filler on the creep performance of the bulk matrix. From Burgers model, the most significant parameters to consider are the elastic modulus E_M which is a measure of the instantaneous elastic creep strain and the retardation time τ which reflects delayed response after removing the applied load. The nanocomposites showed higher E_M values which is a reflection of the improved tensile properties. They also showed lower retardation times which are an indication of improved elasticity as compared to the bulk matrix. The amorphous amEP matrix also showed a similar trend, where E_M of the compositions with 1% and 3% MLS where higher than the bulk matrix. The results confirm the reinforcement characteristics of MLS. An alternative function that has been successfully used to describe the creep of predominantly semi-crystalline polymers is based on the KWW function. The parameters from this function are used to describe the variation of the breadth of relaxation and the characteristic retardation time

during the creep process. An increase in the breadth of relaxation is observed for both amEP and PE nanocomposites which is an indication of a strengthening of the coupling between the relaxing species and the medium and is related to an overall decrease of the molecular mobility. The variations of the retardation time from the KWW are in agreement with those from Burgers model indicating that both functions can be used to describe the structure-property relation of the nanocomposites.

In the second section of the study, temperature and stress effects on the overall properties of the nanocomposites were considered. This is of importance due to the fact that these materials are to be used in structural applications where they experience complex load and temperature histories, so that is important to design for different stress and temperature scenarios.

The effect of stress on creep properties of LLDPE nanocomposites was investigated at room temperature. Like other thermoplastic polymers, polyethylene exhibits time dependent load response and is characterized as a viscoelastic material. At low stresses, the stress-strain is independent of stress/strain independent, however, PE is in general a nonlinear viscoelastic material and the material time dependent properties cannot be defined by a single creep compliance-time curve and a group of compliance-time curves at different stress levels are needed to characterize its time-dependent behavior. In our study, three stress levels of 10, 25, and 50% yield stress were chosen. The nonlinear time-dependent behavior of the different materials at the different stress levels were correlated to the fitting parameters of Schapery's nonlinear equation. The results showed the time dependent behavior of the different compositions to be nonlinear.

The nonlinear behavior was attributed to the "undisturbed" amorphous region far from the crystals as proposed by Struik. All maleated PE compositions showed a reduction in the nonlinear response as obtained from Schapery's fit parameters. The effect of the different material properties was investigated by normalizing the stress levels applied to the yield stress of each material. The stress dependent parameter g_0 showed a decreasing trend with increasing stress indicating material hardening. The addition of MLS to PE or the pure amorphous amEP matrix showed lower values which is an indication of the reinforcement characteristics of MLS.

The effect of temperature on tensile and creep properties was investigated by running these tests in the range of -100° to 25°C. The stress level in the creep tests was kept constant at 50% yield stress ensuring the material response is in the linear viscoelastic region. The tensile properties of the different compositions at temperatures below the softening or glass transition temperature show an increasing trend with decreasing temperature. This is due to the fact that the below the glass transition, the amorphous and semicrystalline domains are brittle and rigid. For the compositions considered, the addition of MLS caused an increase in the yield stress and modulus with decreasing temperature. The maximum increase was obtained for a combination of amEP and MLS which was the same trend obtained for the room temperature results. These results showed that MLS acts as a reinforcing agent even at temperatures as low as -100°C. The molecular relaxation behavior of the bulk PE and amEP matrices can be related to the yield behavior at low temperatures by considering the dynamic temperature response of the materials. The storage moduli E' of the nanocomposites were higher than those of the pure LLDPE over the entire temperature range. The highest increase in storage modulus

(23% at -80°C and 27% at 25°C) was for samples in which a combination of 1% amEP and 1% MLS was used. This increase can be explained by the synergic interaction between amEP and MLS and is reflected by the tensile test results at these temperatures. The decreased work hardening evidenced by the drop in stress following UTS in the tensile test results below -50°C is an indication of a relaxation processes in the matrix. The effect of amEP and MLS on the viscoelastic properties at different temperatures was investigated by comparing the variations in tan β peaks of the two relaxation processes. The addition of amEP did not affect the maxima of the PE for the α transition, indicating no influence of the amorphous compatibilizer on segmental relaxation, while the addition of MLS hada pronounced effect on themaxima,supporting the conclusion that MLS provides an interface that affects the relaxation in the PE matrix.

The effect of temperature on the structure-property relationship was investigated by considering the variations of the Burgers model and KWW function parameters with temperature. A similar trend in the creep-recovery behavior at room temperature was observed with decreasing temperature. All maleated compositions showed increasing % recovery as compared to the pure PE matrix. It was suggested that MLS particles act as hingesinthe amorphousmatrixincreasing the elasticity of the bulk matrix. A comparison of the different parameters from Burgers model showed that all maleated compositions had higher E_M, higher E_K and η_K, and lower retardation times for temperature above the beta transition temperature of PE. The results were related to the reinforcing effect of the clay particles. Below the β-transition temperature, retardation time increases linearly with decreasing temperature. This behavior is exhibited because below the beta transition temperature, the material is in its glassy state where molecular mobility is hindered,

reducing the polymer elasticity. The analysis of the KWW parameters showed the same trend in the retardation times which further confirms the analysis from Burgers model.

The effect of temperature on the nonlinear time dependent behavior was investigated. In order to evaluate the various functions to modify the linear compliance to predict the nonlinear response, a set of creep tests were performed at different stresses and temperatures. The different materials showed a strong nonlinearity with decreasing temperature similar to that observed with increasing stress levels at room temperature. It was important to note that the determination of the dependence of the nonlinear strain on stress and temperature is a key in the design of any linear or nonlinear viscoelastic material. The different parameter in the Schapery's model showed to be both stress and temperature dependent. The values of h_2 which represent the response of the material with no stress applied allowing the separation of stress effects during creep from material effects during recovery. The magnitude of h_2 was shown to increase with temperature for all LLDPE samples. It was observed that the values of h_2 are higher when MLS is added as compared to pure LLDPE. The addition of amEP serves to increase the values. The values of h_2 for all maleated nanocomposites are higher than these containing amEP and MLS separately. This implies that the addition of low concentrations of amEP and MLS leads to a different structure in recovering. The results were explained by structural differences induced with the addition of amEP and MLS, and reinforce the synergistic effects of adding amEP and MLS to PE.

The time-temperature superposition principle was successfully used to predict the long term behavior of LLDPE and amEP nanocomposites. This was important to account

for the long term properties from short term tests. Mastercurves for both systems were constructed. The amorphous nature of amEP was reflected in the use of horizontal shift factors only, where as horizontal and vertical shift factors were used for the PE material which is an indication of its semicrystalline nature. Comparing the two master curves, it was observed that the addition of MLS to both amEP and PE decreased the creep compliance of the bulk matrix. All maleated PE compositions showed lower creep compliance. These results further supported the synergistic effect of adding amEP and MLS separately to the pure LLDPE matrix.

The schematic in Figure 8.1 depicts the prediction of the effect of the combinations. When montmorillonite is added to a semicrystalline polymer (a), it typically resides in the amorphous region, perturbing the chains (b). The introduction of a maleated compatibilizer (c) bridges the polymer to the montmorillonite. Addition of more compatibilizer (d) does not increase the mechanical performance (2% amEP versus 1% amEP) because the intrinsic amEP has significantly lower mechanical performance and beyond offering a chemical bond, limits the incremental mechanical performance of the composite.
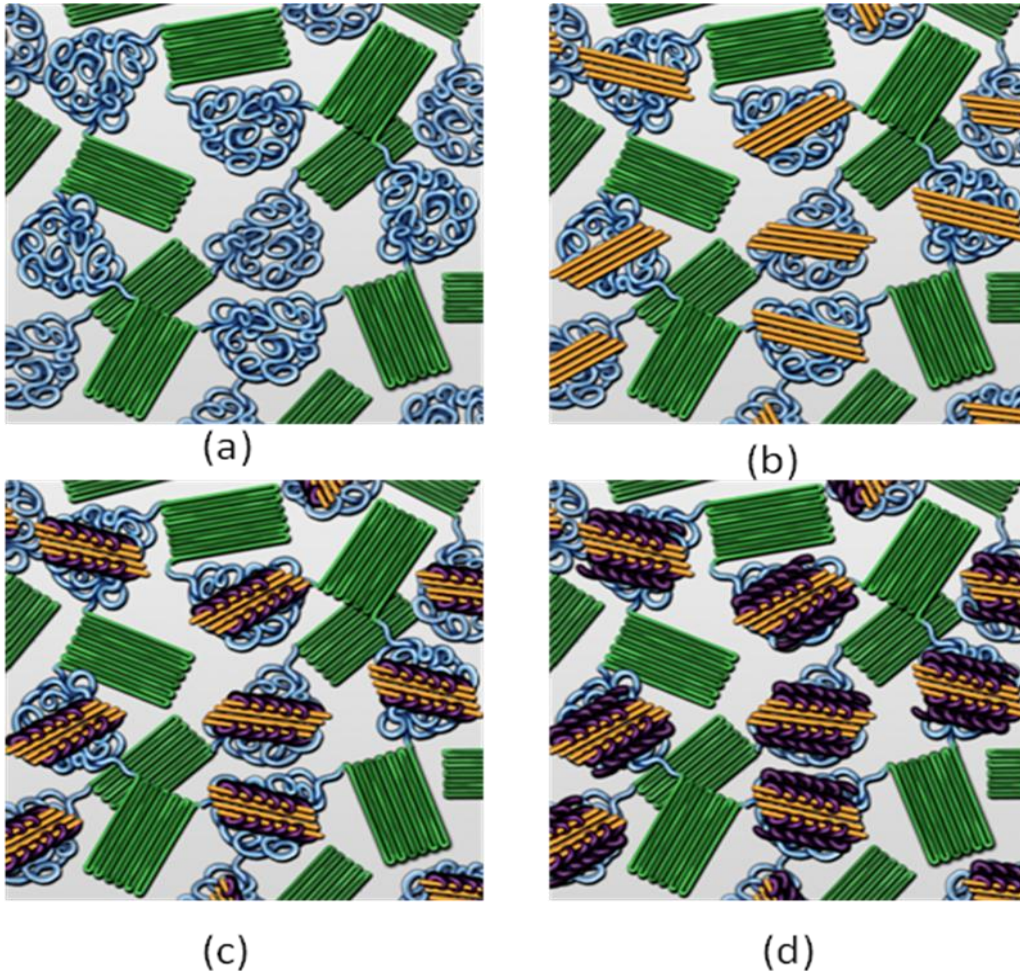
Figure 8.1. Schematic explaining material behavior during deformation.